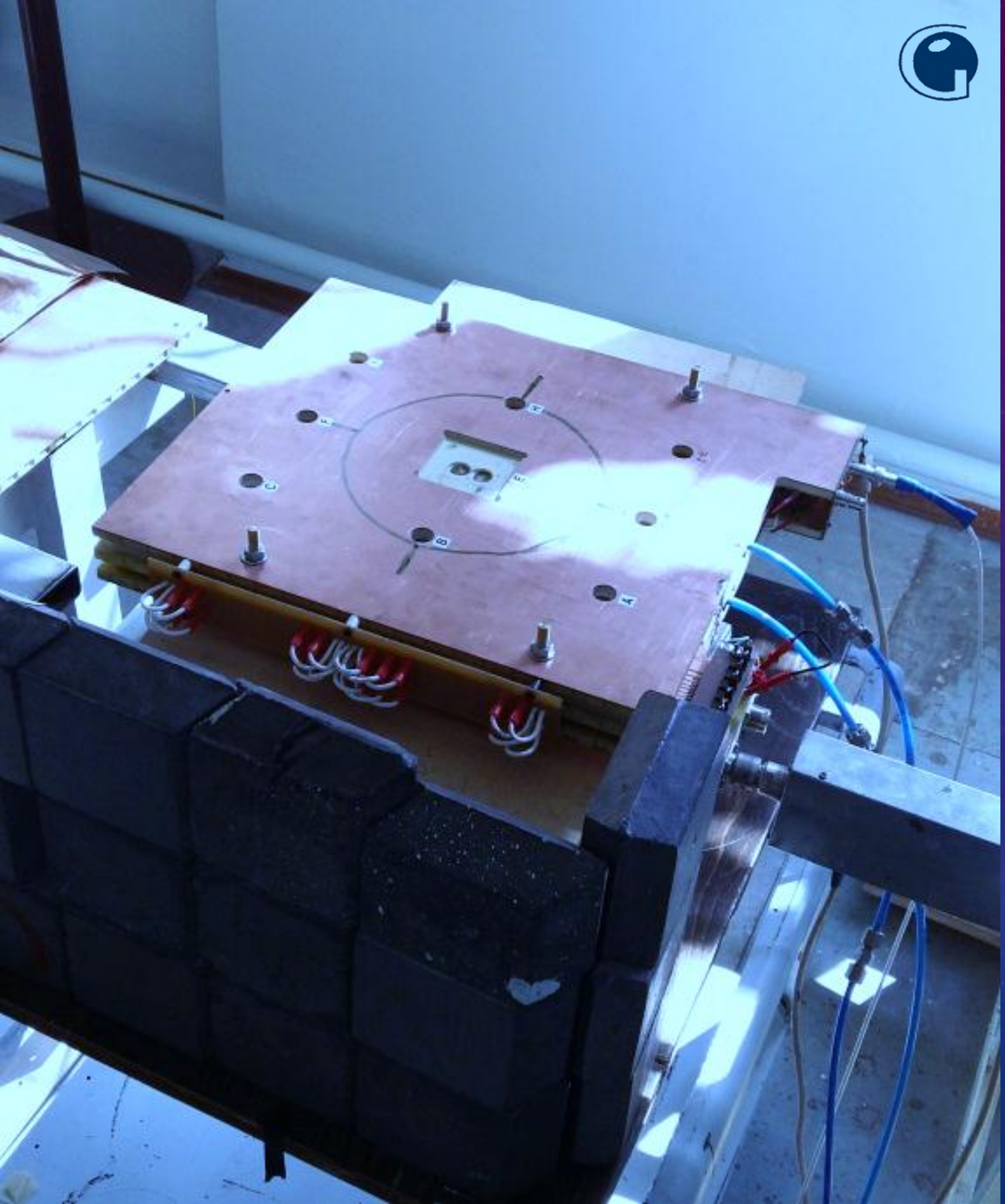

STUDY MALTER EFFECT PHENOMENA WITH CSC PROTOTYPE

G. GAVRILOV, M. BUZOVERIA

B.P. Konstantinov Petersburg Nuclear Physics Institute, Gatchina
National Research Nuclear University MEPhI, Sarov

Motivation: CSC's performance at HL-LHC

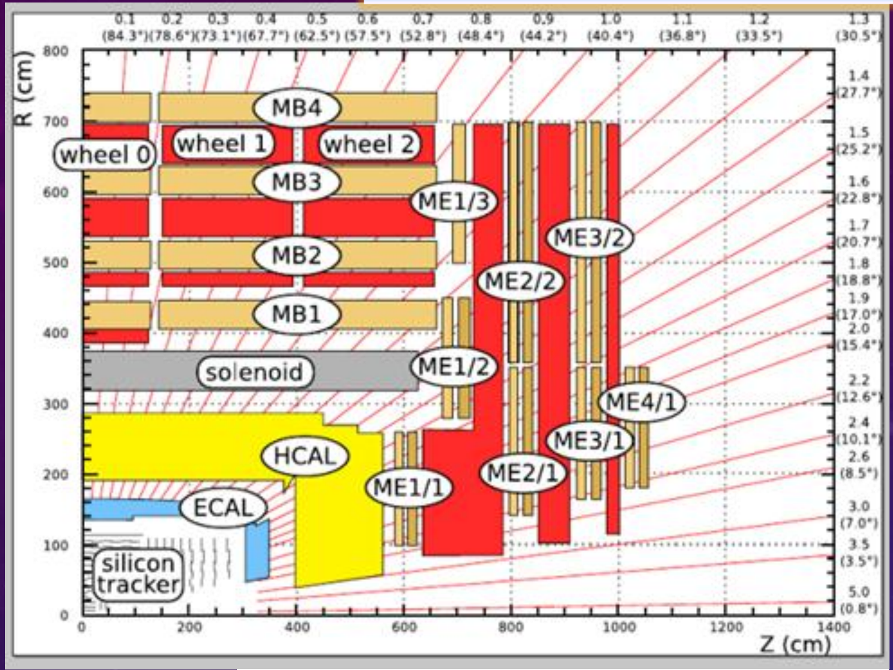

J. Va'vra, January, 2002

Secondary electron emission due to the Malter effect (L.Malter, Phys. Rev. 50(1936)) **:**

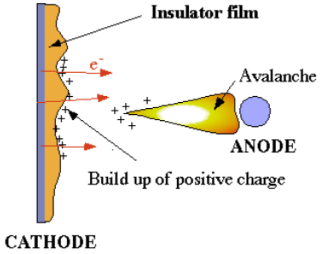

Necessary condition for electron emission:
a) Localized primary ionization deposit.
b) An insulator on the cathode.
c) A rate of the charge build up is higher than its removal rate.
d) Excessive field cathode gradients help to trigger it.
e) **To start the effect, it needs an ignition.**

Effective luminosity determined from current on anode wires

Anode current is proportional to luminosity (example from ME2/1)

Andrey Korytov

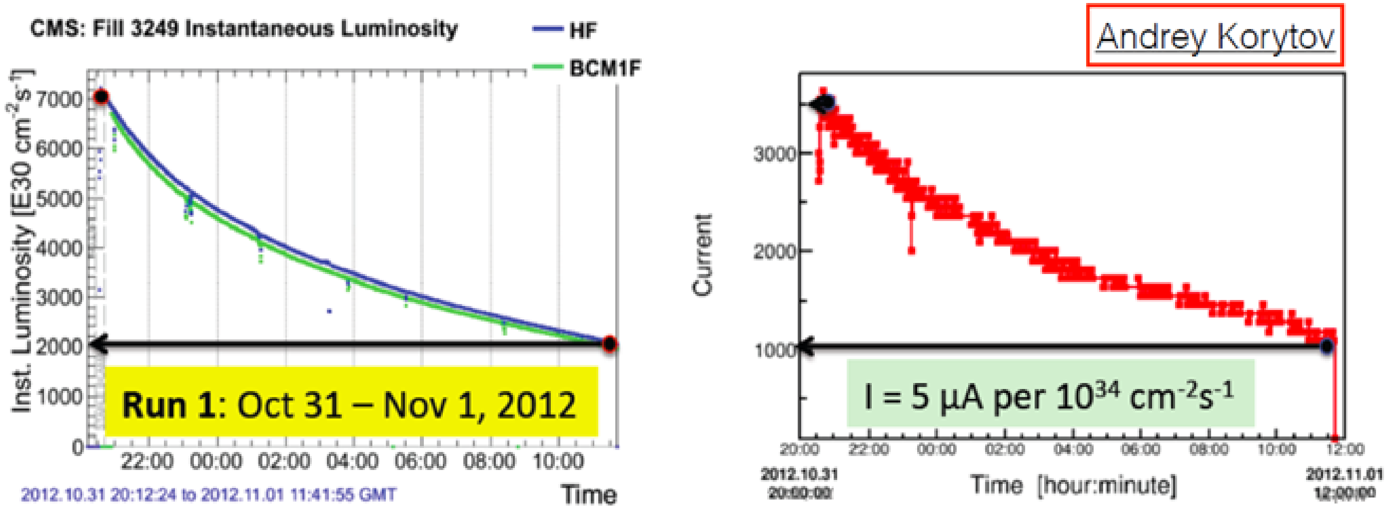

- **Currents observed in Run 1 and Run 2**
  - **ME1/1: $I \approx 2$ μA per 10^{34} cm^{-2}s^{-1}**
  - **ME2/1 (HV#1): $I \approx 5$ μA per 10^{34} cm^{-2}s^{-1}**
  - Current per lumi is about the same at 8 and 13 TeV

?

- **Extrapolation toward HL LHC L = 5×10^{34} cm^{-2}s^{-1}**
  - **ME1/1: $I_{HL-LHC} \approx$ 10-15 μA**
  - **ME2/1 (HV#1): $I_{HL-LHC} \approx$ 25 μA**

Motivation: CSC's performance at HL-LHC

CMS Muon upgrade plan

2012	2013	2014	2015	2016	2017	2018	2019	2020	2021	2022	2023
	LS1					LS2				LS3	

Detector consolidation

Anticipated phase-2 upgrades

GE1/1 installation
CSC + GEM trigger

HL-upgrades

Additional detectors GEM+ME0+iRPC in forward region of all 4 stations

Rapidity extension of tracker, CAL, muon to |η|~4

Detectors

ME4/2 + RE4/2 installed

Move part of DT electronics from detector to cavern and redesign in higher performance µTCA technology.

Electronics

Upgrade ME1/1 electronics.

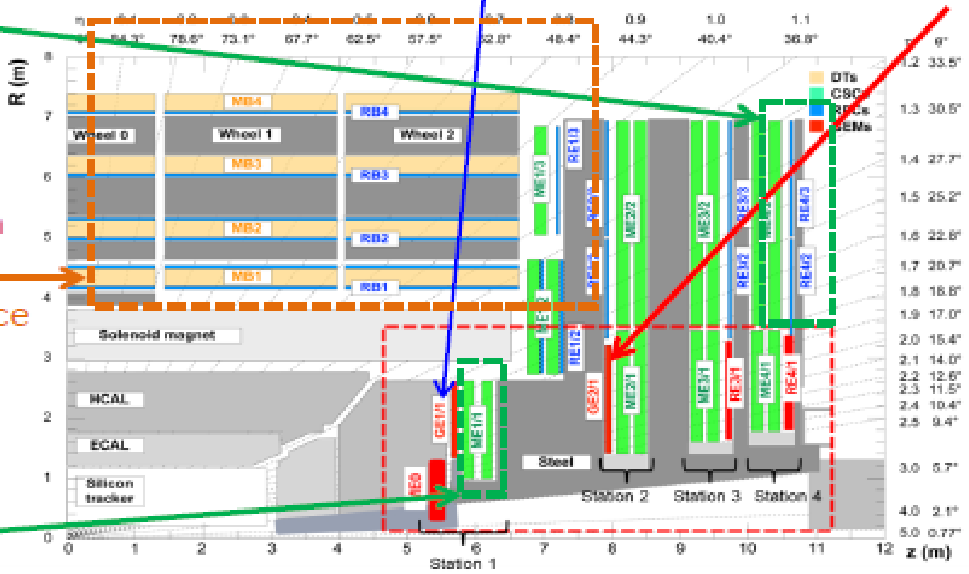

Redesign of DT on-chamber electronics

Other CMS upgrades, e.g. L1 trigger

Malter current effect is …

Malter current effect (MCE) is secondary electron emission which appears when:

1. an insulating layer exists on the cathode,
2. the rate of ion build-up is higher than its removal from the insulating layer,
3. some ignition mechanism take place

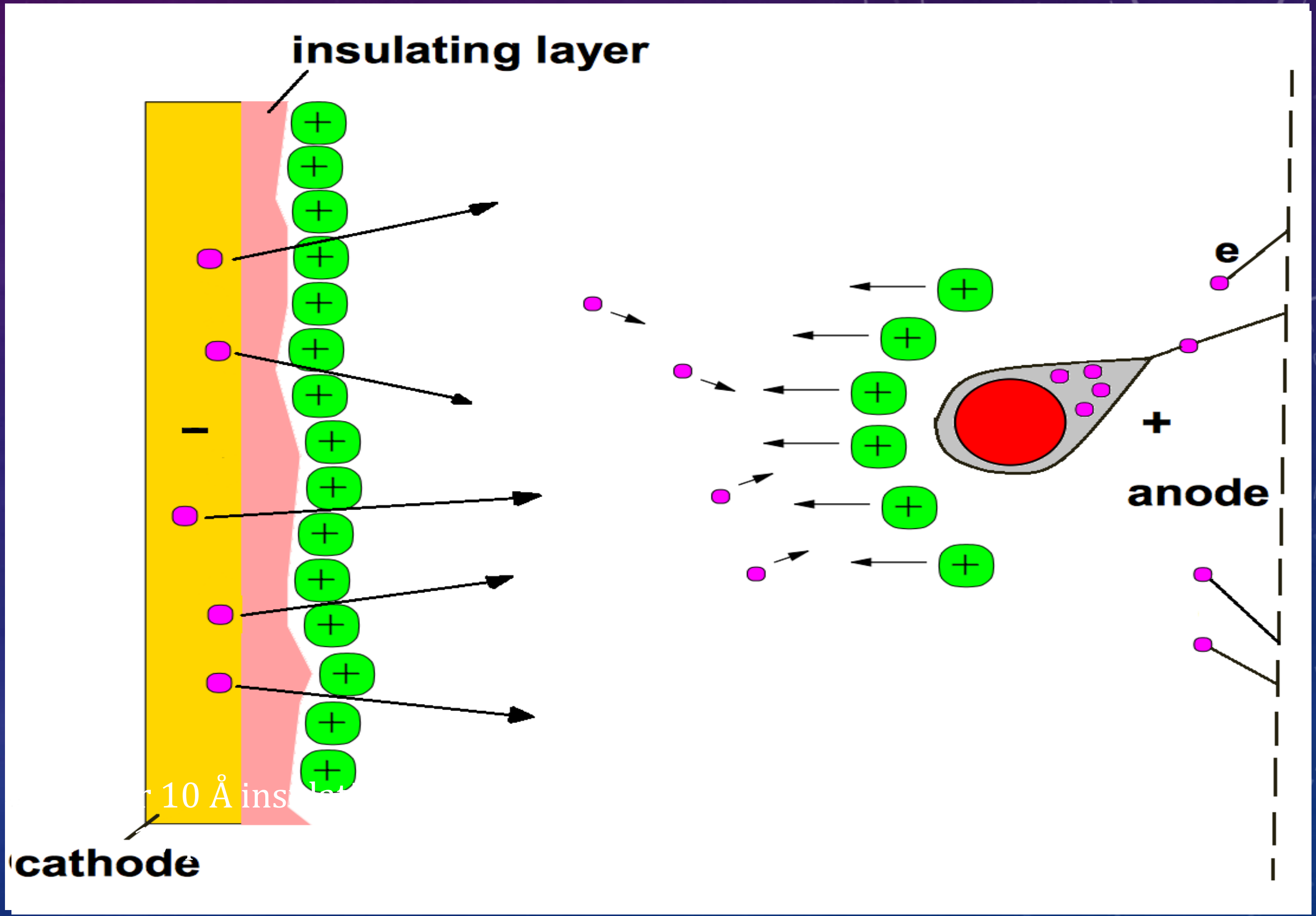

Manifestation of MCE:

1. self-sustained discharge ignited by high intensity irradiation and micro sparks;
2. sustained O(1) μA current independent from external irradiation;
3. spurious signals which hard to see in data or DQM (can be too small, DAQ is LST driven).

Curing is possible:

- Make cathode again conductive by
  - Adding water/alcohol vapours (not good for FR4 cathode strips);
  - Clean (etch) insulating layer with training at presence of O•, F• and CF_3•
- Wait until insulating layer rises up to 1 μm (??)

Malter currents: CSC CMS

CSCs Malter currents status:

- 2% (9 out of 432) ME1/1 Layers are operating with lowered HV:

ME-1/1/02 L6 (-100V)
ME-1/1/04 L3 (-100V)
ME-1/1/05 L2 (-200V)
ME-1/1/07 L1 (-100V)
ME-1/1/09 L1 (-50V)
ME-1/1/09 L2 HV=off
ME-1/1/25 L4 (-100V)
ME-1/1/25 L6 (-100V)
ME-1/1/01 L5 HV=off

6% (25) of the remaining Layers occasionally show the Malter

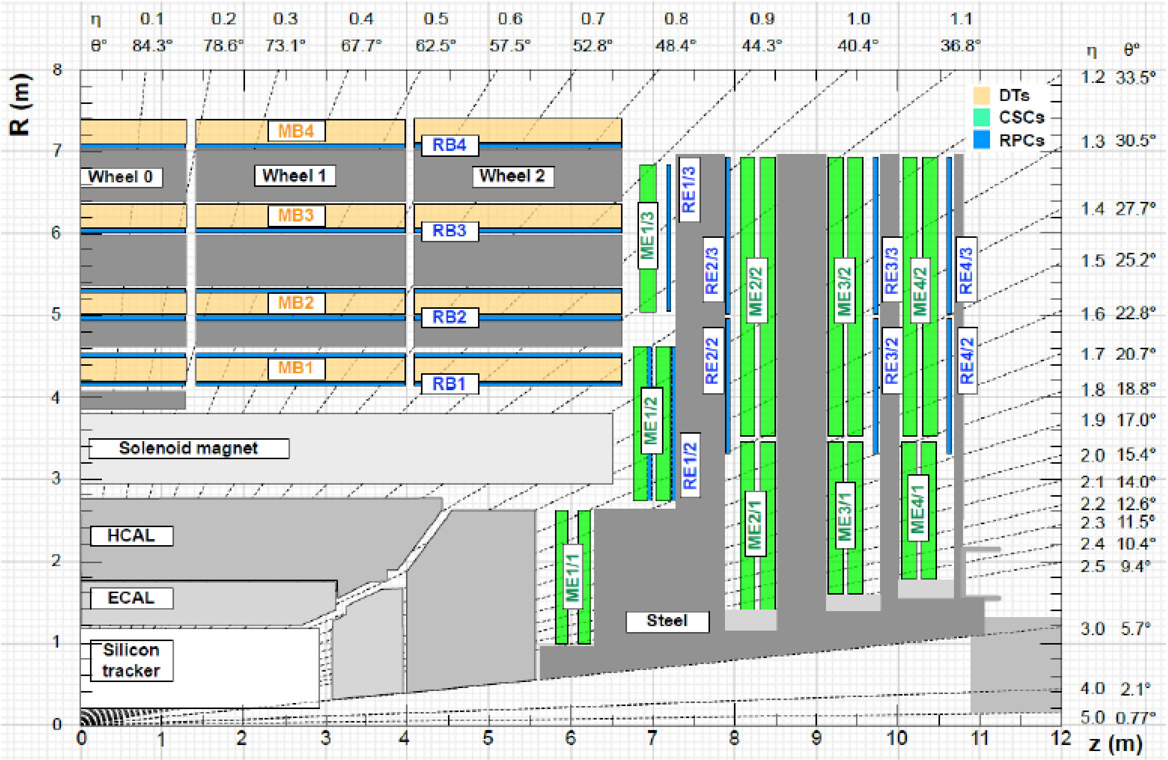

Fill 5068 Lumi=8.1×10^{33} cm-2 sec-1

- 71% (21 out of 72) of ME1/2 chambers showed HV instabilities during LHC 5068 fill
- ~25% (9 out of 36) of ME2/1 chambers (in 3 chambers the classic Malter effect was observed).
- 8% (3 out of 36) ME3/1 rings - showed single spikes.
- ME4/1 rings - 1 HV channel showed 1 current spike

B=0T

- ❑ **ME1/1, ME1/2, ME2/1, ME3/1 and ME4/1 show Malter-like HV instabilities.**
- ❑ **At B=0 T Malter current is easy ignited in ME1/1, ME1/2, ME2/1 and extinguishes at B=3.8 T (???)**

RECOVERY OF LHCb MUON CHAMBERS FROM MALTER

I. MCE curing procedure on the beam consists in keeping of the Malter current until it drops down at the level below of the HV trip threshold. For the training the threshold is specially raised up to ~40 μA

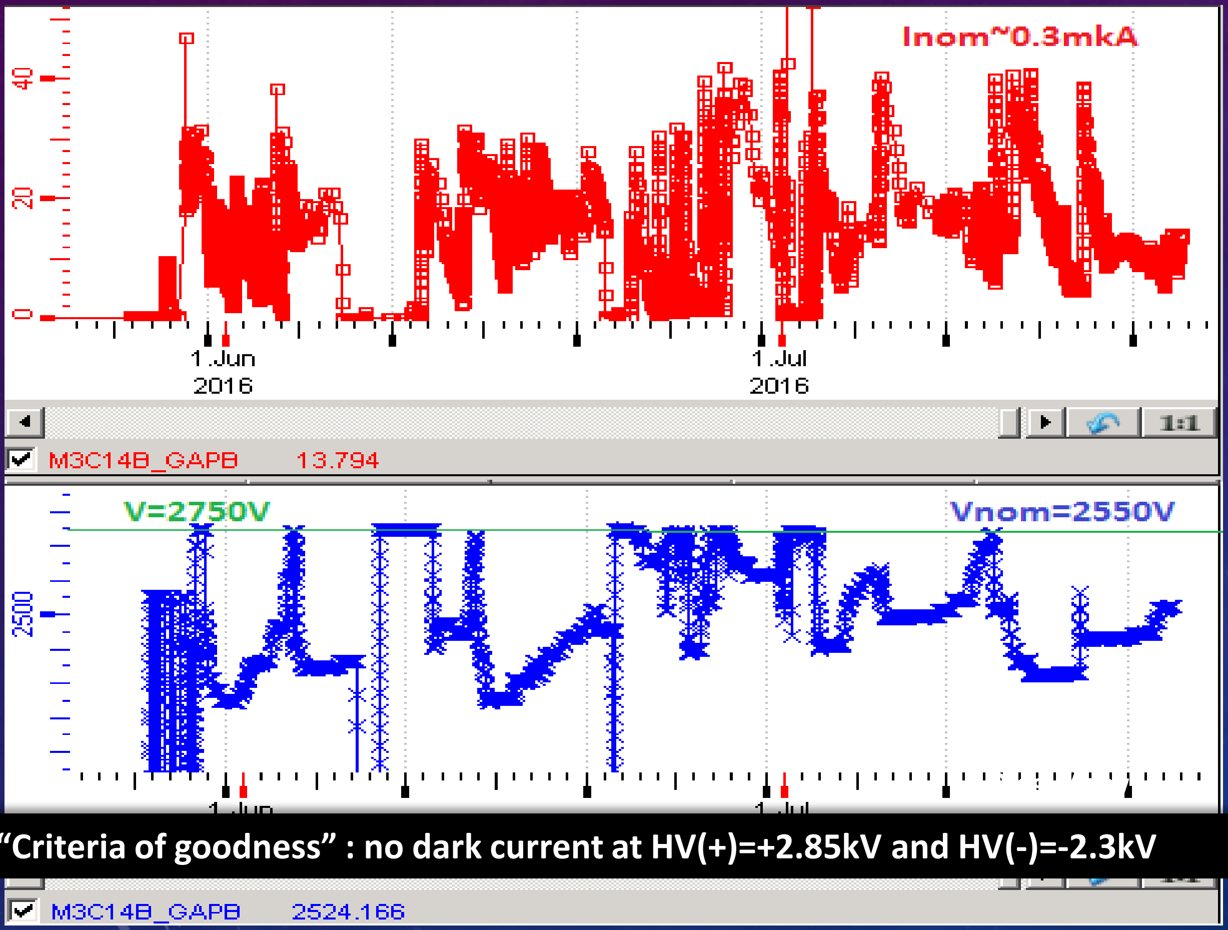

"Criteria of goodness" : no dark current at HV(+)=+2.85kV and HV(-)=-2.3kV

II. MCE curing procedure without beam is similar to the previous with beam, but includes the training with inversed high voltage as well.

During each long period for access (>4 days) the most problematic gaps had been treated with negative polarity.

- 47% gaps of MUON system passed in situ the training with HV(-).
- In addition, 5 regions, M1R2 and M2/3 R1/R2, passed through the conditioning with HV(-) on GIF before installation (336 gaps).
- *In total –2582 gaps (52.2%)*

CSC LHCb, Ar/CO2/CF_4 (40 : 55 : 5)

Malter currents MUON LHCb:
recovery with 2% O_2 adding

Reactions of oxygen impact dissociation and excitation significant for avalanche electron energy 1-15 eV:

$$e^- + O_2 \rightarrow O^- + O^{\bullet\bullet} \quad (1)$$

$$e^- + O_2 \rightarrow {}^*O_2 + e^- \quad (2)$$

O_2 molecules (1) happens at electron energies ~5 eV,
CO_2 electron impact dissociation starts only at ~13 eV.

The atomic oxygen, $O^{\bullet\bullet}$, and the excited molecular oxygen, $^*O_2$, are chemically aggressive.
Atomic oxygen $O^{\bullet\bullet}$ interacts with O_2 molecules forming ozone:

$$O^{\bullet\bullet} + O_2 \rightarrow O_3^* \quad (3).$$

Ground state ozone, O_3, can participate in the processes of plasma chemical etching on the cathode surface or recombines with free oxygen radicals:

$$O_3 + O^{\bullet\bullet} \rightarrow 2O_2 \quad (4).$$

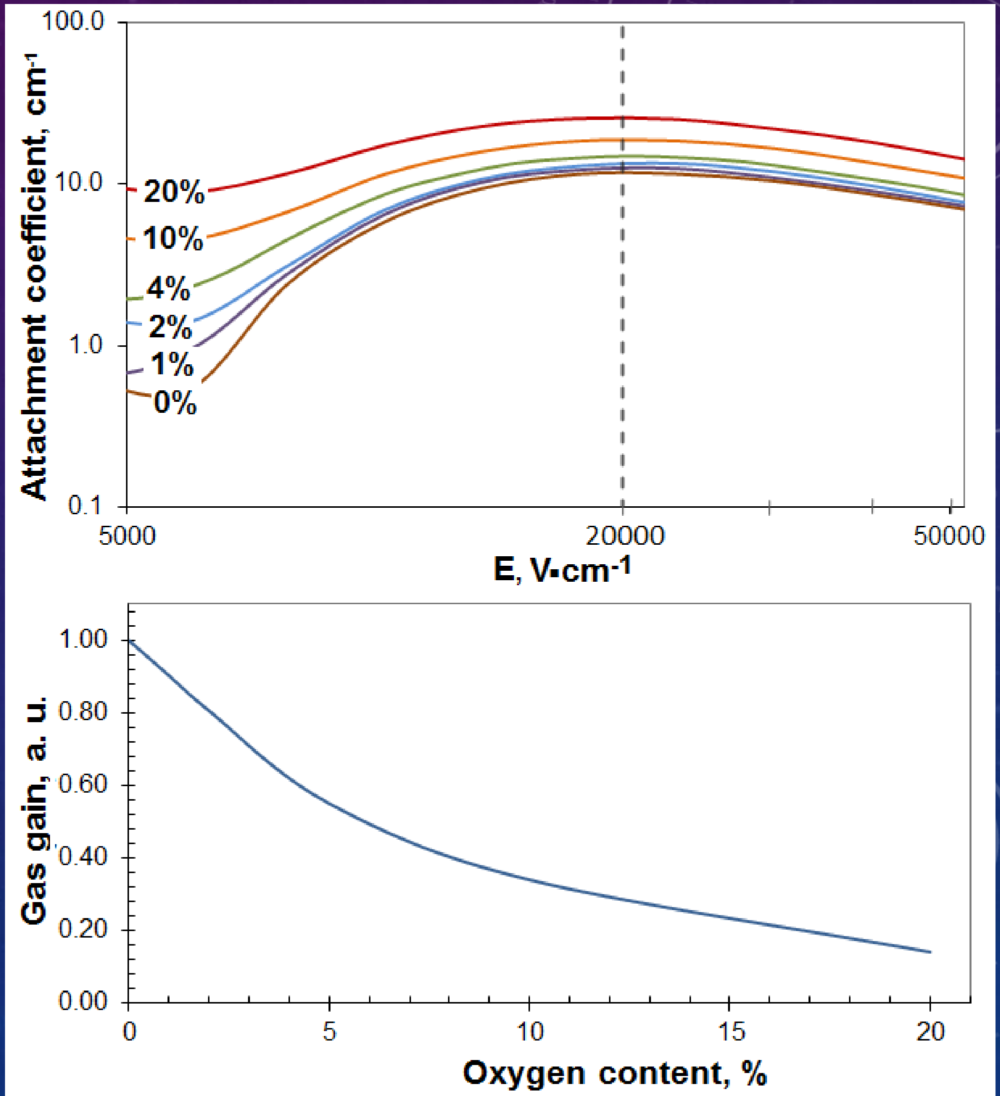

D.Maysuzenko, O. Maev, S. Nasybulin

Malter currents MUON LHCb:
recovery with 2% O_2 adding

III. MCE curing procedure is similar to the previous without beam, but in Ar/CO2/CF4 (40 : 55 : 5) 2% of Oxygen is added.

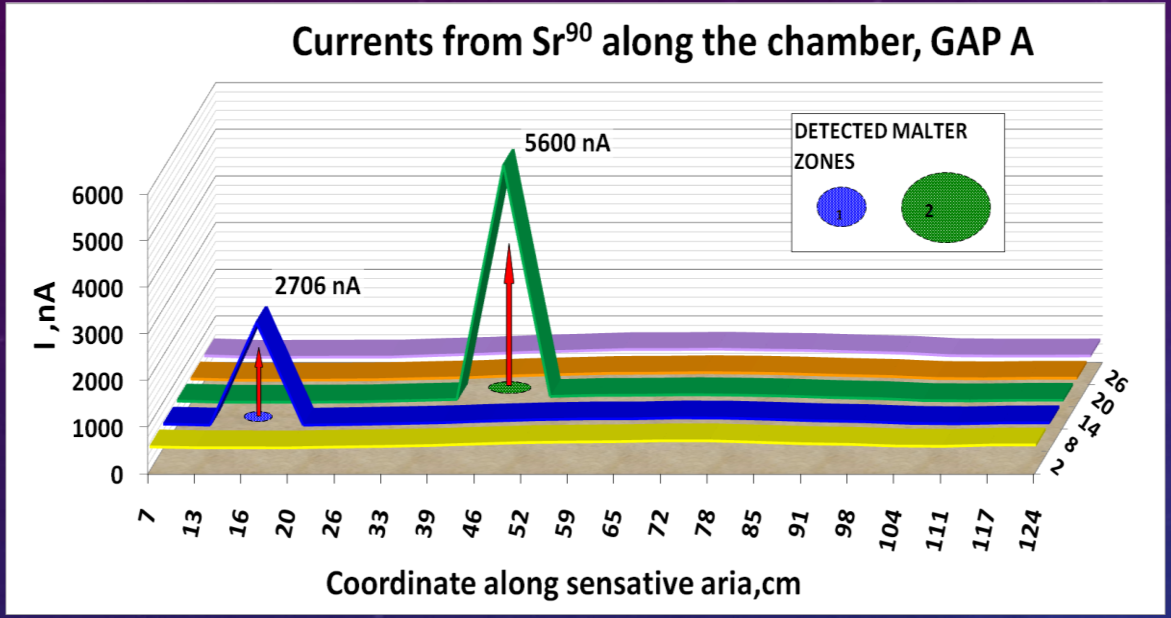

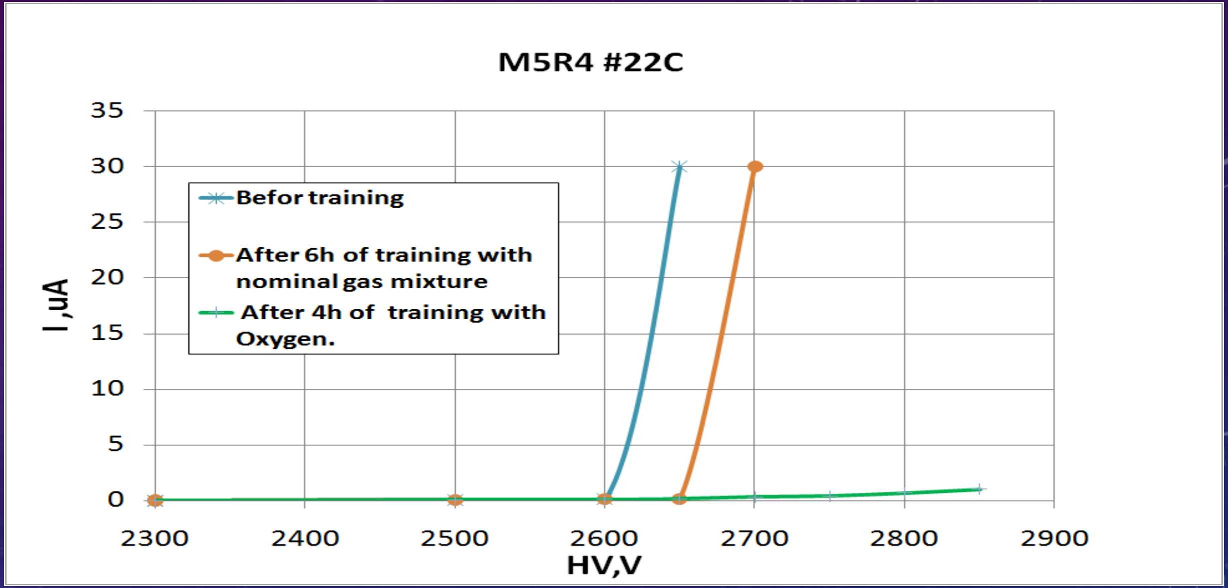

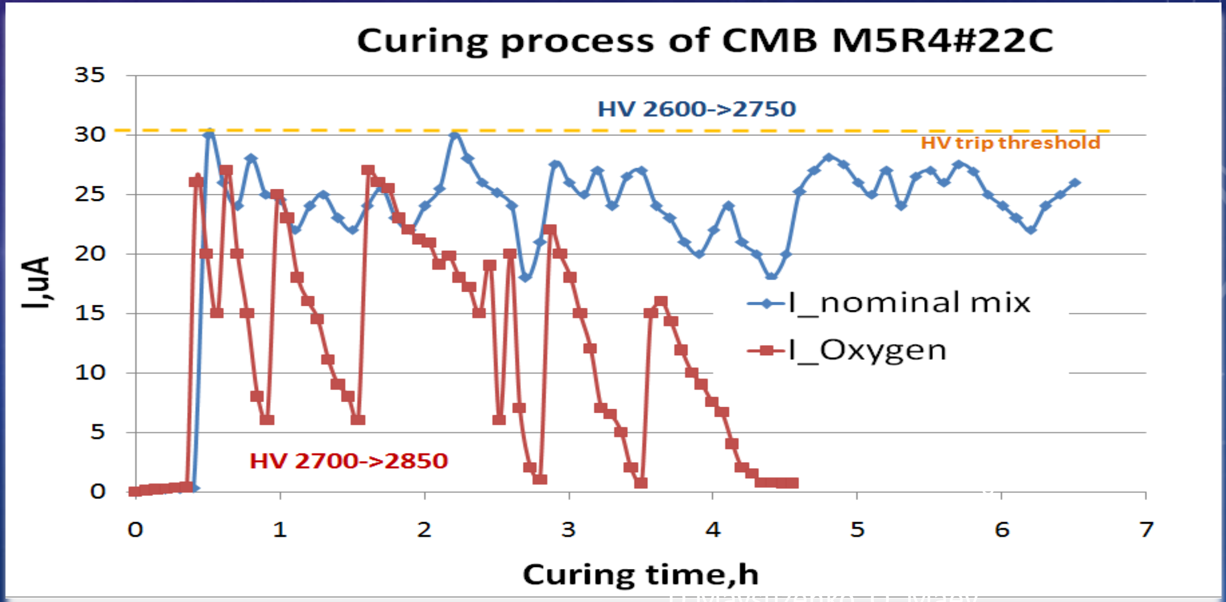

✓*Removal of organic polymeric material with oxygen containing plasma (H. Boeing, Plasma Sci.&Tech., page 281, (1987).*

✓ *Cleaning of mirrors contaminating films by a glow discharge in oxygen plasma. (R. Gillette et al., Vac. Sci. Tech., 7(1070)534)*

✓ *Recovery from the Malter effect deposits by Oxygen (A. M. Boyarski, Additives That Prevent Or Reverse Cathode Aging in Drift Chambers With Helium-Isobutane Gas, Nucl. Inst. And Meth. A515, 190-195(2003).*

✓ *M. Blom, I. Mous, and N. Tuning, Effects of adding oxygen to the outer tracker gas mixture," LHCb, vol. 064, 2008*

Malter currents: CSC CMS

Summary:

- **The number of the MCE touched chambers may increase at HL-LHC.**
- **We need an early diagnostic based on HV monitoring system.**
- **From LHCb CSCs experience follows that recovery techniques for CMS CSC's have to be developed.**
- **Laboratory tests with small scale prototypes are actual for this purpose.**

CSC's aging study history

MCE historical summary at CSCs of CMS and LHCb:

CSC CMS, $Ar/CO2/CF_4$ (40 : 50 : 10)

- 1998 – Local aging test of first CSC prototype (^{90}Sr - Q~12 C/cm, 75 Volume/day+ Q~2 C/cm 1 Volume/day);
- 1999 - Aging test of 1m prototype on GIF (^{137}Cs – Q=0.218 C/cm, 1 Volume/day);
- 2000-2001 - Aging test **of full-scale** CSC chamber on GIF (^{137}Cs – Q=0.35 C/cm, 1 Volume/day);
- 2010 – **First signs of MCE** in the **full-scale** ME1/1 (V.Perelygin DOC Report 25.04.2012).
- From 2016 – Ongoing aging test of **full-scale** CSC chamber on GIF++ (^{137}Cs -Q~0.1 C/cm, 1 Volume/day);
- 2016 - Local benchmark aging test of CSC prototype (^{90}Sr - Q~1.36 C/cm, 3.5 Volume/day).
- 15.09.2018 - Local benchmark aging test of CSC prototype (^{90}Sr - Q~ 356 mC/cm, 3.5 Volume/day).

CSC LHCb, $Ar/CO2/CF_4$ (40 : 55 : 5)

- 1998 – 2000, M1R2 and M2/3 R1/R2 - 5 regions, passed through the conditioning with HV(-) on GIF before installation (336 gaps). In total –2582 gaps (**52.2%**);
- **2010 - 2018 Ongoing training procedures for recovering from Malter current.**

Oleg Maev, LHCb General meeting, 12 September 2016

TARGETING AGING TEST IN PNPI

- Local aging tests under ^{90}Sr irradiation are performed with compact CSC prototype modules fed by standard CSC gas mixture and modified gas mixture 36.6%Ar+61.75%CO_2+1.65%CF_4;
- Accumulated charge 1.36 C/cm is obtained with standard gas mixture and 0.39 C/cm with modified. The absence of amplitudes degradation matches with the previous tests;
- Despite of the strong oxidation and presence of Si on cathodes surface, no MCE manifestation have been detected

Note

The CSC's of the CSC muon tracker in CMS mainly are under irradiation by the muons, neutrons (1 MeV) and electrons (1-10 MeV).

There is no facility for laboratory aging tests providing the study of the effect of more than one radiation source.

The solution consists in study a separate aging effects from singular radiation source. ^{90}Sr β-source with maximum E_β = 2.28 MeV is capable provide both classical aging due to plasma chemistry processes and radiation damage of the cooper foil surface.

CSC prototype for longevity tests in PNPI

- 2 planes, each with 7 controlled anode wires;
- 50 μm gold-coated anode wire;
- 285 x 270 mm² sensitive area, 693 cm³ gas volume;
- S = 3 mm ;
- L = 4.5 mm ;
- Identical geometry and construction materials to CSC ;
- Gas flow during aging test was 2.5 sccm

that is ~ 4 volumes per day ;

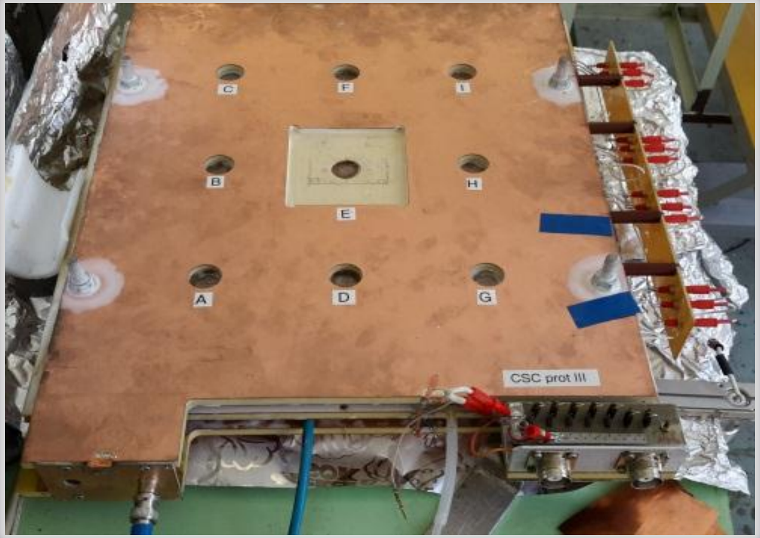

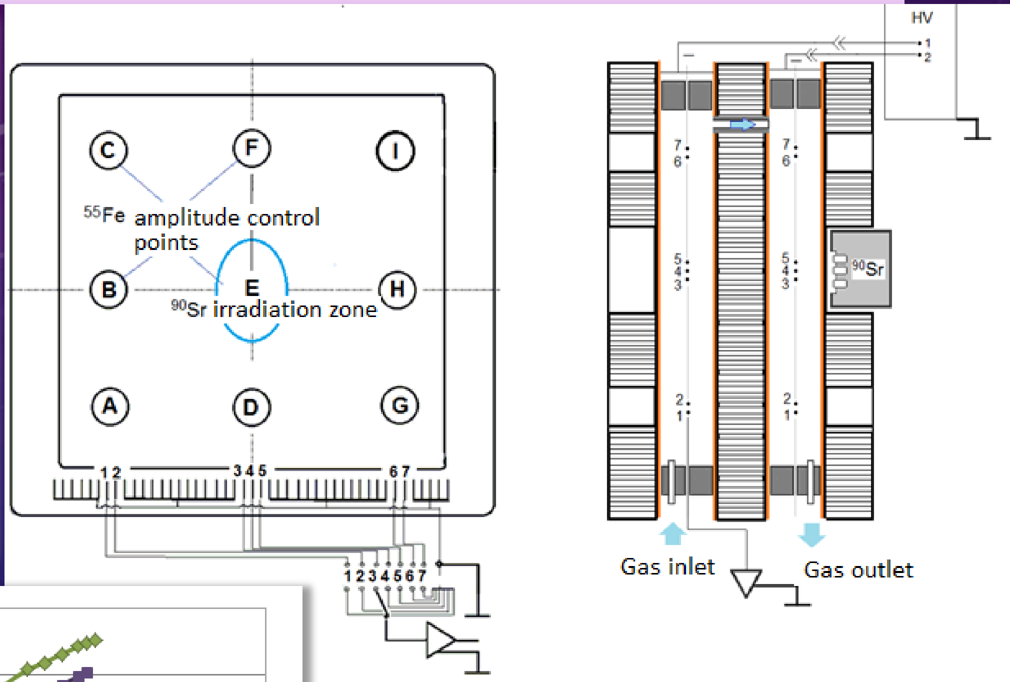

BUT

- Readout from anode wires;
- No gas mixture recirculation;
- HV applied to the cathode.

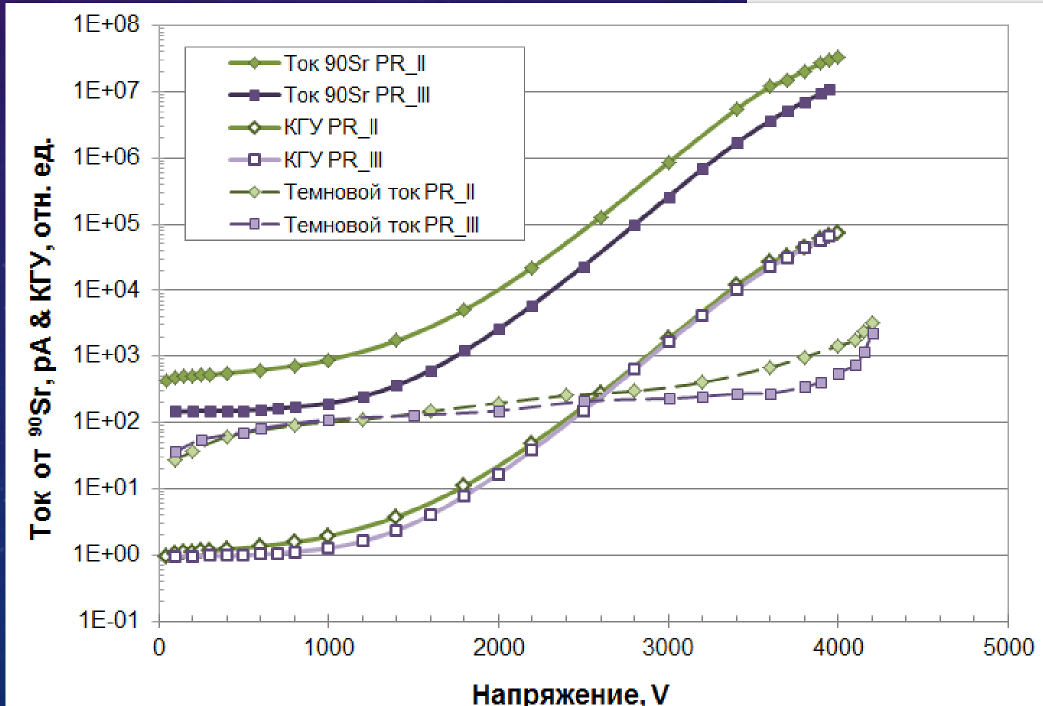

Gas gain 5×10^4
HV = 3750 V

Disassembled detector after accumulation of Q=1.36 C/cm with $40\%Ar+50\%CO_2+10\%CF_4$

Q= 0.0 C/cm

Dark current vs Acc. Charge

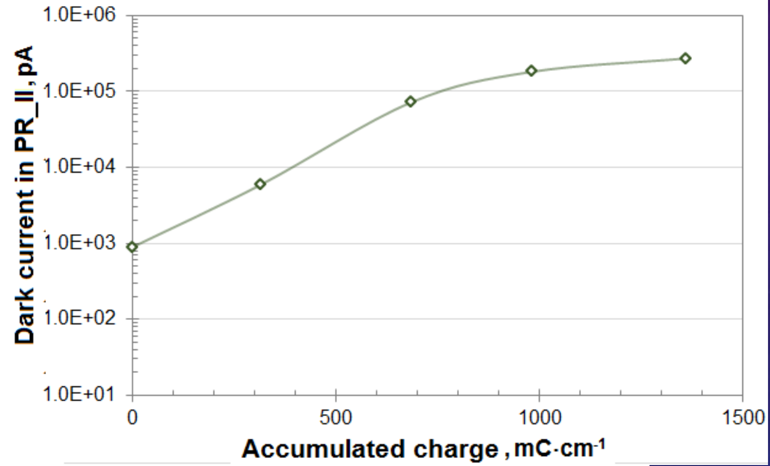

D. Acosta et al. / Nuclear Instruments and Methods in Physics Research A 494 (2002) 504–508

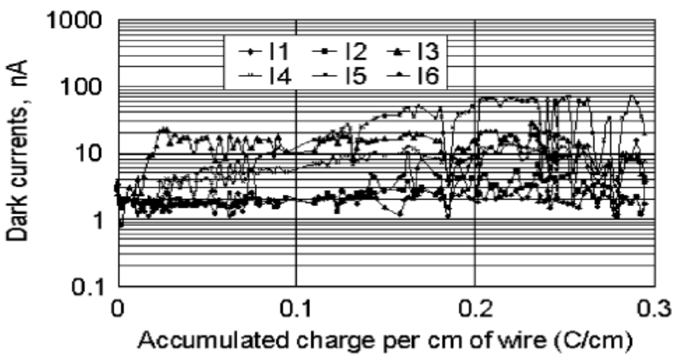

Fig. 4. Increase in dark current over 0.3 C/cm accumulated charge.

Gas gain vs Acc. Charge

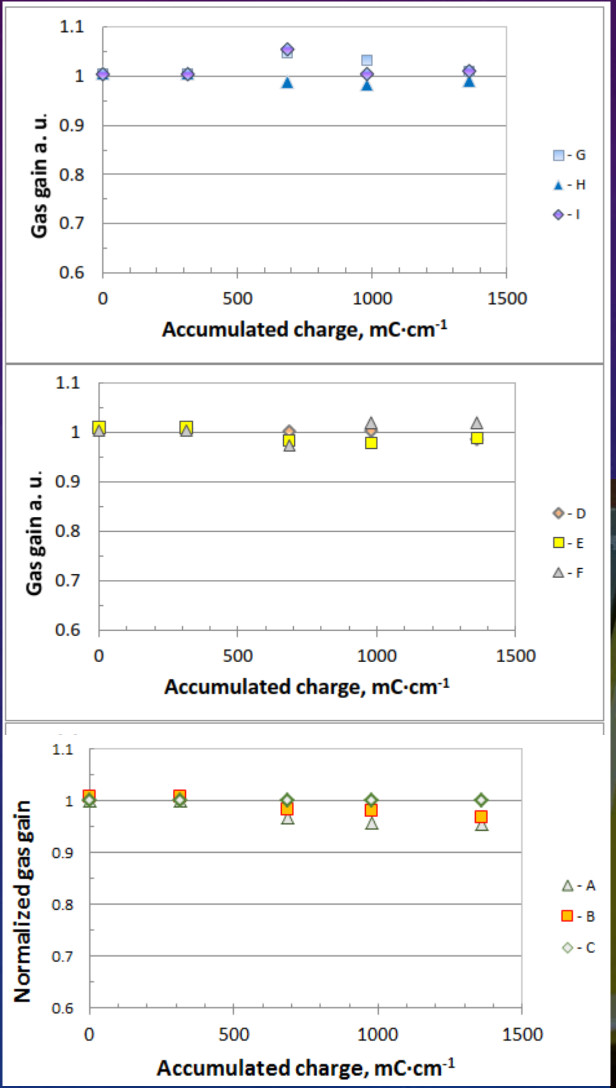

Q=1.36 C/cm

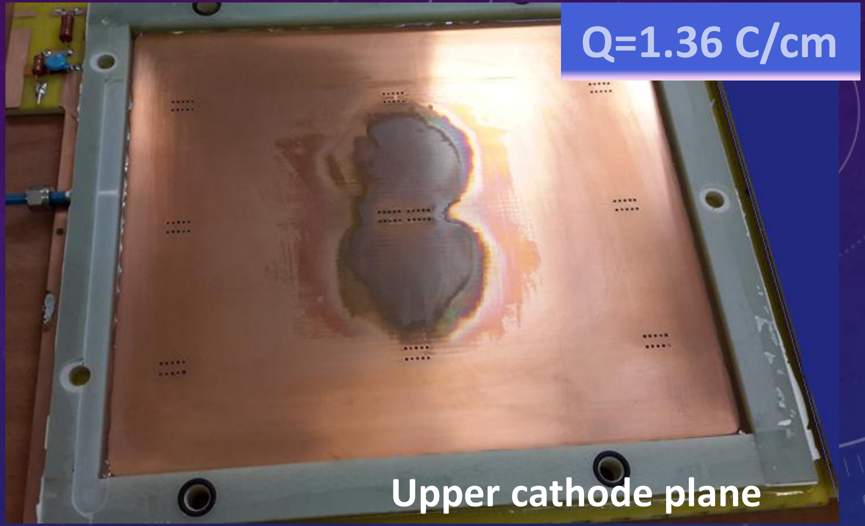

Upper cathode plane

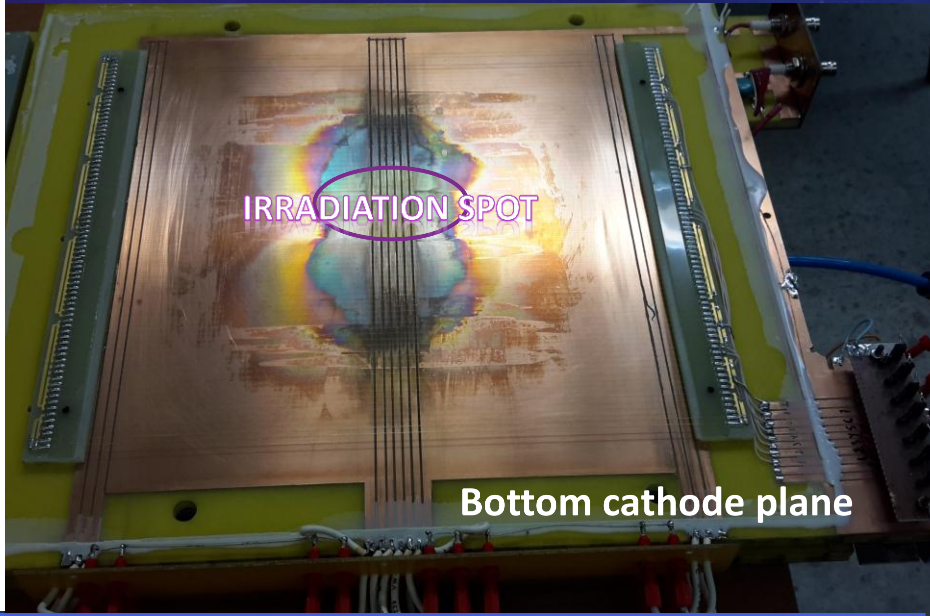

Bottom cathode plane

Damaged (toughed by oxidation) zone
is 10 times bigger of irradiated spot (~6 cm2)

Disassembled detector after accumulation of Q= 0.39 C/cm aged with $36.6\%Ar+61.75\%CO_2+1.65\%CF_4$

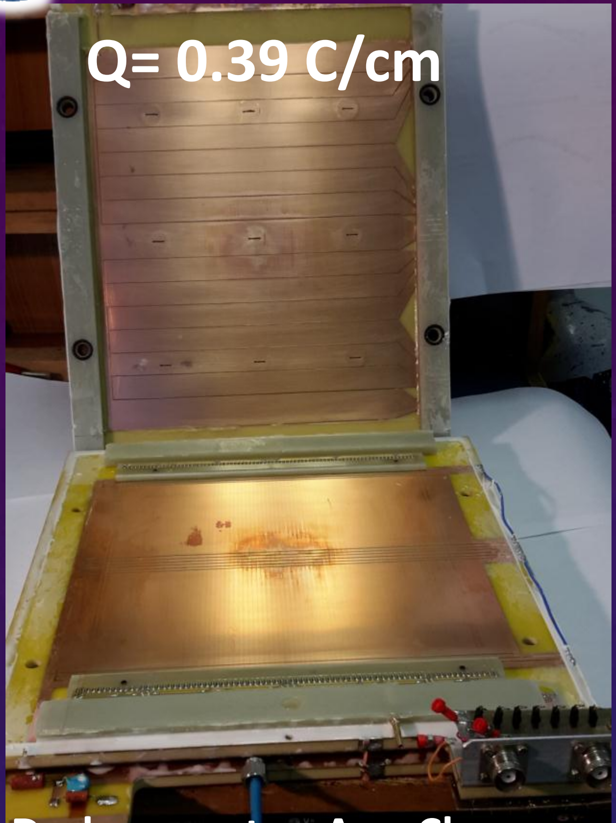

Dark current vs Acc. Charge

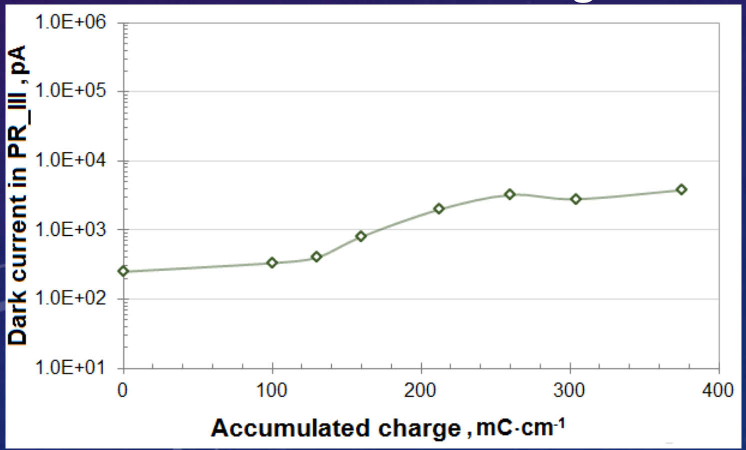

Gas gain vs Acc. Charge

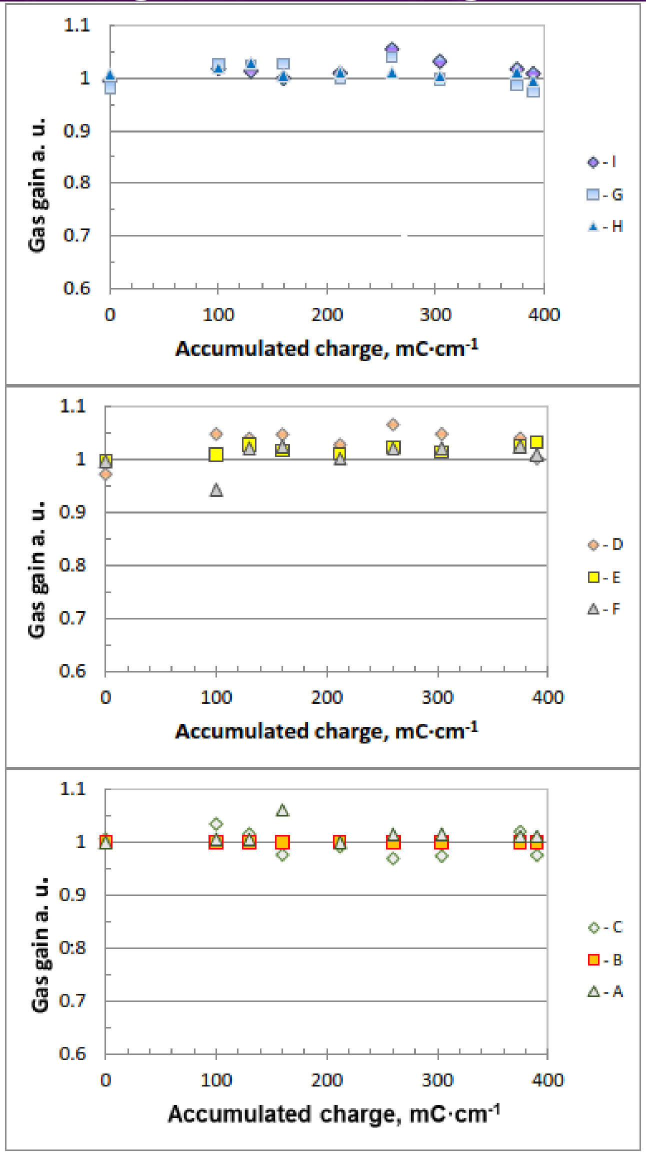

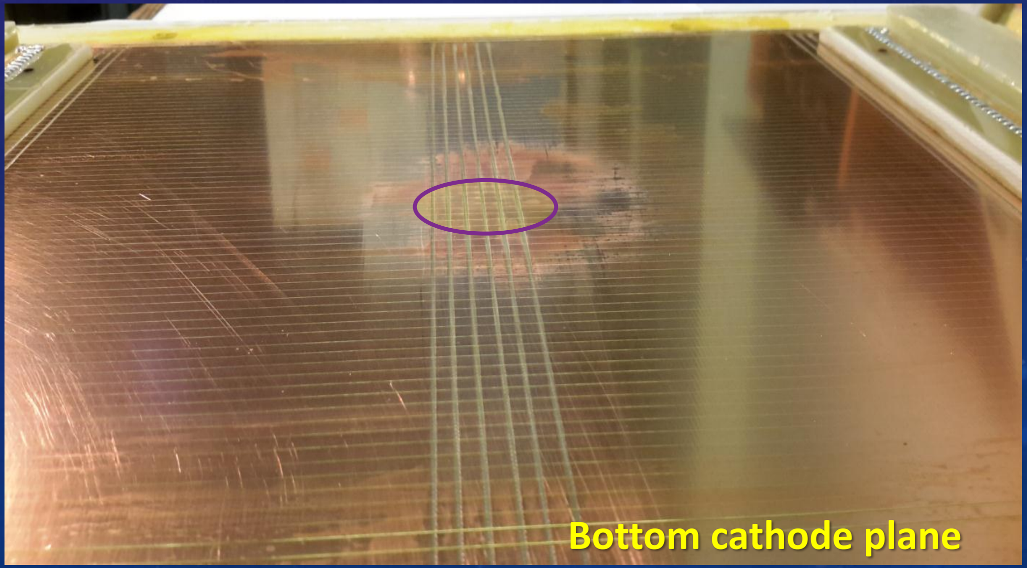

MALTER CURRENT IGNITION TEST

Scan with ^{90}Sr over the whole CSC prototype area

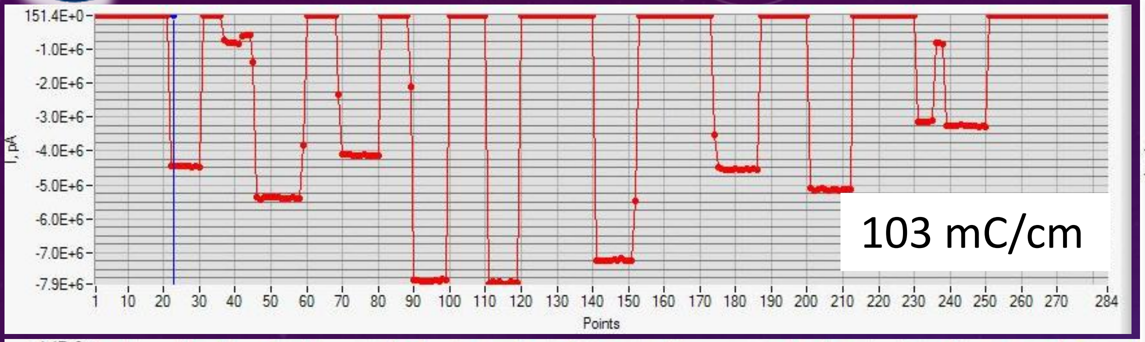

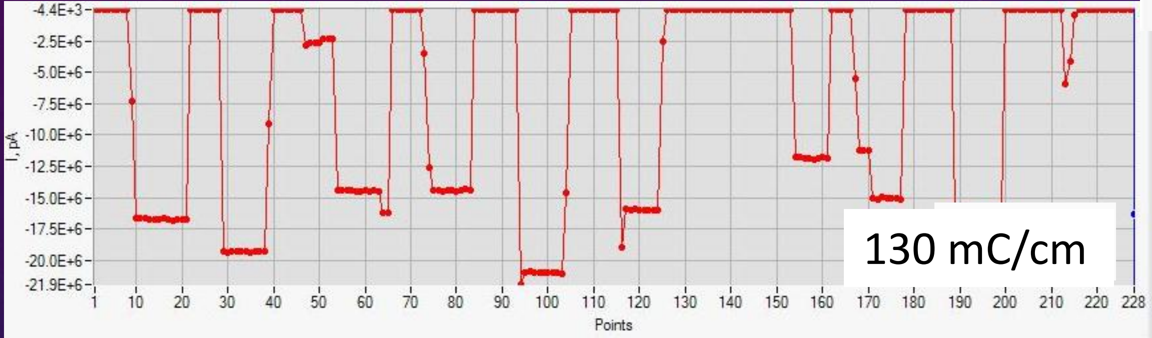

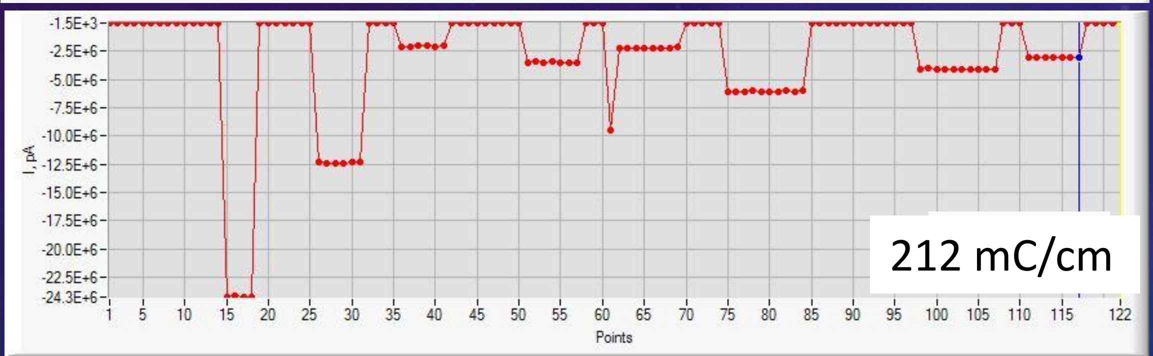

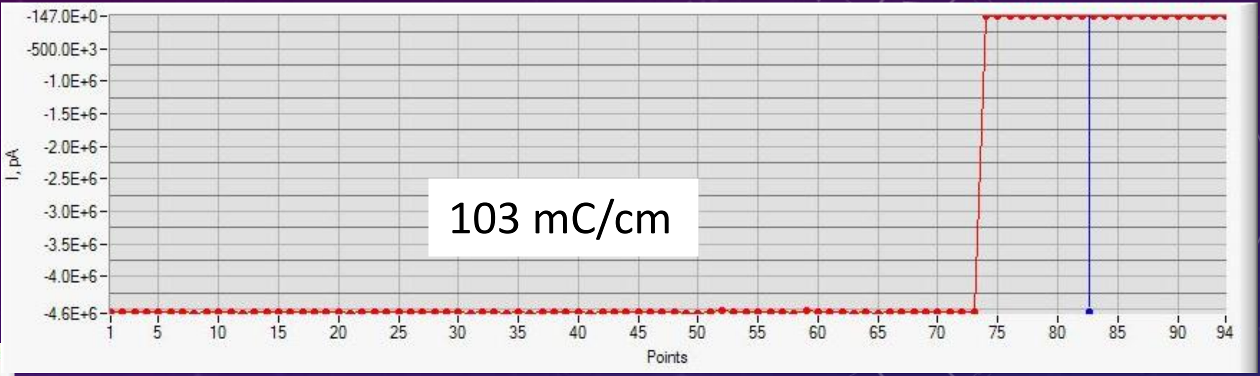

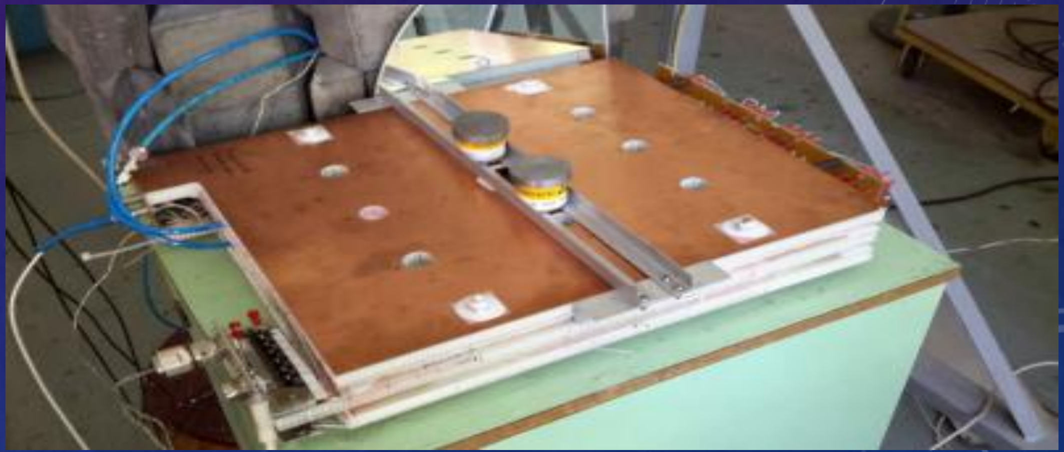

“SLOW” AGING TEST – SEARCH FOR MALTER

- ❑ CSC prototype local aging test under ^{90}Sr irradiation with $40\%Ar+50\%CO_2+10\%CF_4$ working gas mixture is in progress
- ❑ Ionization current in the two per ~6 cm^2 irradiated zones is 1.1 μA that provides charge accumulation rate ~ 4 mC/cm per day
- ❑ An accumulated charge per 1 cm of wire length in the prototype module is Q = 356 mC/cm
- ❑ No signs of Malter effect have been obtained

^{90}Sr scan currents at HV=3950 V

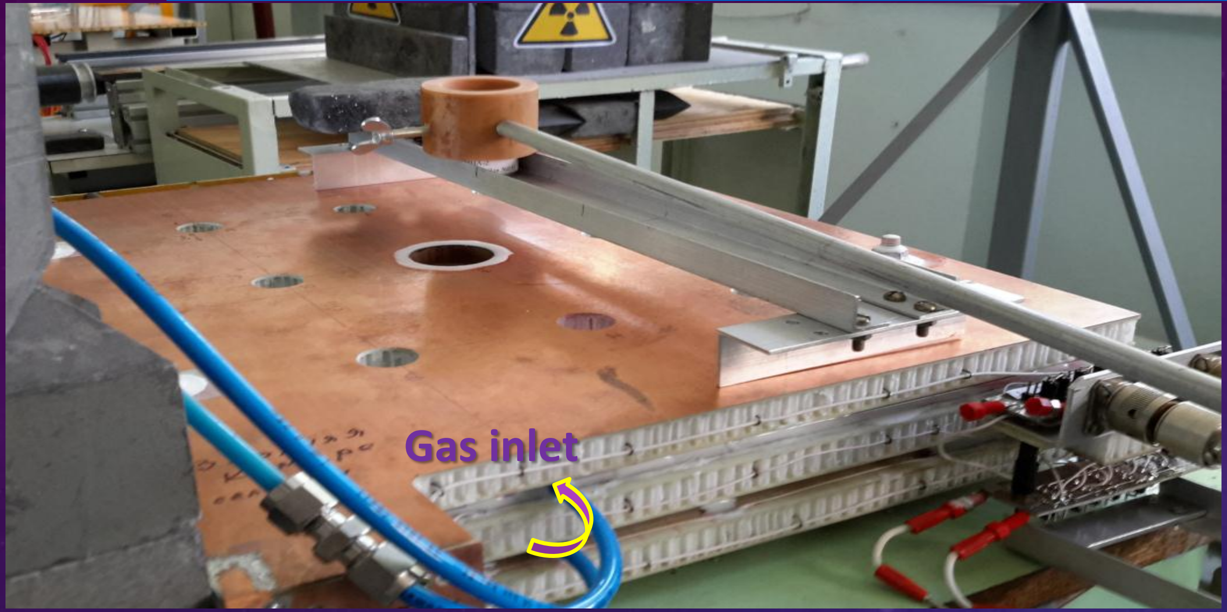

Scan for ME with ^{90}Sr at ~3 cm height from prototype surface

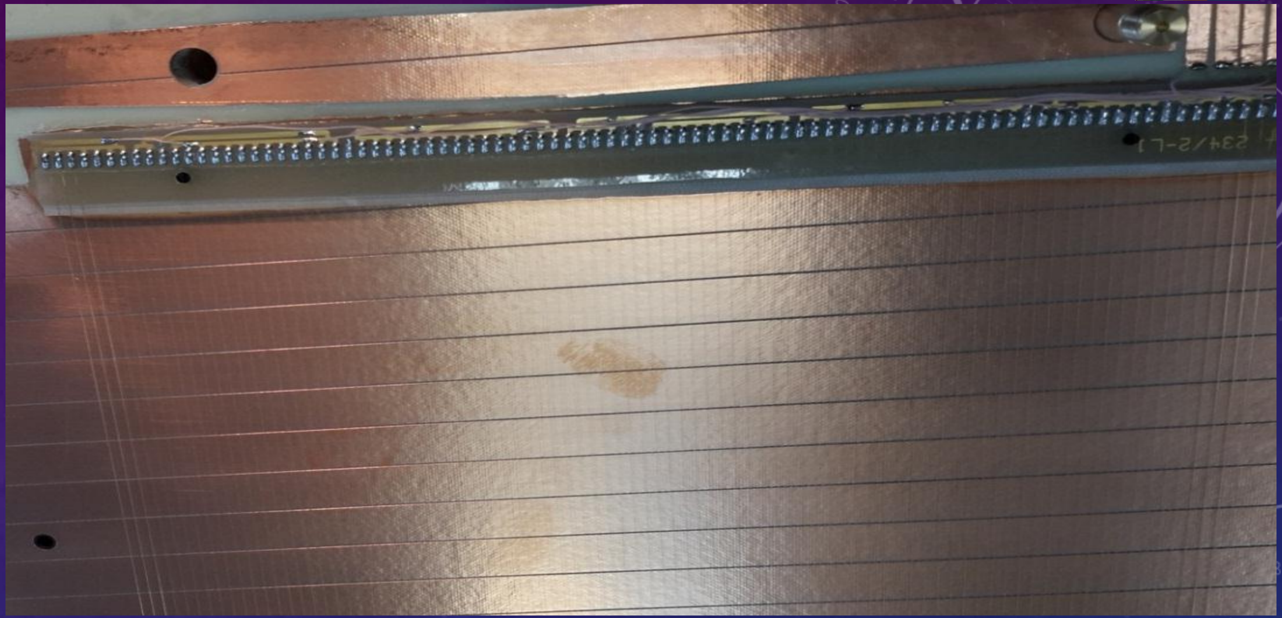

Fingerprints between B and E control points

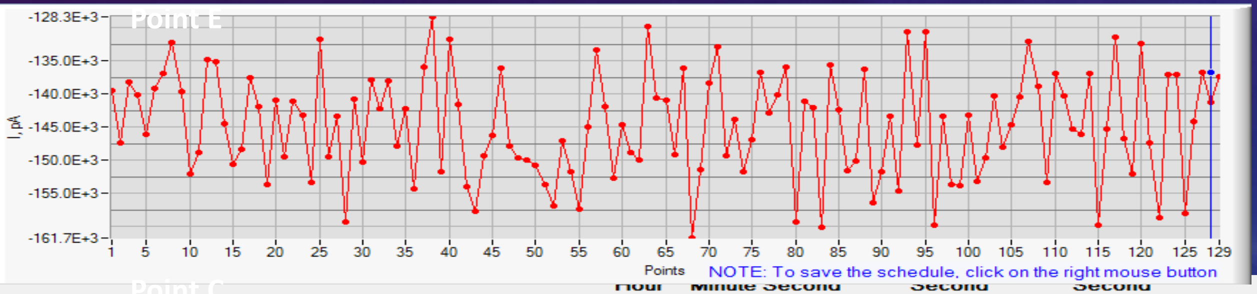

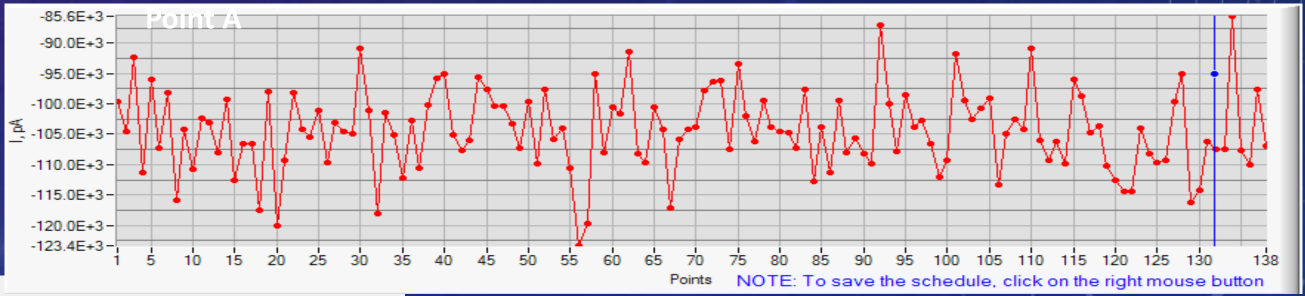

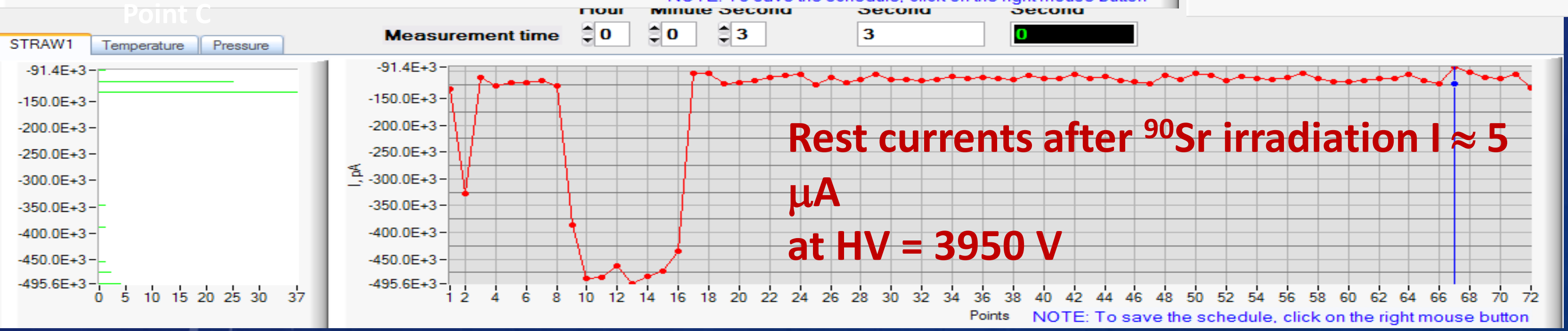

Rest currents after ^{90}Sr irradiation I ≈ 5 μA at HV = 3950 V

Q = 103 mC/cm

^{55}Fe amplitudes measurements in the control points

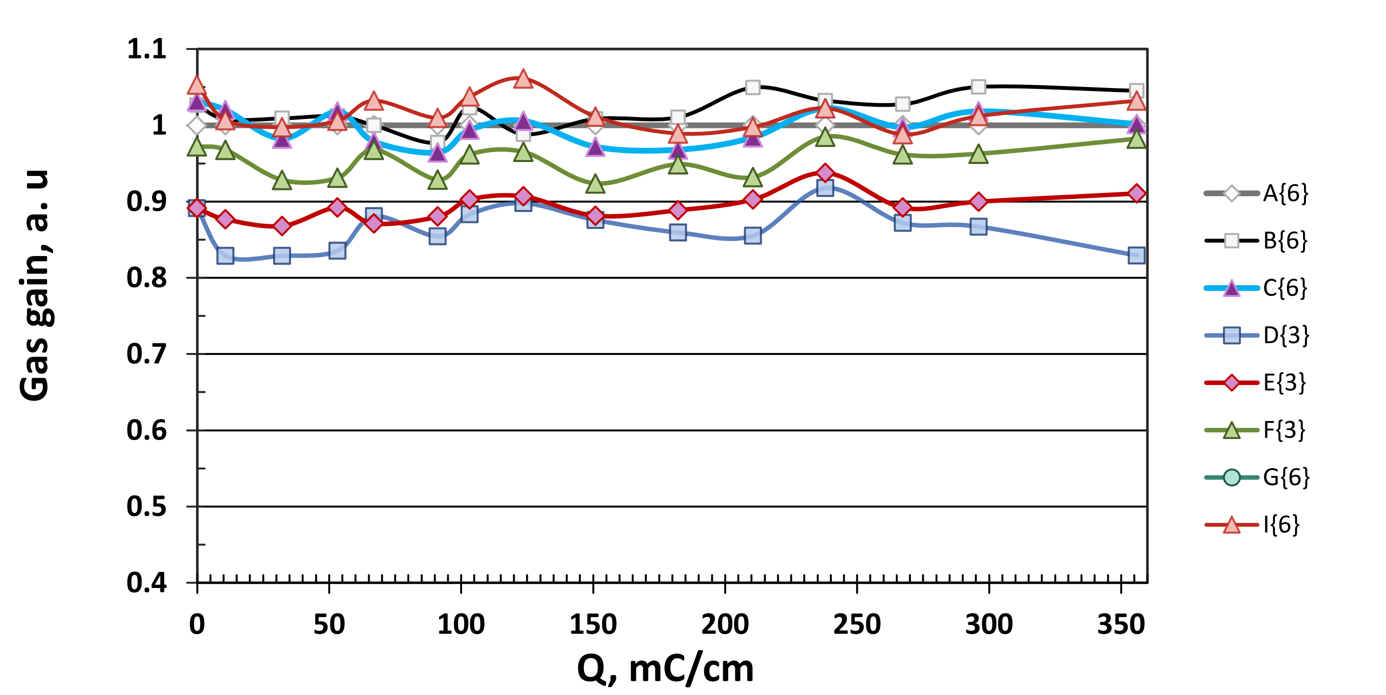

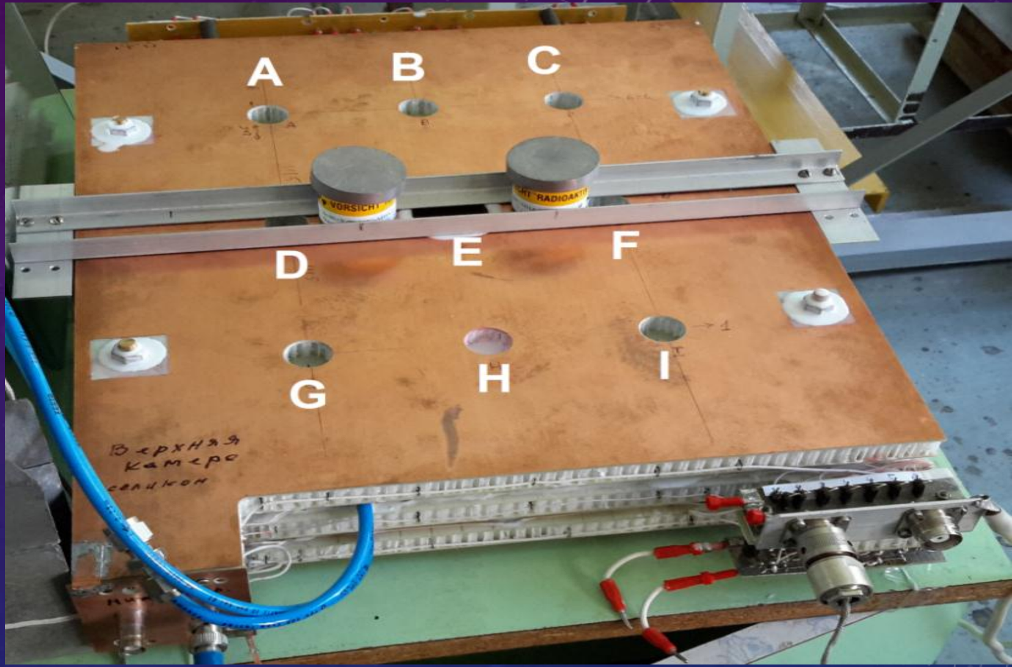

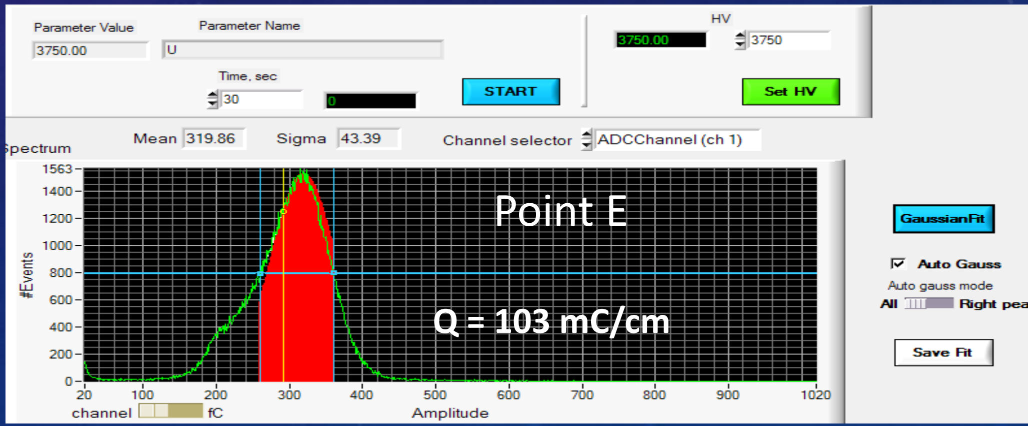

Monitoring parameters:

- ^{90}Sr irradiation current, correspondent pressure and temperature
- ^{55}Fe amplitudes in the control points A ….I
- ^{55}Fe count rated in the control points
- Dark currents per plane and monitored wires
- ^{90}Sr scan per plane and control points looking for ME

DARK CURRENTS

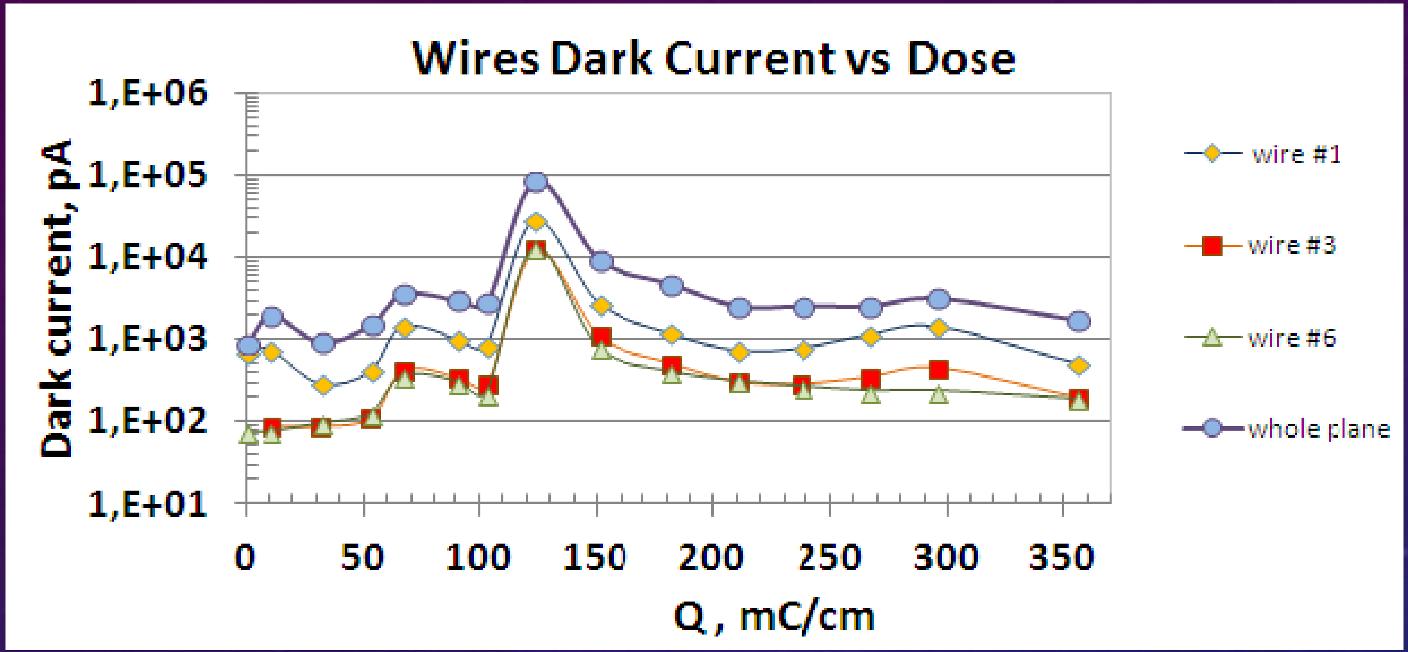

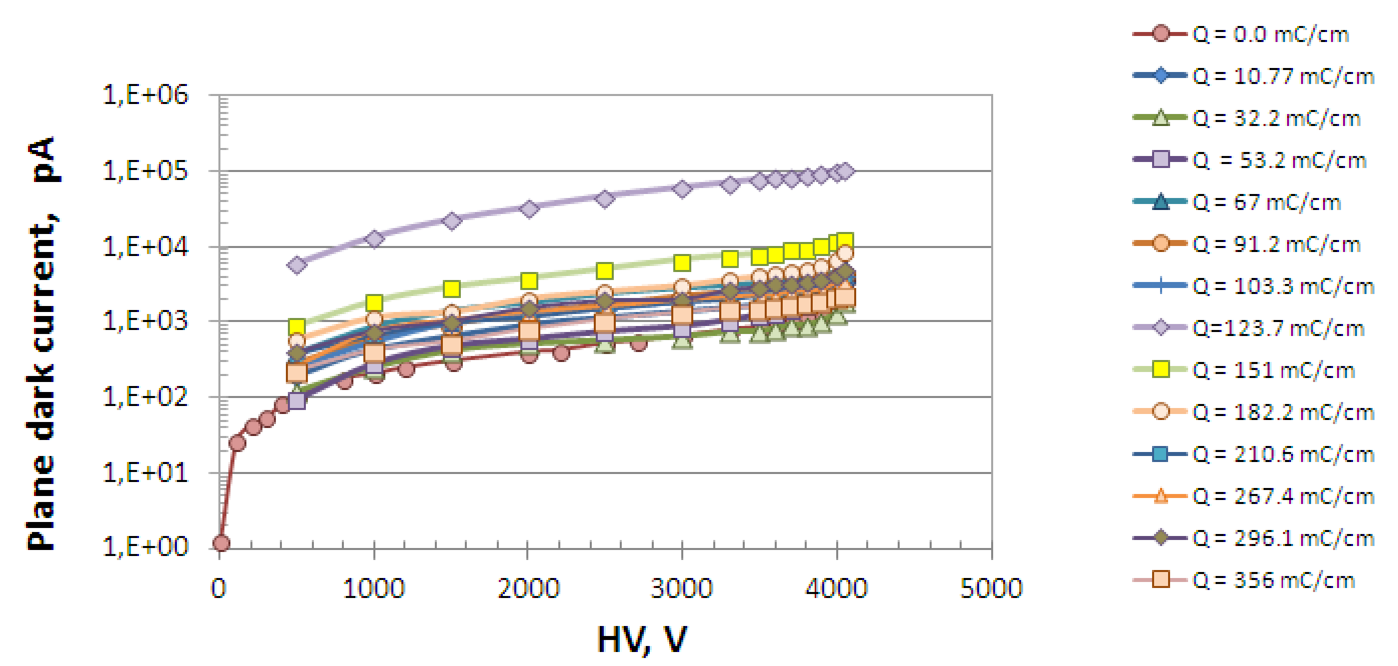

Study of Malter effect provoking mechanism

To remind: $CF_3^\bullet$, $F^\bullet$, $O^\bullet$ are produced in avalanche at 3 – 6 eV

$e^- + CF_4 \rightarrow CF_3^\bullet + F^\bullet + e^-$;	(1)
$e^- + CF_4 \rightarrow CF_3^\bullet + F^-$;	(2)
$e^- + CF_4 \rightarrow CF_2^\bullet + 2F^\bullet + e^-$;	(3)
$e^- + CO_2 \rightarrow CO^\bullet + O^\bullet + e^-$;	(4)
$e^- + CO_2 \rightarrow CO^\bullet + O^-$;	(5)
$e^- + CO_2 \rightarrow CO^- + O^\bullet$.	(6)

$4F^\bullet + Si \rightarrow SiF_4\uparrow$;
$4F^\bullet + SiO_2 \rightarrow SiF_4\uparrow + O_2\uparrow$;
$Si + CF_3^\bullet + F^\bullet + 2O \rightarrow SiF_4\uparrow + CO_2\uparrow$.

$O^\bullet + CF_3^\bullet \rightarrow COF_2^\bullet + F^\bullet$;	(7)
$O^\bullet + CF_2^\bullet \rightarrow COF^\bullet + F^\bullet$;	(8)
$e^- + COF_2 \rightarrow COF^\bullet + F^\bullet + e^-$;	(9)
$O^\bullet + COF^\bullet \rightarrow CO_2\uparrow + F^\bullet$.	(10)

Presence of $O^\bullet$ stimulates additional generation of $F^\bullet$ which provides etching of Si and other organics

To provide an effective cleaning from silicon and organic deposits a high current about of 20-40 μA is needed

Etching rate can be accelerated with adding O2 in the gas mixture.

MAP OF THE SAMPLES FOR ANALYSIS

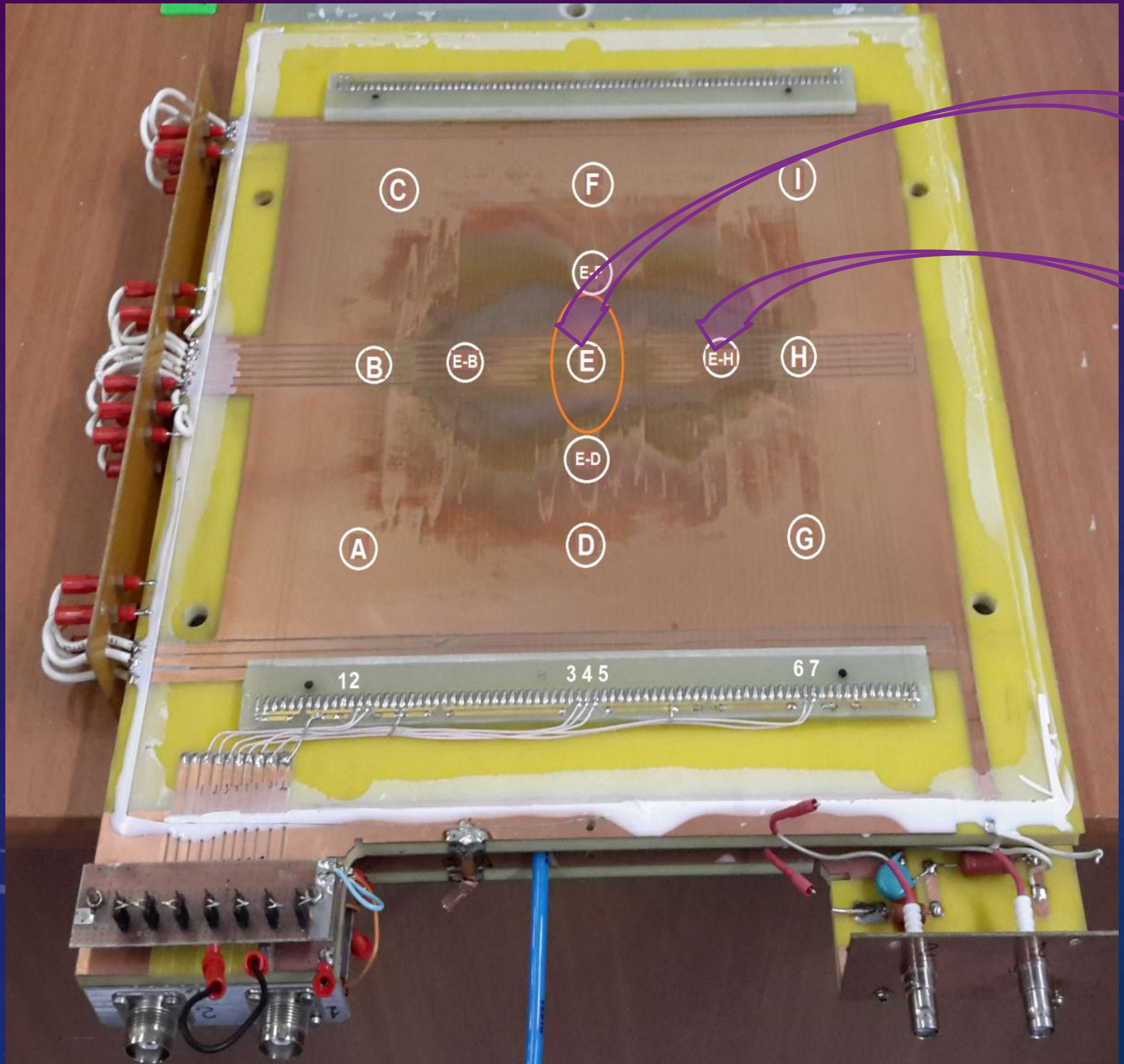

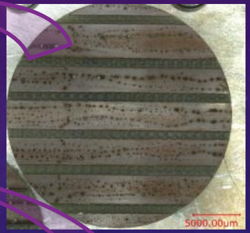

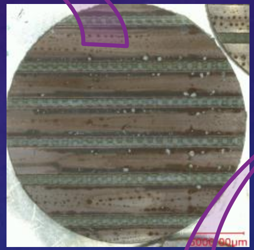

Top

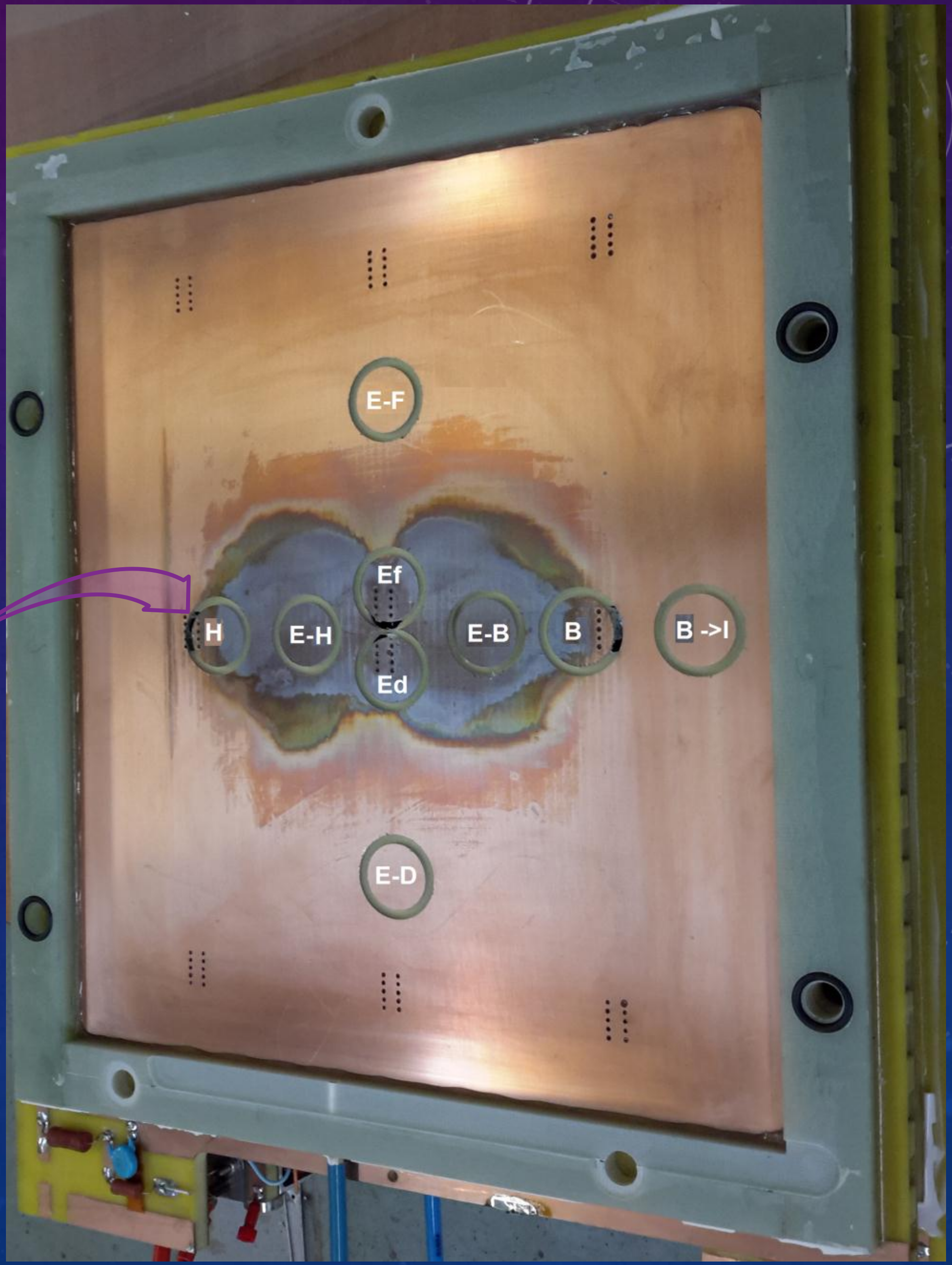

DETAILED SEM/EDS OF AGED CATHODE SURFACE OF CSC PROTOTYPE IN PNPI

- Small (<0.1cm[2]) samples from E and B-I (most irradiated and “reference”)
- Zeiss XB540 FIB/SEM with Oxford Instruments X-Max Silicon Drift Detector
- Use of FIB=”Focused Ion Beam” for milling a x-section

Optical microscope

PR II

Sample E - surface

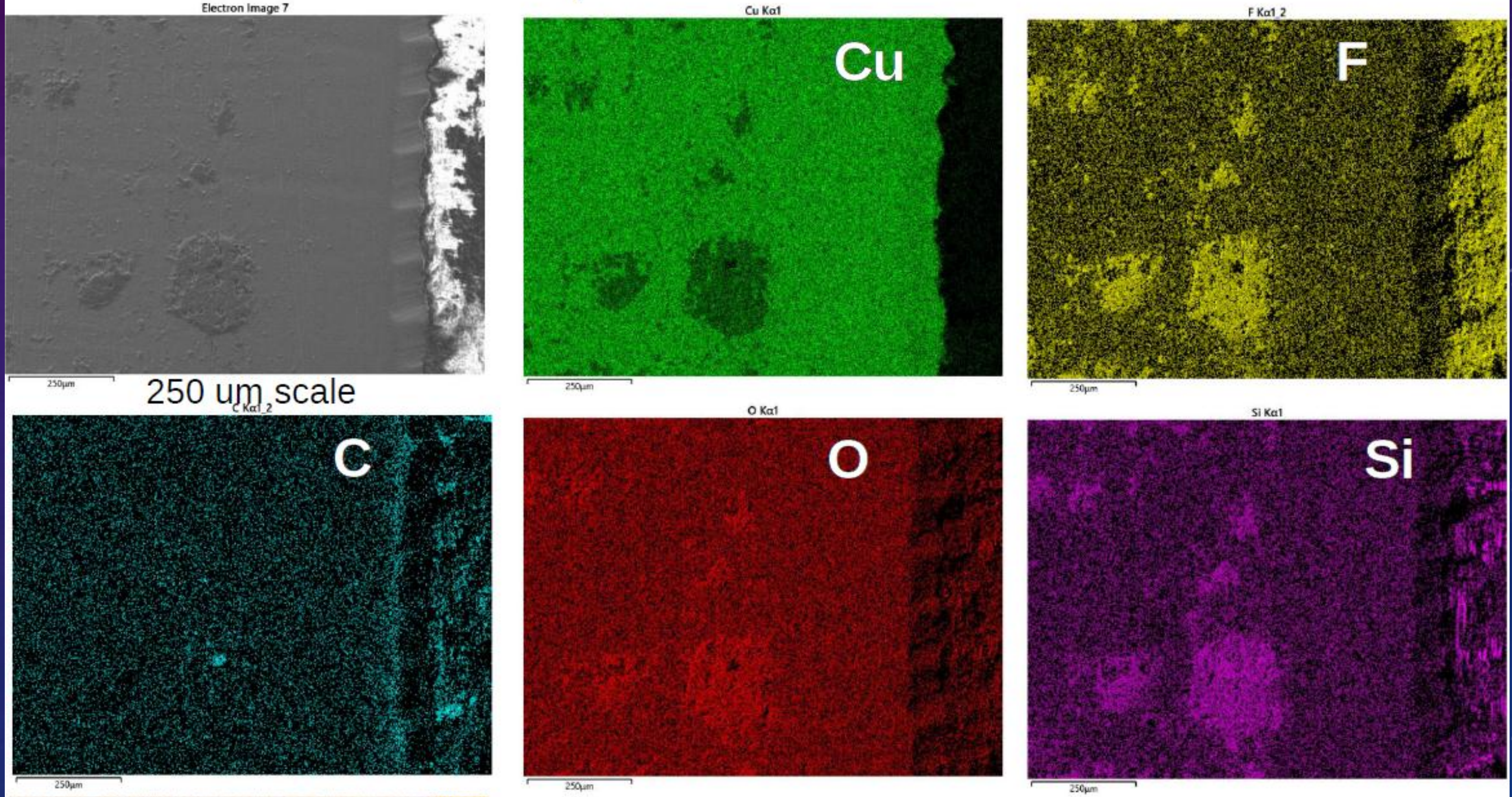

- The spots are formed from Si, F and O
- F is also presented inside the groove
- C?… only one place

PR II DETAILED SEM/EDS OF CATHODE SURFACE OF AGED CSC PROTOTYPE IN

CATHODE SAMPLES:
E – CENTER OF THE IRRADIATED ZONE (4 GY)

CSC accumulated dose: Q = 1.36 C/cm
Cooper foil accumulated dose: ~4 Gy/cm^2

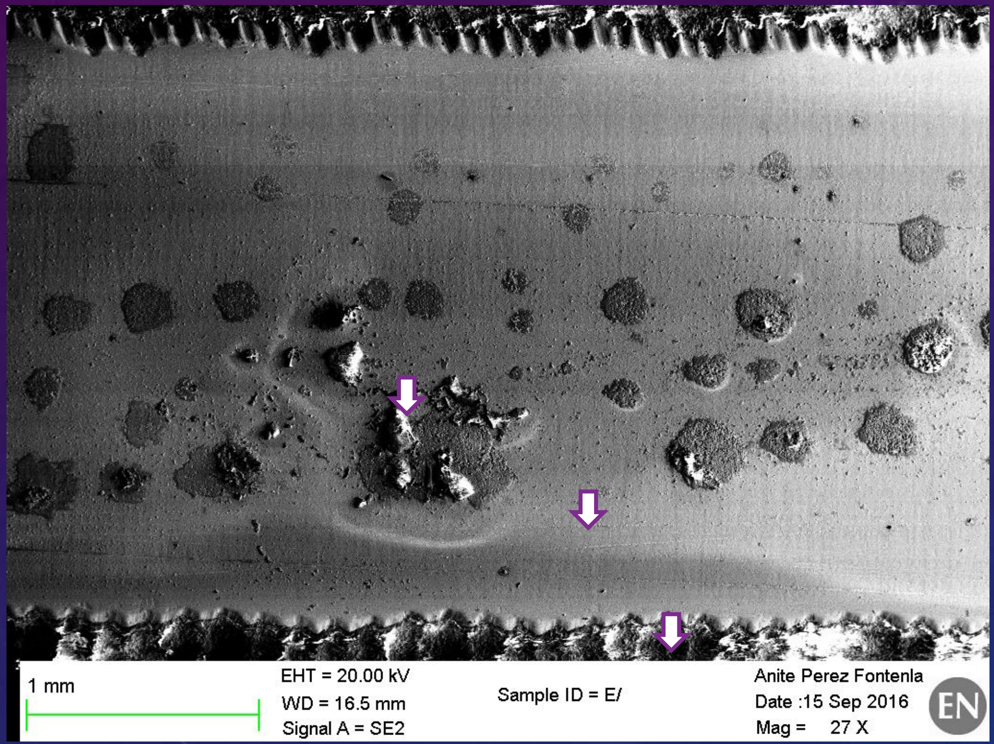

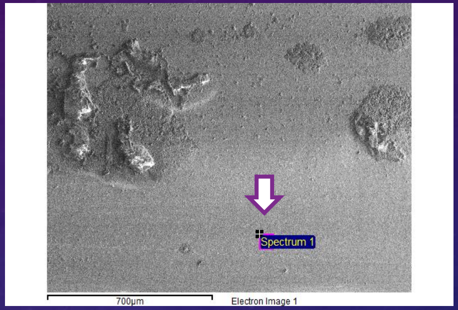

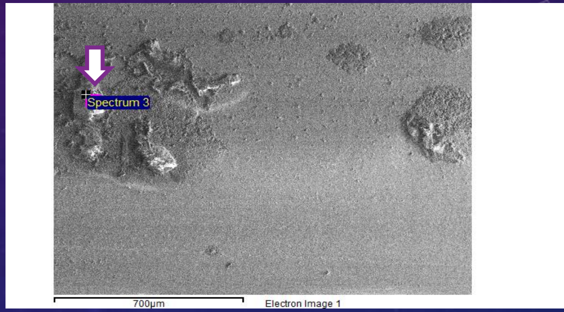

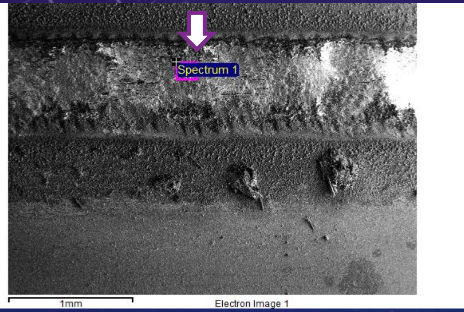

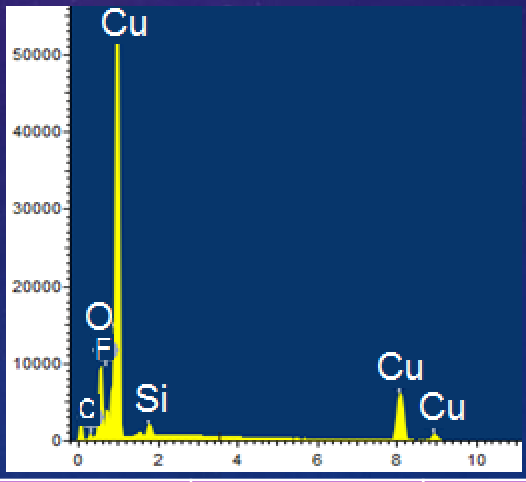

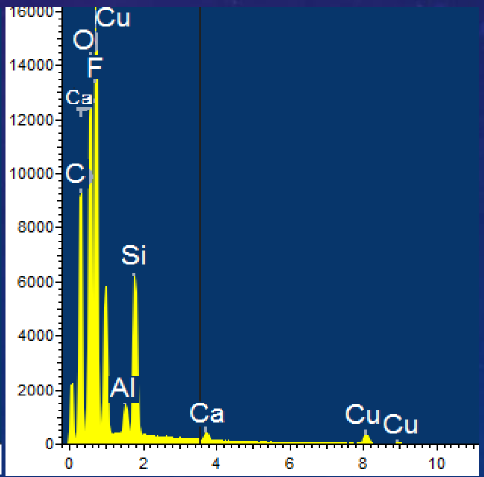

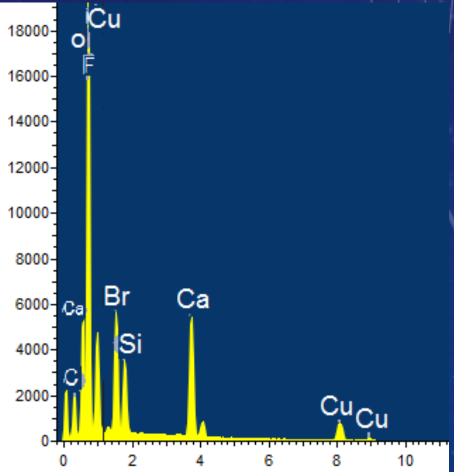

Element	Cu (wt%)	O (wt%)	C (wt%)	F (wt%)	Si (wt%)	Ca (wt%)
Sample B-I	84.5 ± 0.1	3.0 ± 0.0	12.3 ± 0.1	0.0	0.3 ±0.0	0.0
Sample E	73.4 ± 0.1	11.5 ± 0.0	8.0 ± 0.1	4.6 ± 0.1	1.8 ± 0.0	0.7 ± 0.0

DETAILED SEM/EDS OF CATHODE SURFACE OF AGED CSC PROTOTYPE IN PNPI

PR II

CATHODE SAMPLES:
H – APART FROM THE IRRADIATED ZONE

CSC accumulated dose: Q = 1.36 C/cm
Cooper foil accumulated dose: ~4 $\times 10^{-3}$ Gy/cm^2

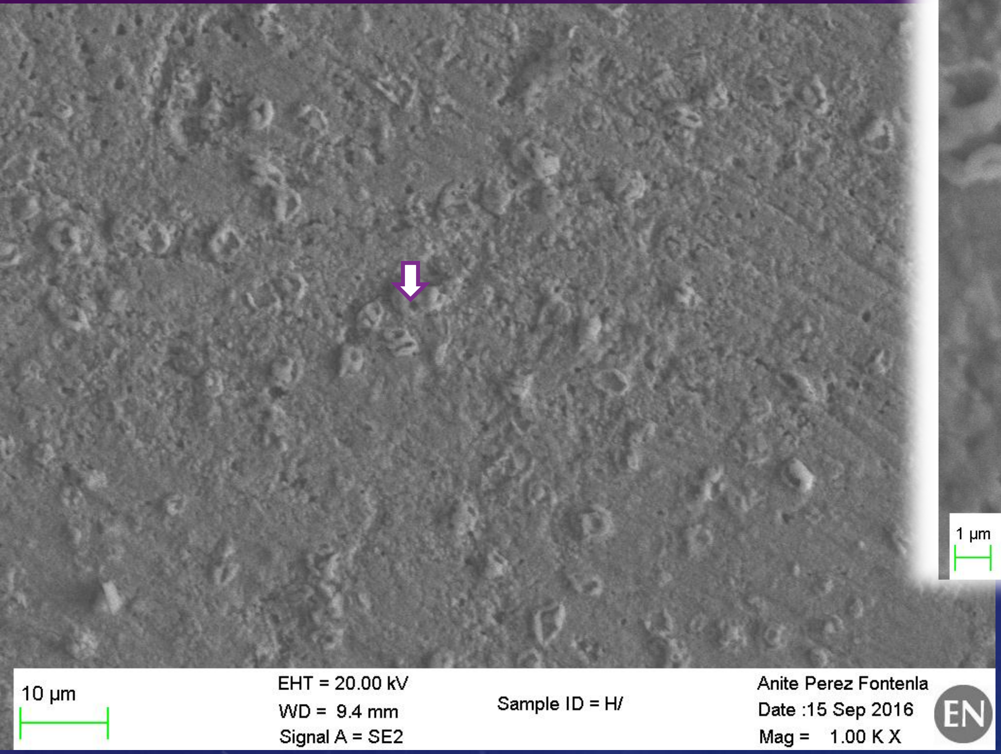

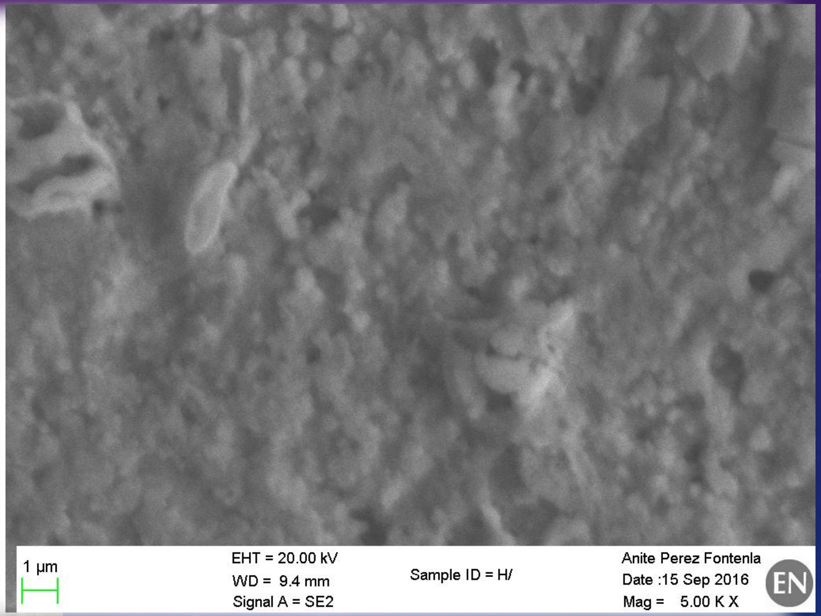

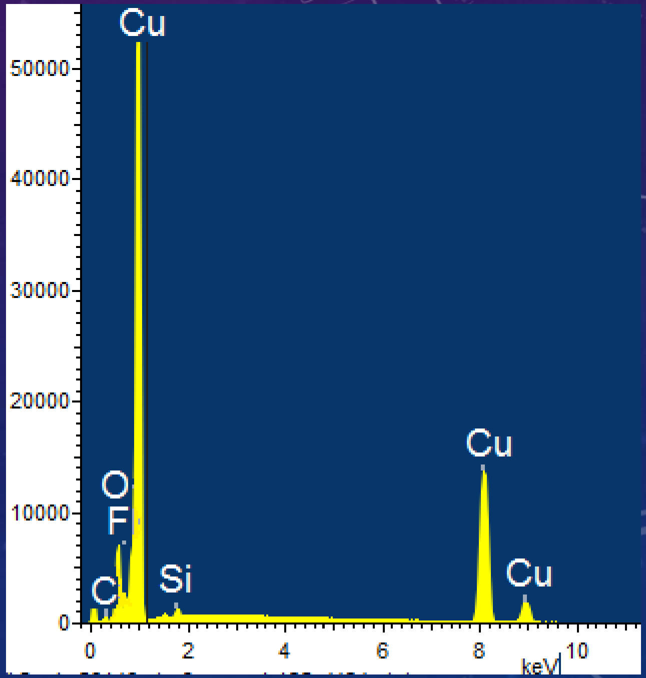

PR II

ANODE WIRE SAMPLE:
E – CENTER OF THE IRRADIATED ZONE

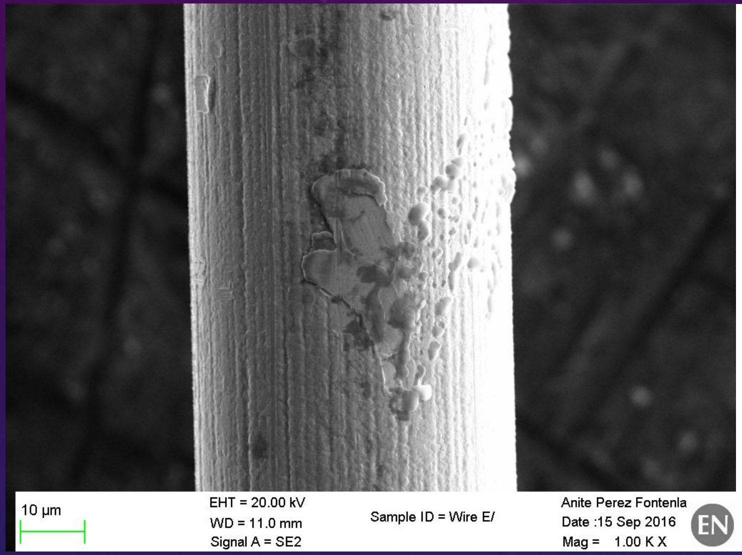

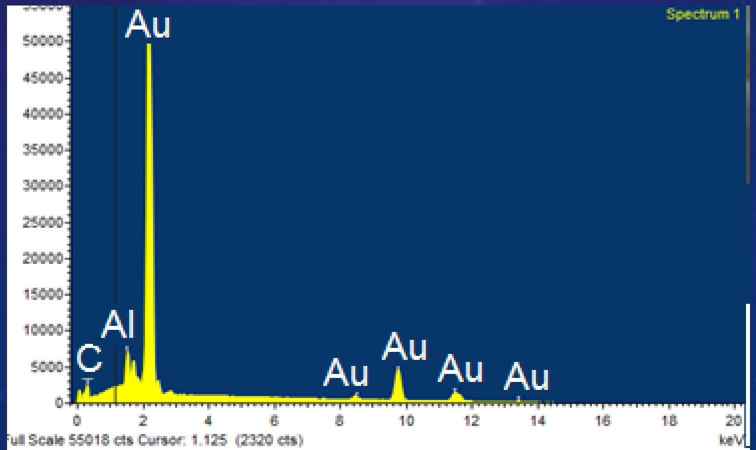

Accumulated dose Q = 1.36 C/cm

EDS OF FIB MILLED CROSS SECTIONS IN CU COATED CSC MUON CHAMBER PROTOTYPES

PR G

CSC accumulated dose: Q = 1.36 C/cm
Cooper foil accumulated dose: ~4 Gy/cm^2

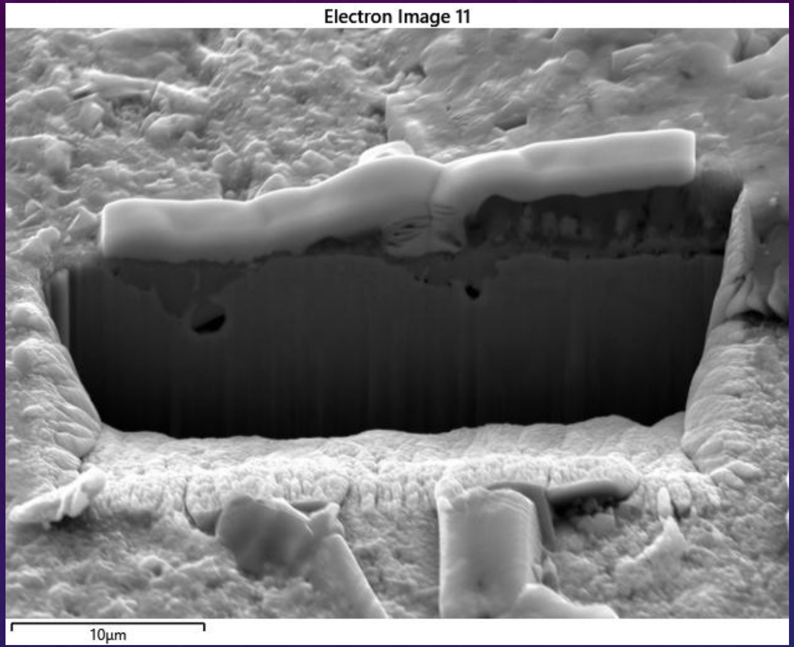

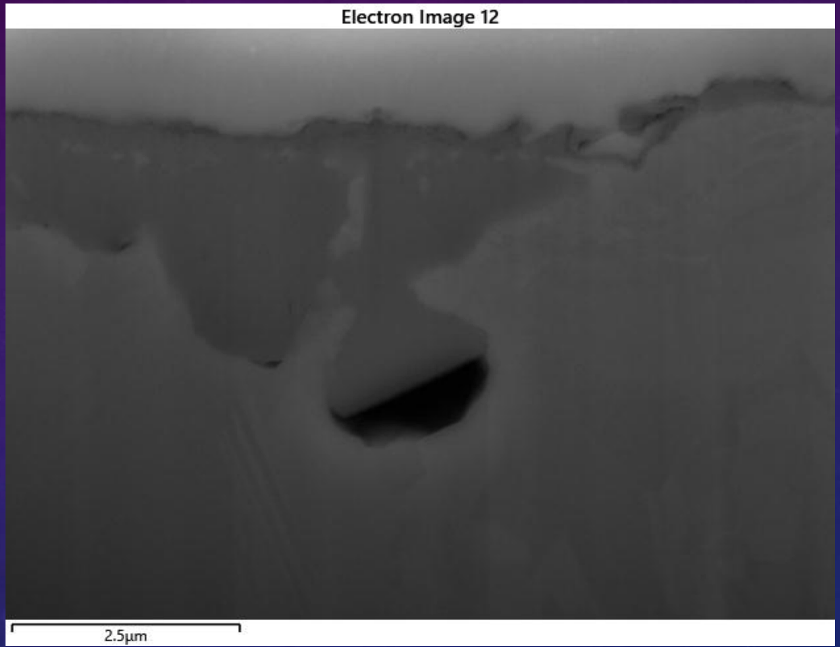

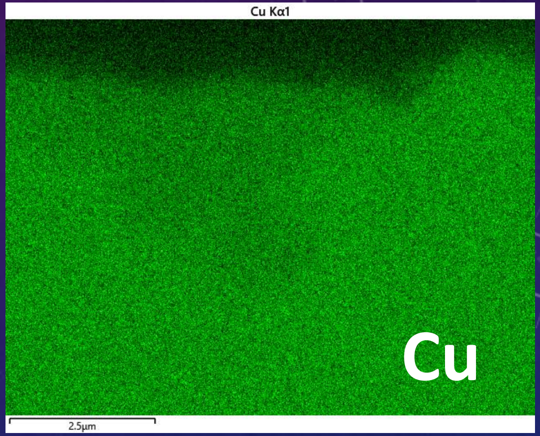

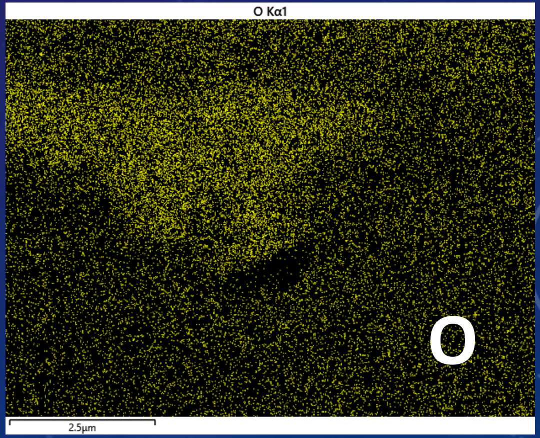

High resolution EDS mapping revealed that this darker region has a lower concentration of Cu and a higher O concentration than the surrounding Cu. This suggests that the irradiation on the sample surface has resulted in the formation of copper oxide in the near surface region (3-4 µm).

DOCUMENT PREPARED BY:	DOCUMENT CHECKED BY:	DOCUMENT APPROVED BY:
A. J. G. Lunt EN-MME-MM Client: Katerina Kuznetsova EP-UCM	F. Léaux EN-MME-MM	F. Léaux EN-MME-MM

Results: Cathode E_top- SEM

General appearance

AsB detector

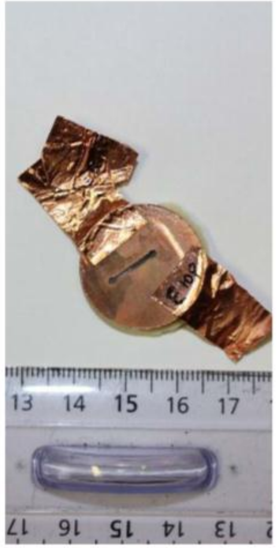

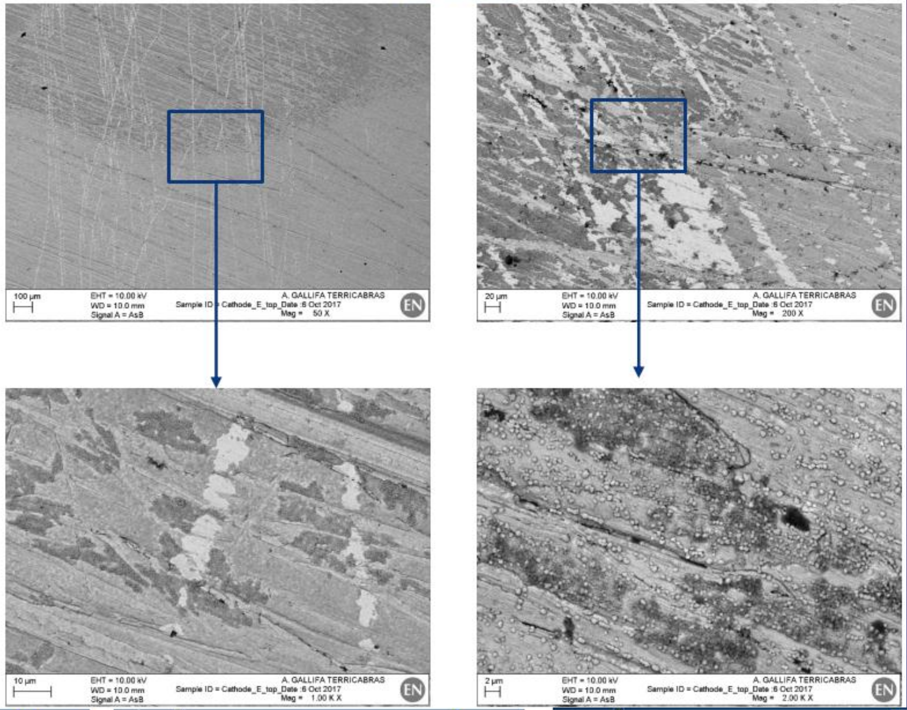

PR III

Results: Cathode E_bottom- SEM

General appearance

SE2 detector

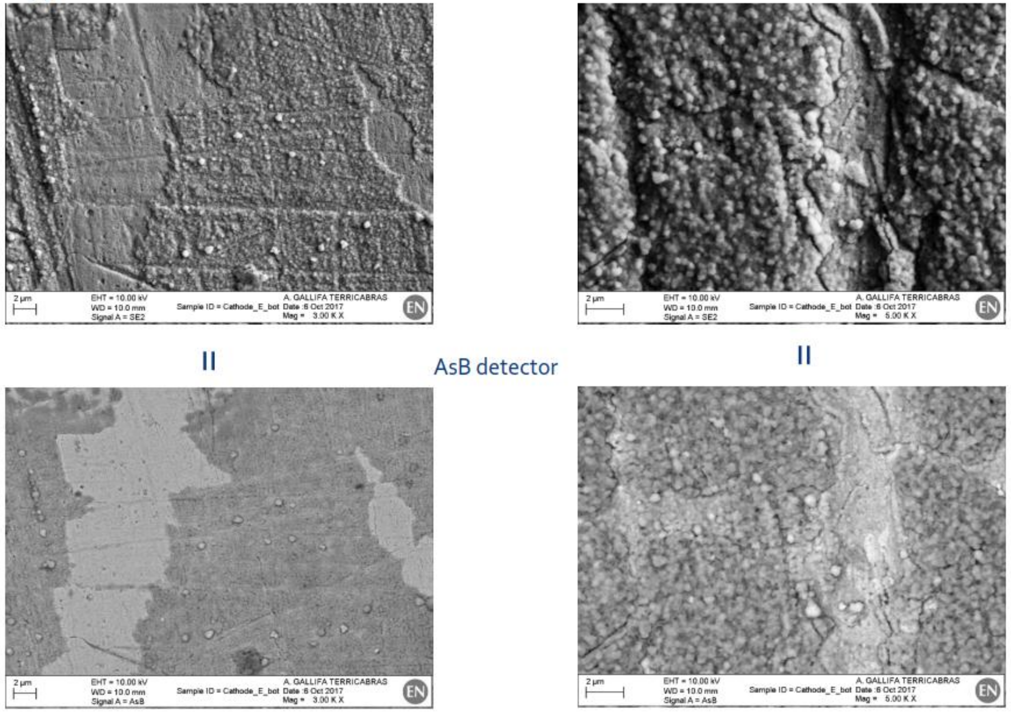

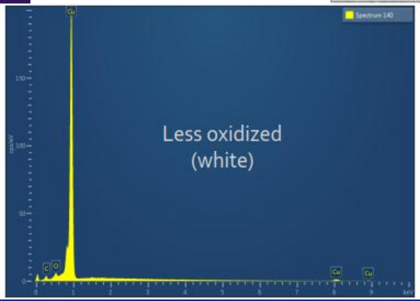

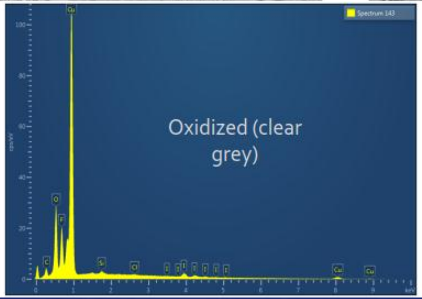

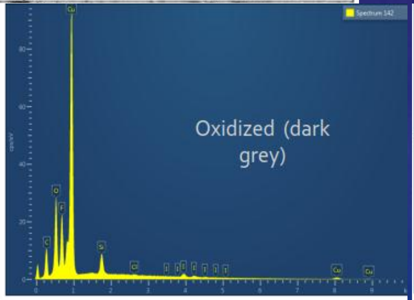

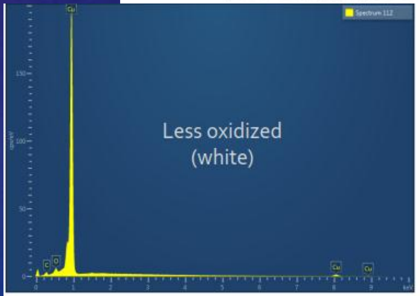

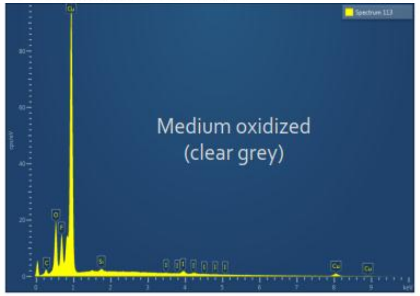

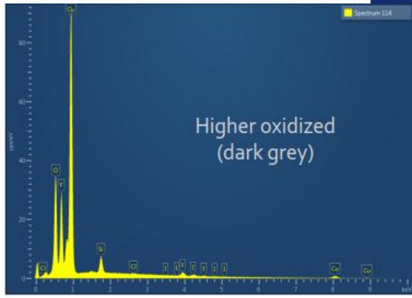

CSC accumulated dose: Q = 390 mC/cm
Cooper foil accumulated dose: ~1.65 Gy/cm^2

Presence of evident damages of the cooper foil indicates that besides of the intensive oxidation processes the cathode surface suffer from radiation damages, too.

B-sample PR III

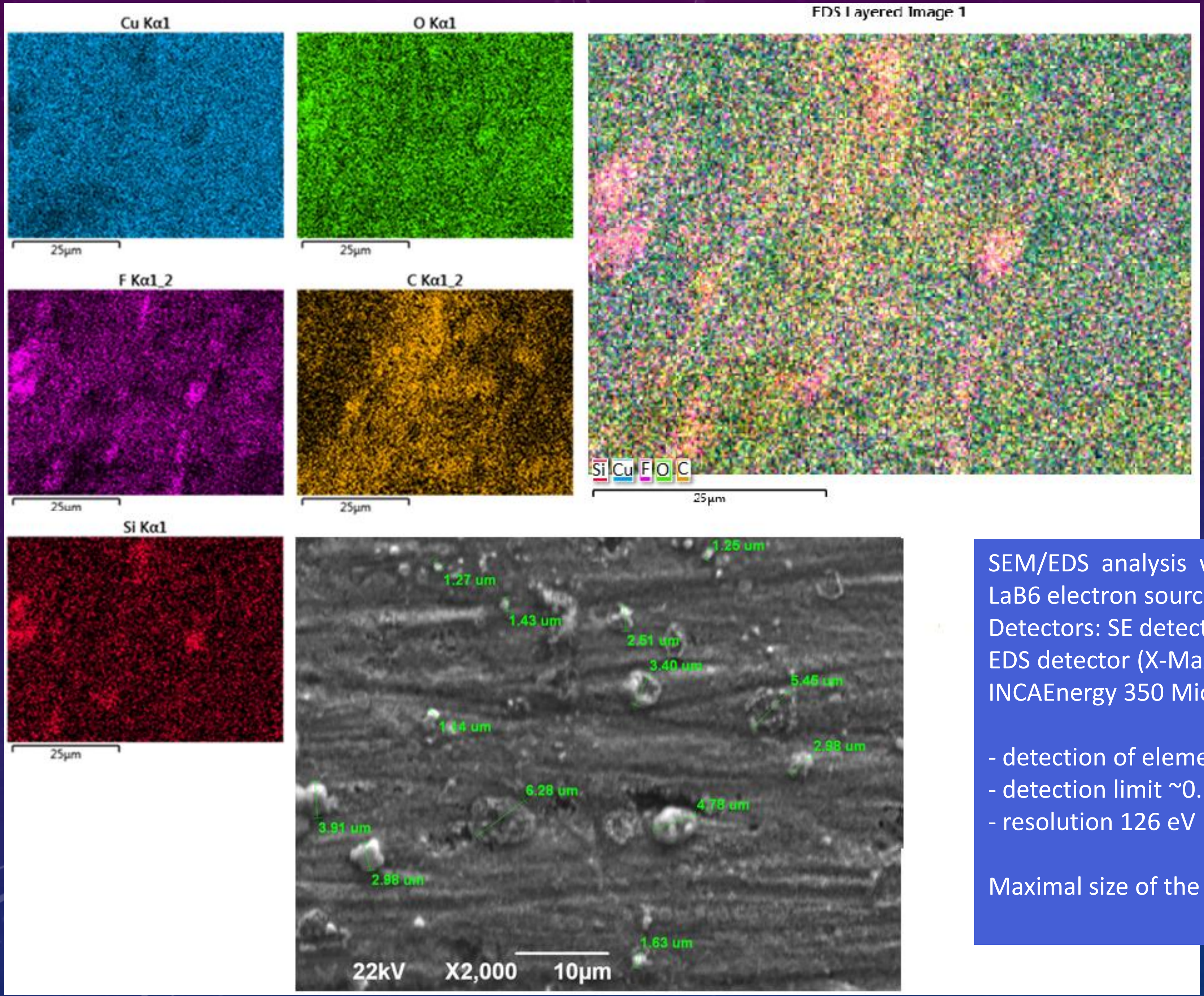

CSC accumulated dose: Q = 390 mC/cm

Cooper foil accumulated dose: ~0.2×10^{-3} Gy/cm^2

SEM/EDS analysis was conducted on **Jeo66l JSM-10LV** with W and LaB6 electron source (U=0.3-30kV).
Detectors: SE detector, BDE detector, CL detector
EDS detector (X-Max Large Area Analytical Silicon Drift connected with INCAEnergy 350 Microanalysis System)

- detection of elements **Z ≥ 5**
- detection limit ~0.1 mas%
- resolution 126 eV

Maximal size of the sample: 20cm (width), 8cm (height), 1kg (mass)

XRD (X-RAY DIFFRACTION ANALYSIS)

B-sample PR III

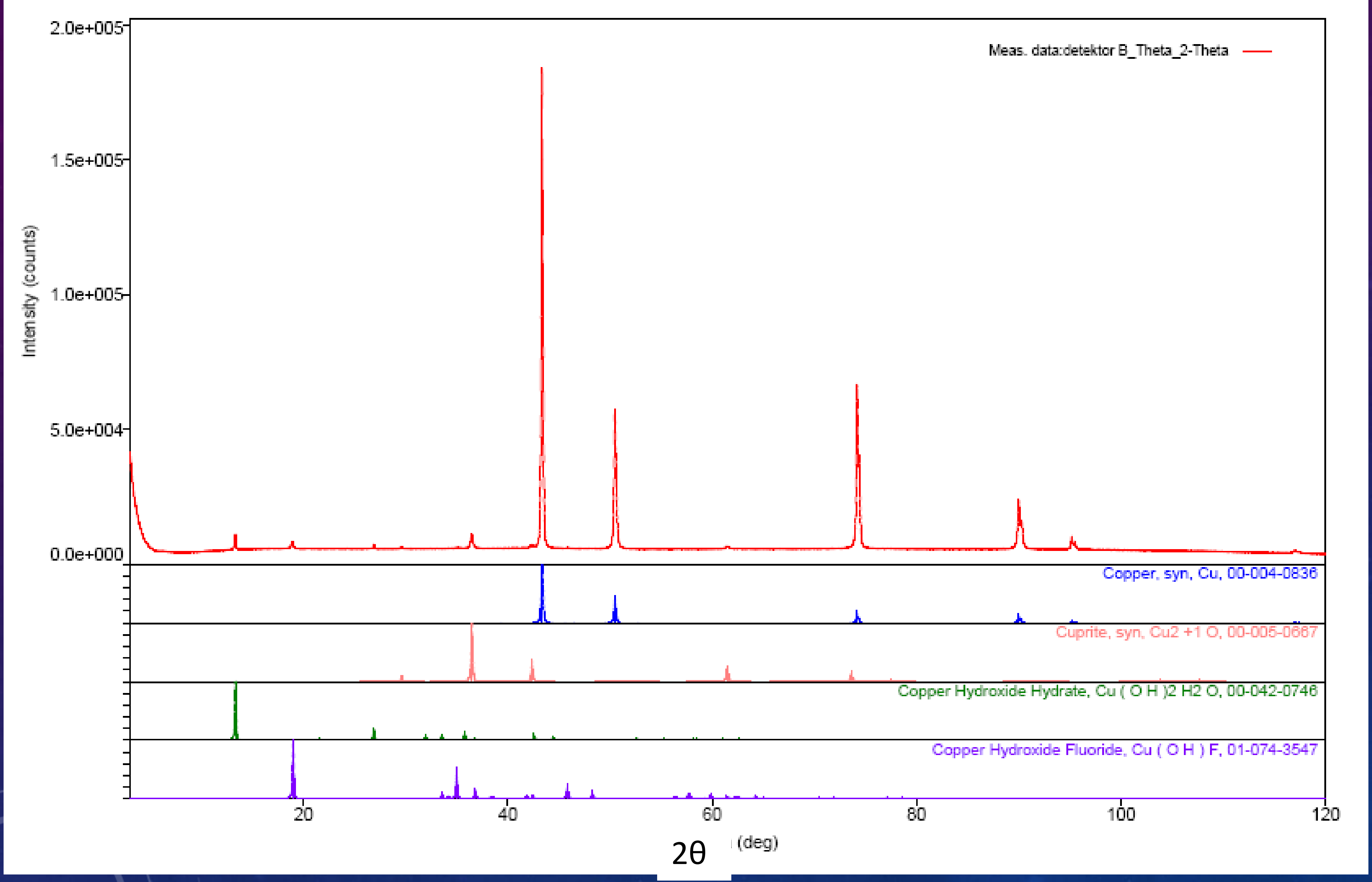

Analyzed area: ~15x15mm
Penetration depth < 1mm
Detection limit: 3%

The X-ray diffraction analysis was conducted on **Rigaku Smartlab** automated multipurpose X-ray Diffractometer in θ-θ geometry (the sample in horizontal position) in parafocusing Bragg-Brentano geometry using D/teX Ultra 250 strip detector in 1D XRF suppresion mode with $CuK_{\alpha 1,2}$ radiation source (U = 40 kV and I = 30 mA).

Identified crystalline phases: Cu, Cu_2O, $Cu(OH)_2H_2O$, $Cu(OH)F$

Irradiation geometry simulation with GEANT4

Model 1

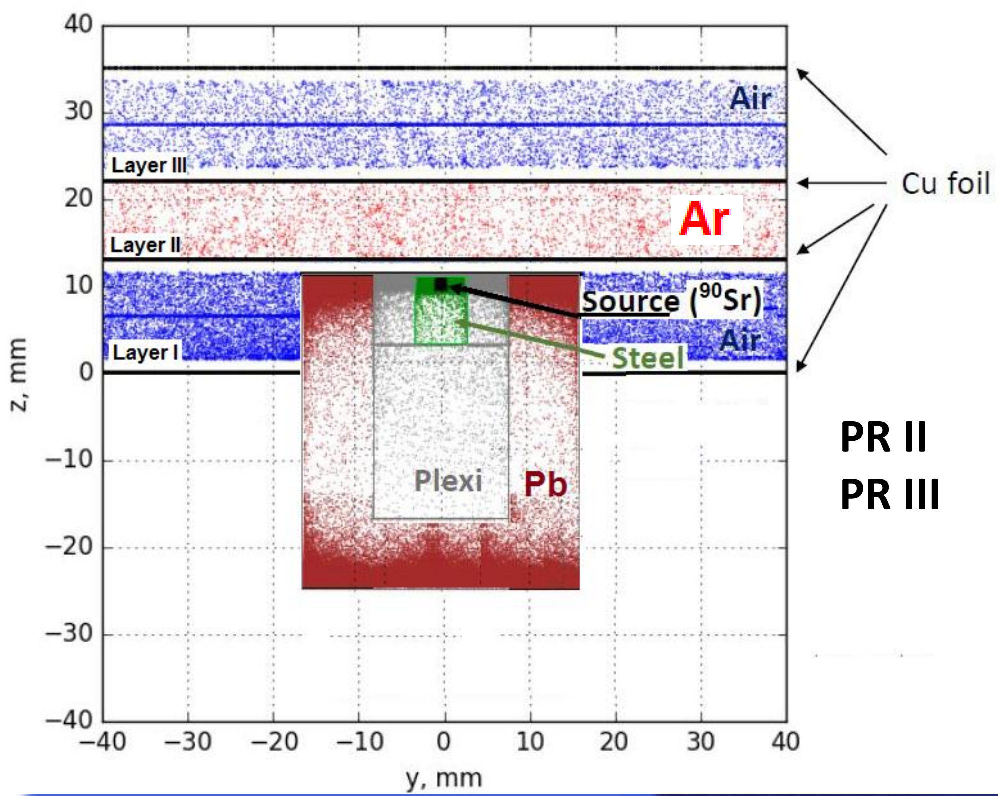

PR II
PR III

Model 2

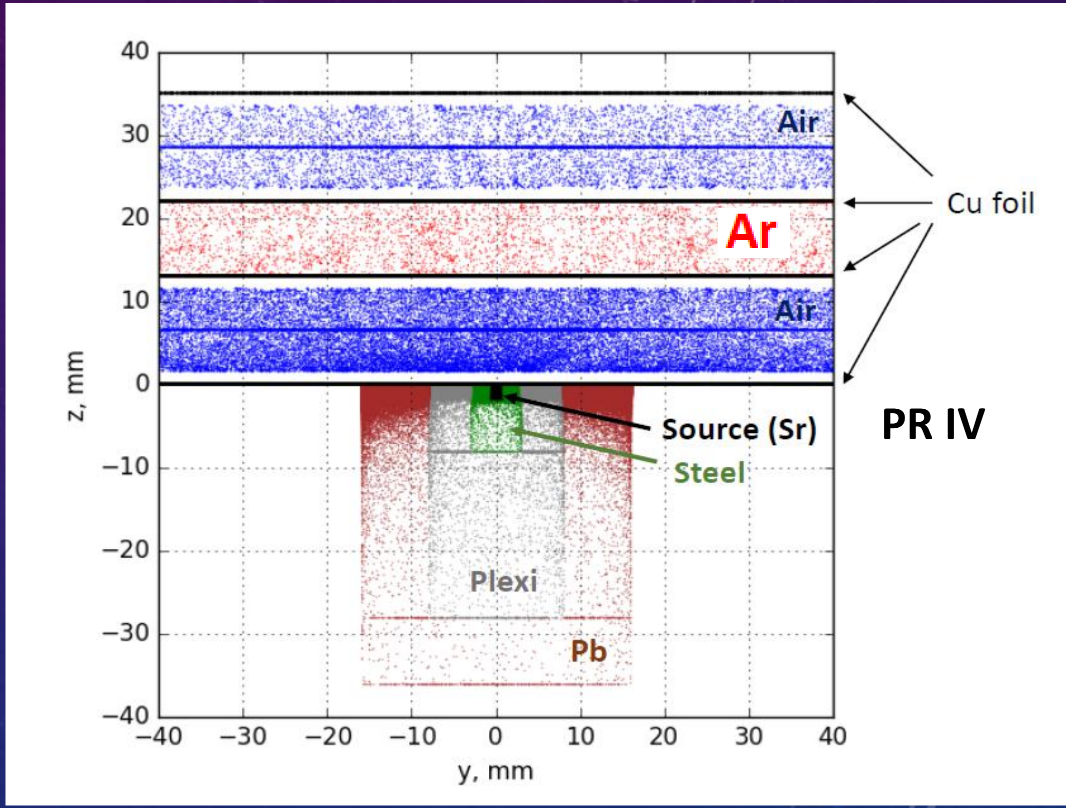

PR IV

Spectrum from ^{90}Sr β-source

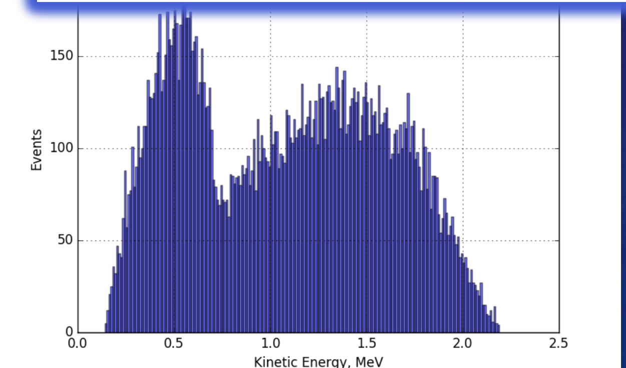

The accumulated doses in the copper layers per second:

Model 1

- Layer 2: 1068.5 ± 7.8 nGy
- Layer 3: 712.2 ± 6.3 nGy

Model 2

- Layer II: 137.7 ± 2.5 nGy
- Layer III: 102.3 ± 2.1 nGy

Int. J. Appl. Radiat. Isot. 34 (1983) 1241

Samples of **PRII**	Number of point like objects	Cooper foil dose, Gy/cm^2
C	153	1.2×10^{-4}
E-D	261	1.6×10^{-3}
H	277	4×10^{-4}
E-H	284	1×10^{-3}
Ef	216	4.0

Irradiation simulation with GEANT4

Flux of the electrons [Hz/cm²] versus the distance from the center of irradiation spot

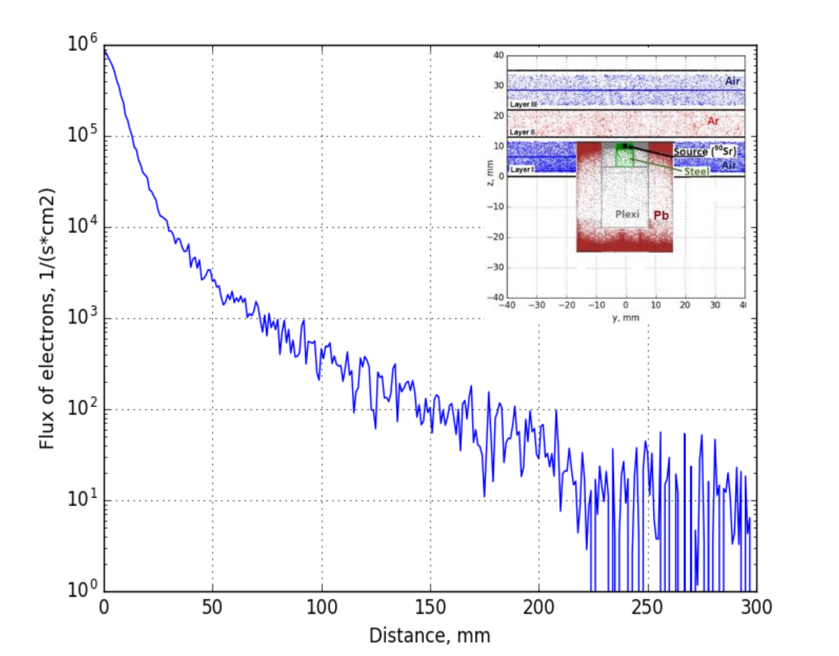

Accumulated dose distributions on the Cu foil at different irradiation models

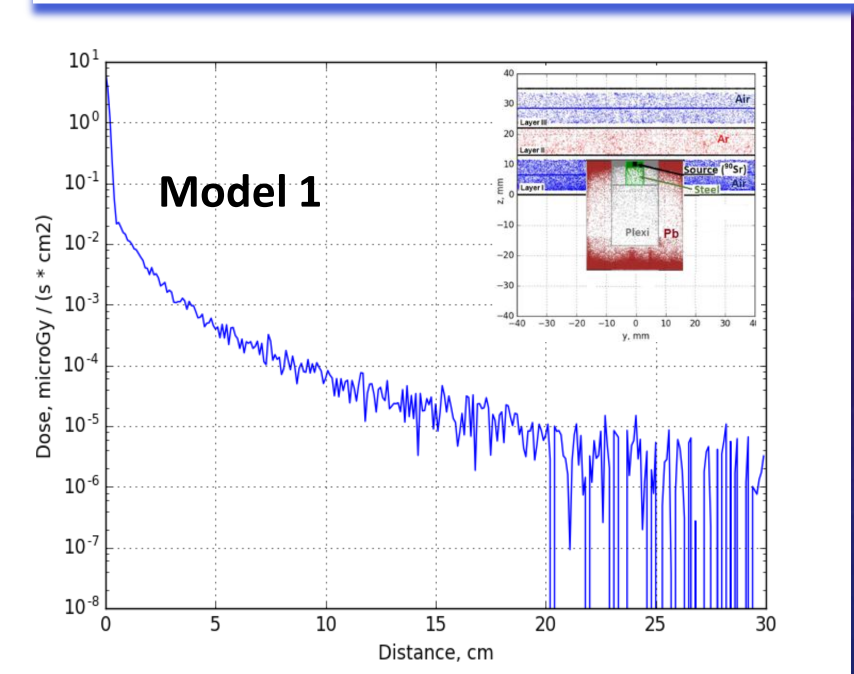

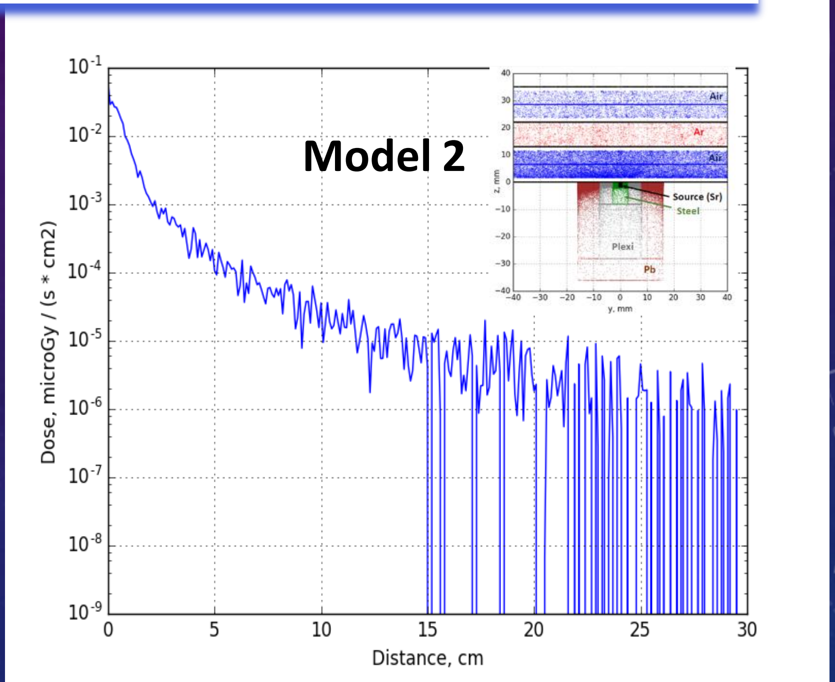

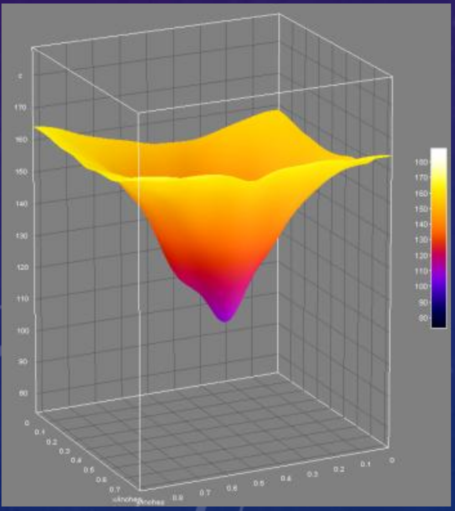

Profile of the 90Sr exposition on a photo film

Cooper foil dose in the **centre of zone (E)**:

PR II ~ 4 Gy·cm^{-2}

PR III ~ 1.65 Gy·cm^{-2}

PR IV ~ 0.124 Gy·cm^{-2}

PR II test with 10%CF4 gas mixture
Time = **1,372,500 s** (Model 1), **I = 17 µA**

PR III test with 1.65%CF4 gas mixture
Time = **2,194,000 s** (Model 1), **I = 4 µA**

PR IV test with 10%CF4 gas mixture
Time = **6,200,000 s** (Model 2), **I = 1.15 µA**

The samples from the aged CSC Prototype have been studied in the National Research Nuclear University MEPhI (Sarov)

Cathode FR4 samples from the points E-D, E-D, H, E^f were analysed with

- Atomic Force Microscope microscopy with “Solver Next” (Zelenograd, Russia);
- Nuclear scanning microprobe analysis (Sarov, Russia).

EGP-10 Electrostatic Rechargeable Accelerator

- Nuclear scanning microprobe setup (ЯСМЗ)
  - E=14 MeV H^+ beam with not less of ±300 μm spot on the target
  - Scanning rate from point-to-point 200 μs.
  - Time of positioning less of 40 μs.

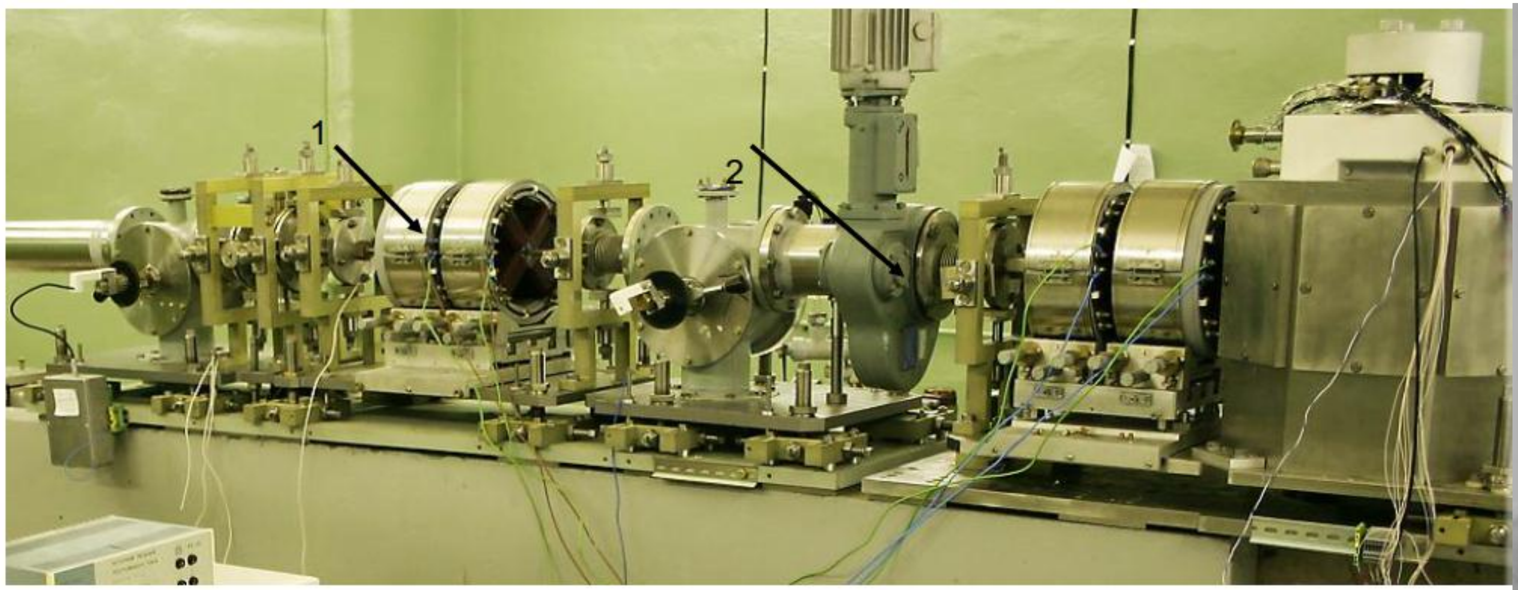

1 – Ions optical focusing system; 2 – beam-sample interaction chamber

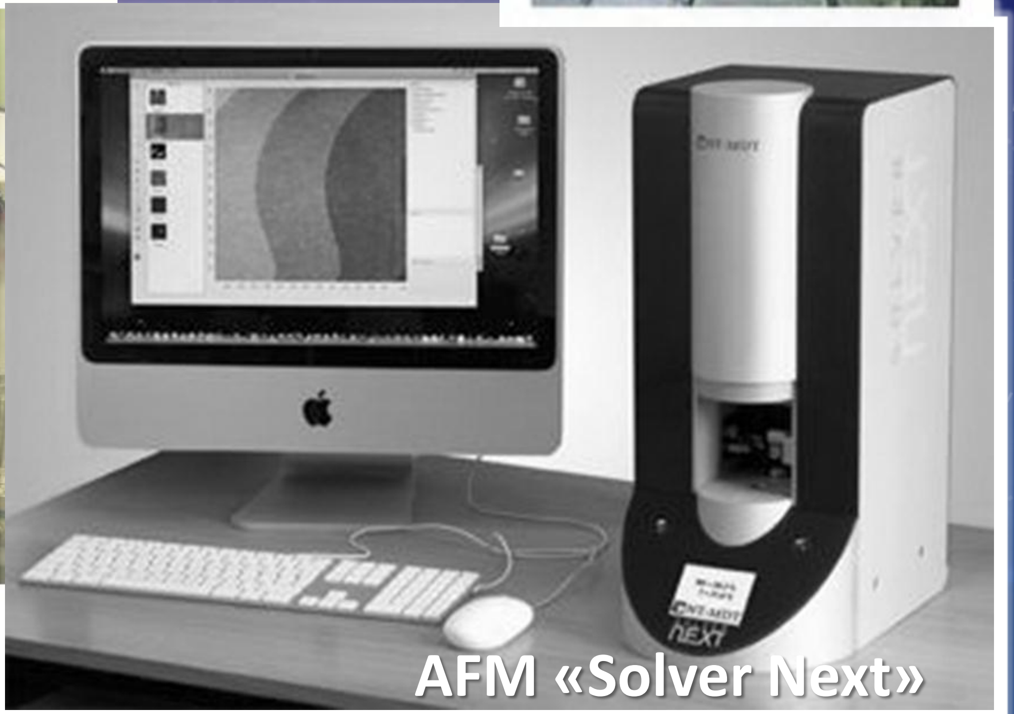

AFM «Solver Next»

Nuclear scanning microprobe analysis of the CSC samples

Vary of concentration of the Oxygen in the Cooper foil with a depth of the analysed layer for different samples

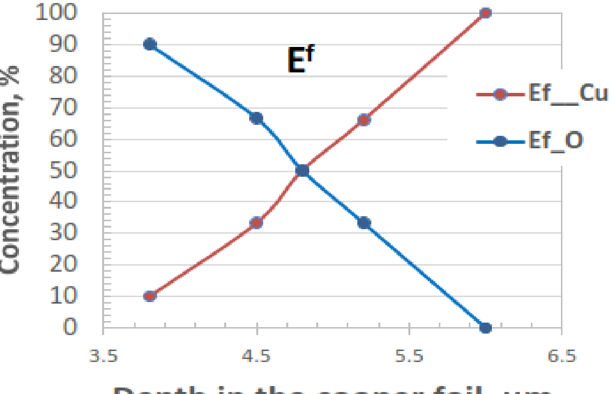

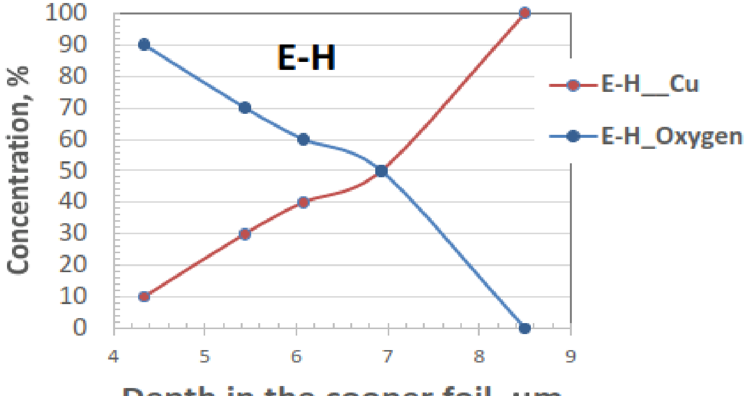

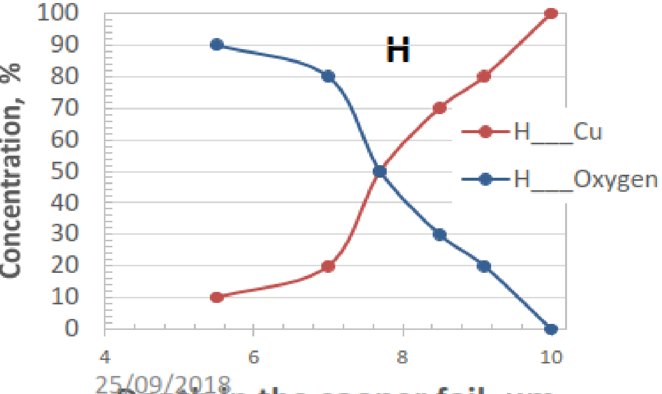

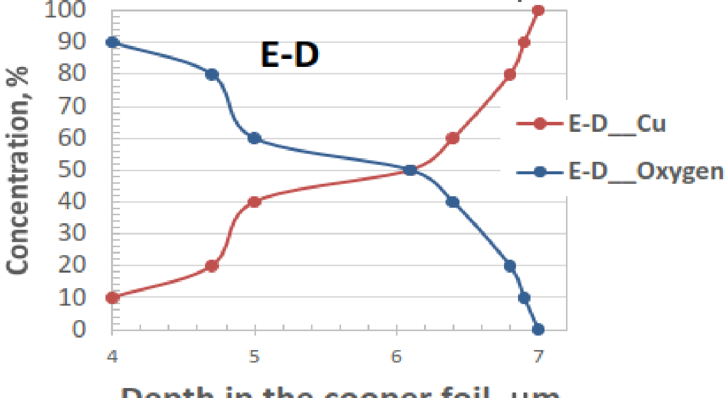

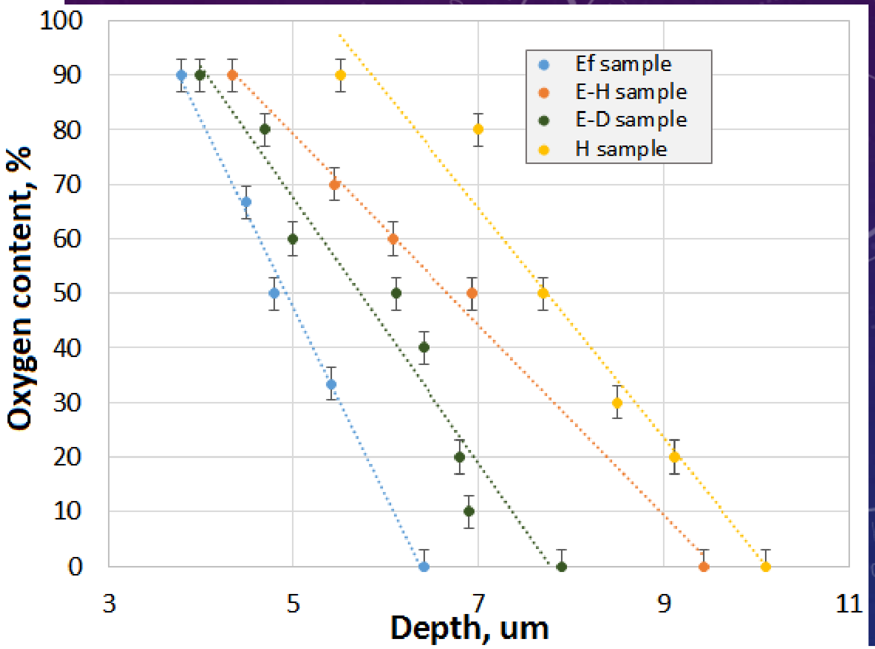

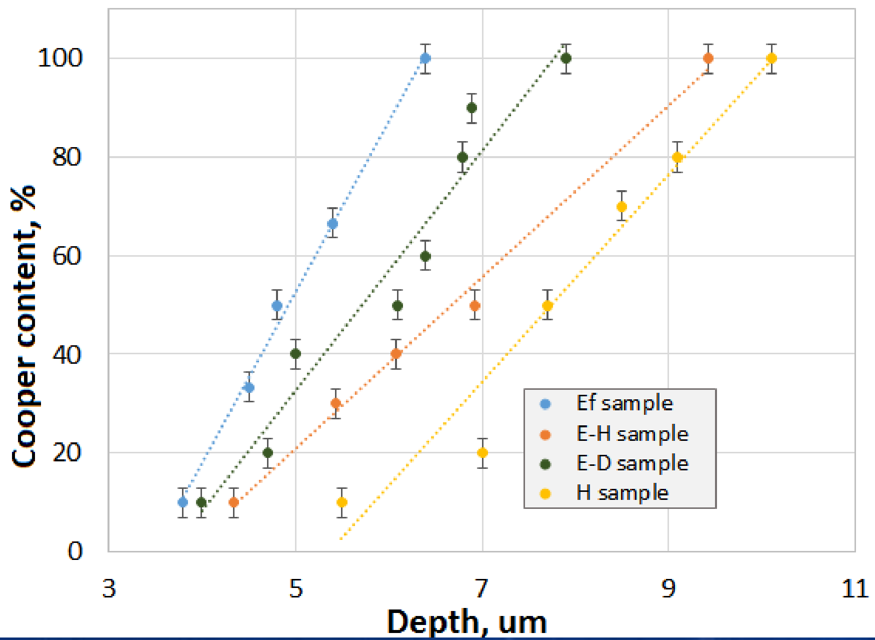

Oxygen concentration changes from 90% at 3-4 um depth up to 0 % at 8-10 um depth from the foil surface

AFM & SEM images of the copper foil surface of not irradiated FR4

Roughness profile has a depth of 0.4 μm

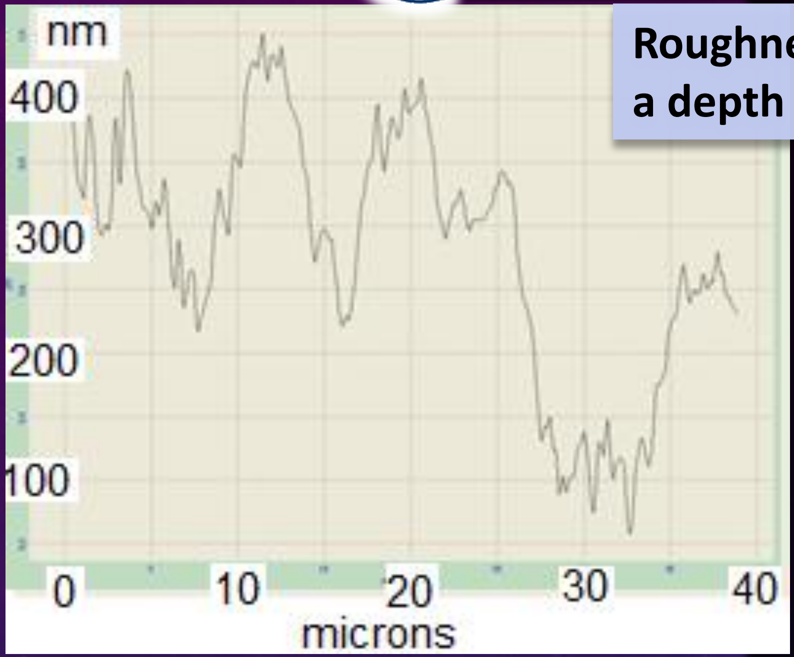

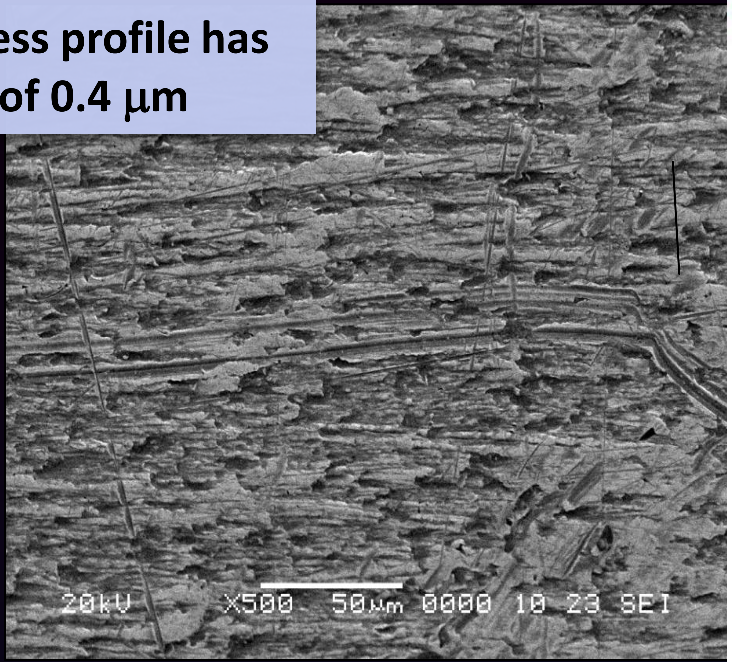

Scanning probe microscopy

Principle of Atomic Force Microscopy

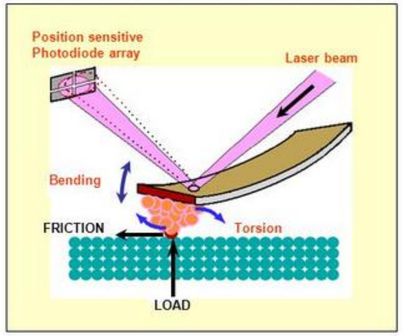

Forces:

Van der Waals force
electrostatic force
Magnetic force
Chemical force
Pauli repulsive force

When the tip is brought into proximity of a sample surface, forces between the tip and the sample lead to a deflection of the cantilever according to Hooke's law.

This deflection is characterized by sensing the reflected laser light from the backside of cantilever with the position sensitive photodiode.

Because force signal (including Van der Waals force, electrostatic force, Pauli repulsive force) is measured, various samples including insulator can be imaged in AFM.

Force microscopy of original FR4

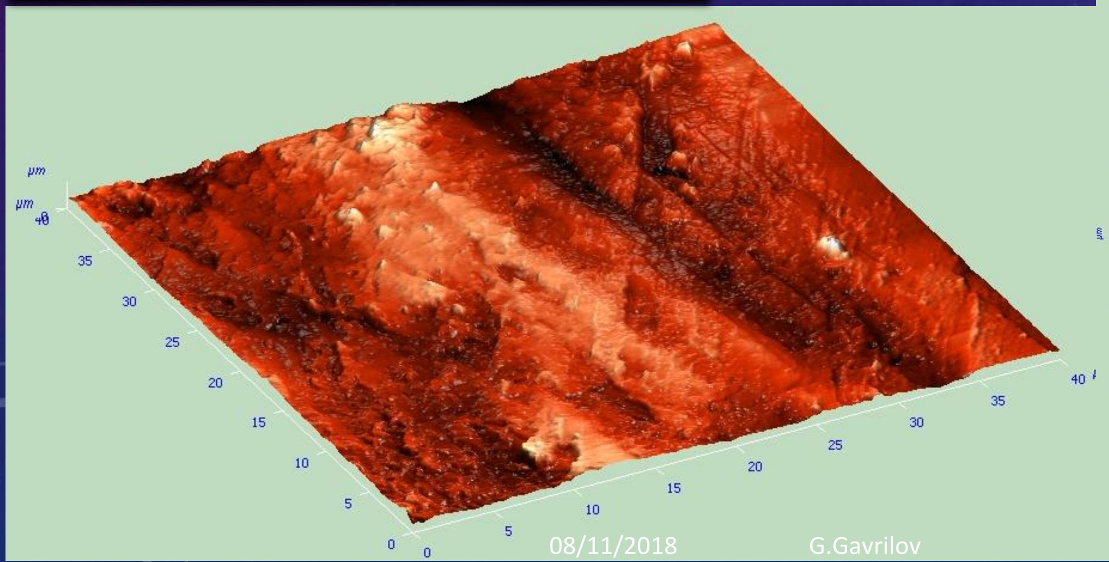

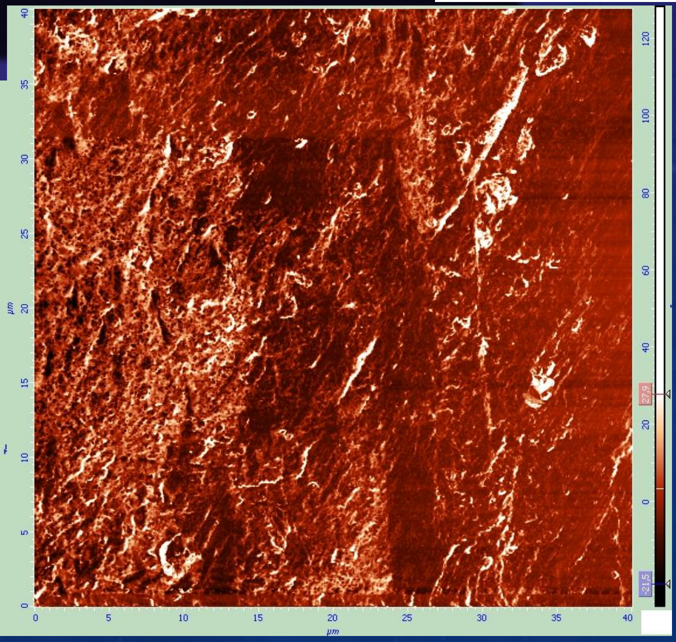

AFM microscopy

200 nm

Sample of FR4 35 μm cooper foil

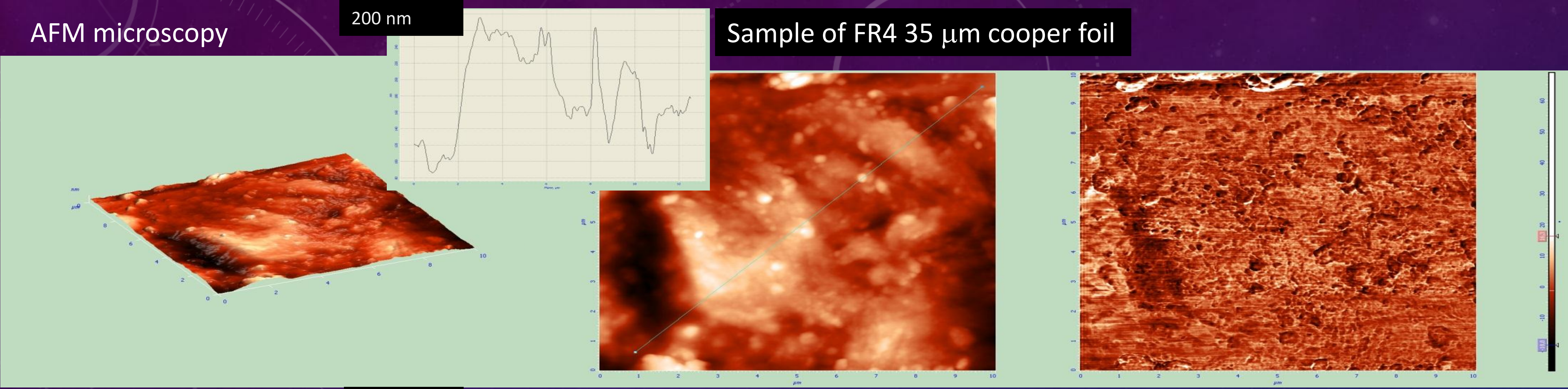

Blisters generation

800 nm

Irradiated FR4 35 μm cooper foil, Dose ~ 1x10E-3 Gy/cm^2

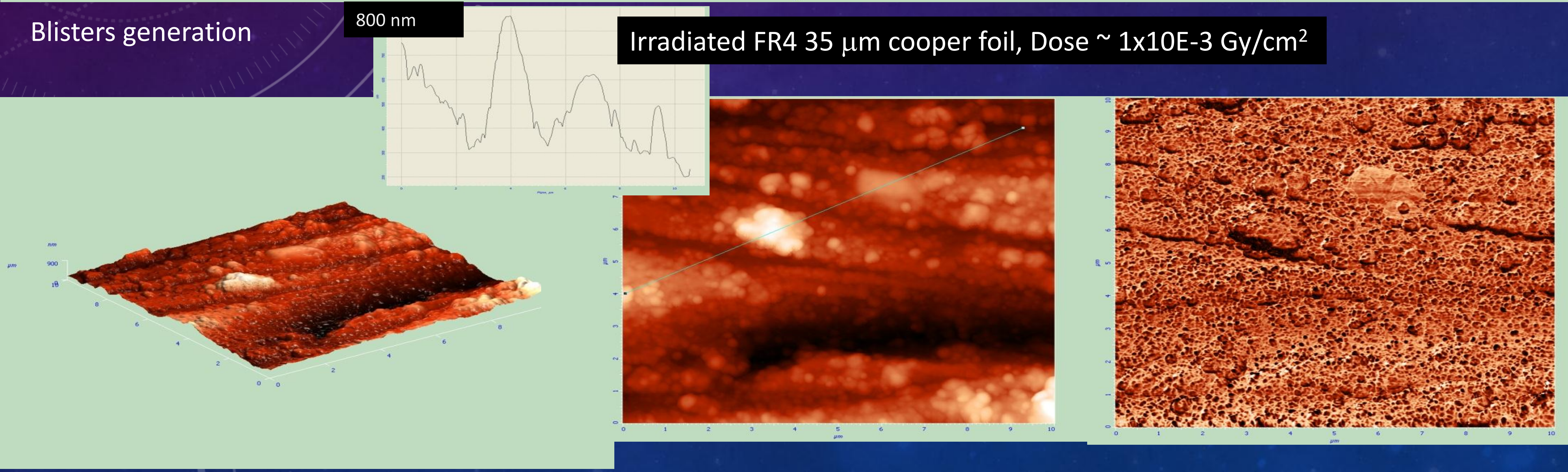

Cathode radiation damages

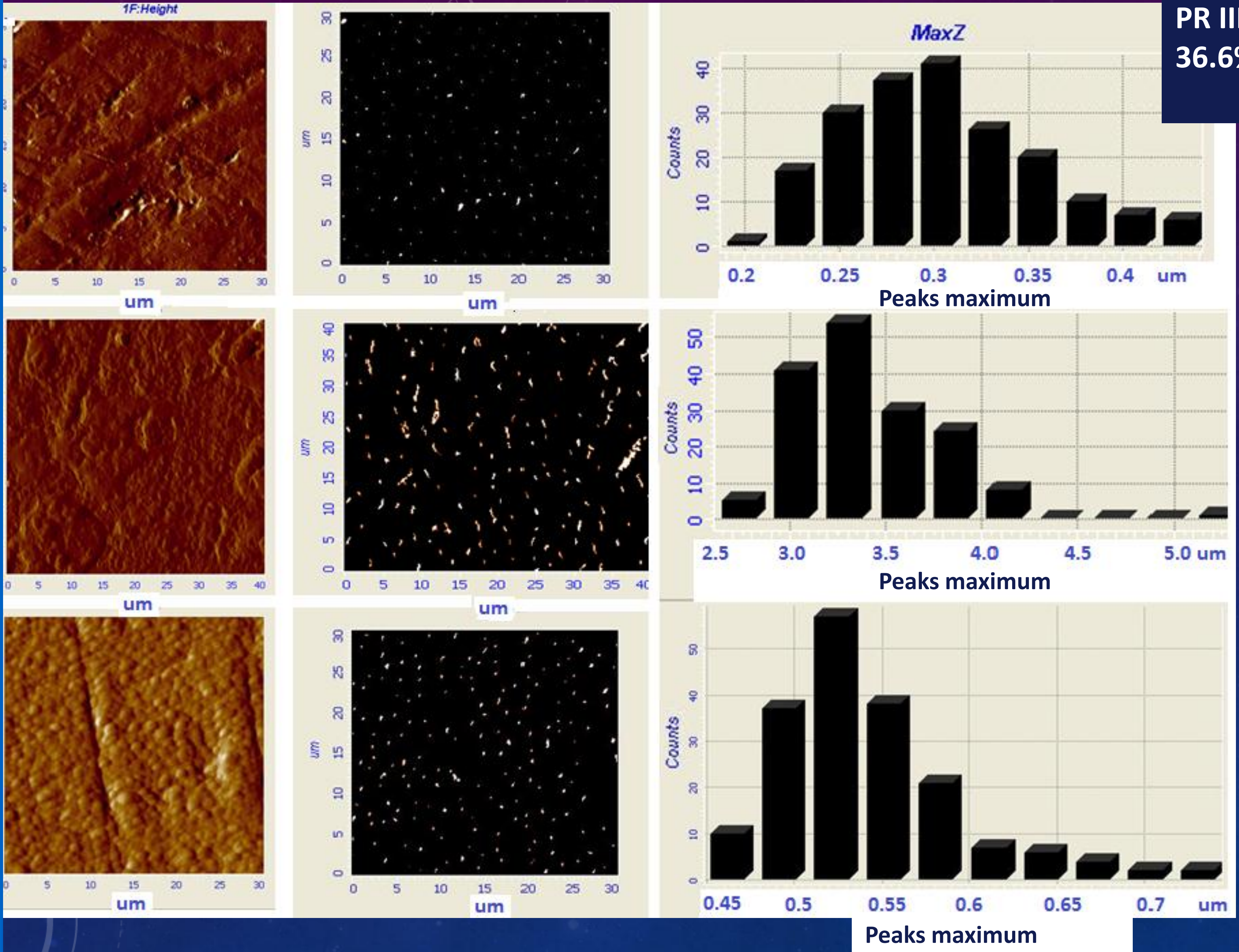

PR III

$36.6\%Ar+61.75\%CO_2+1.65\%CF_4$

The results of processing with Grain Analysis program of AFM scanned image

Sample C,
$Dose^{Cu} \sim 9\times10^{-5}$ Gy/cm^2

Sample E-H,
$Dose^{Cu} \sim 0.348\times10^{-3}$ Gy/cm^2

Sample Eh,
$Dose^{Cu} \sim 1.65$ Gy/cm^2

Optical microscopy of FR4 cooper foil before and after irradiation

Samples of FR4 cooper foil

x 400

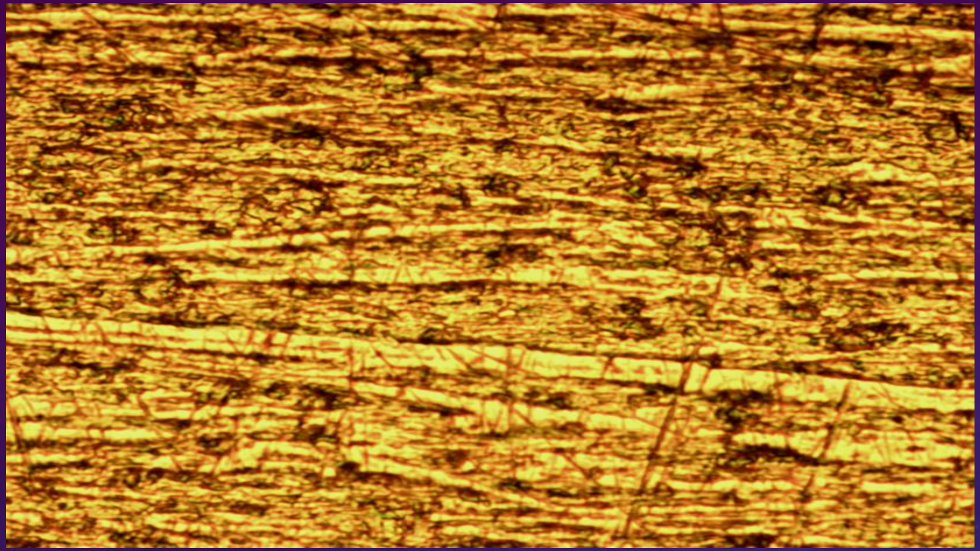

x 800

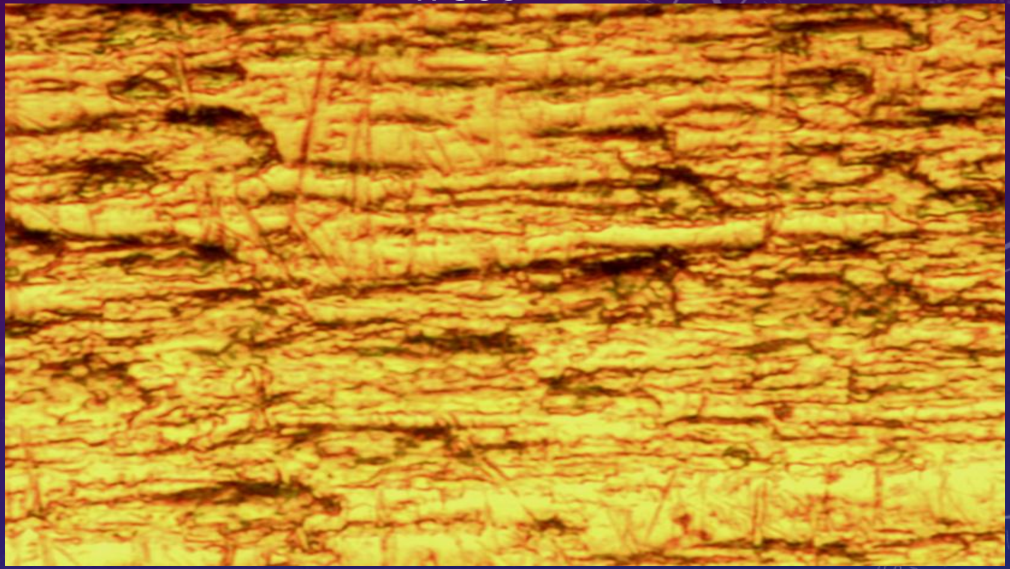

^{90}Sr irradiated FR4 cooper foil

x 200

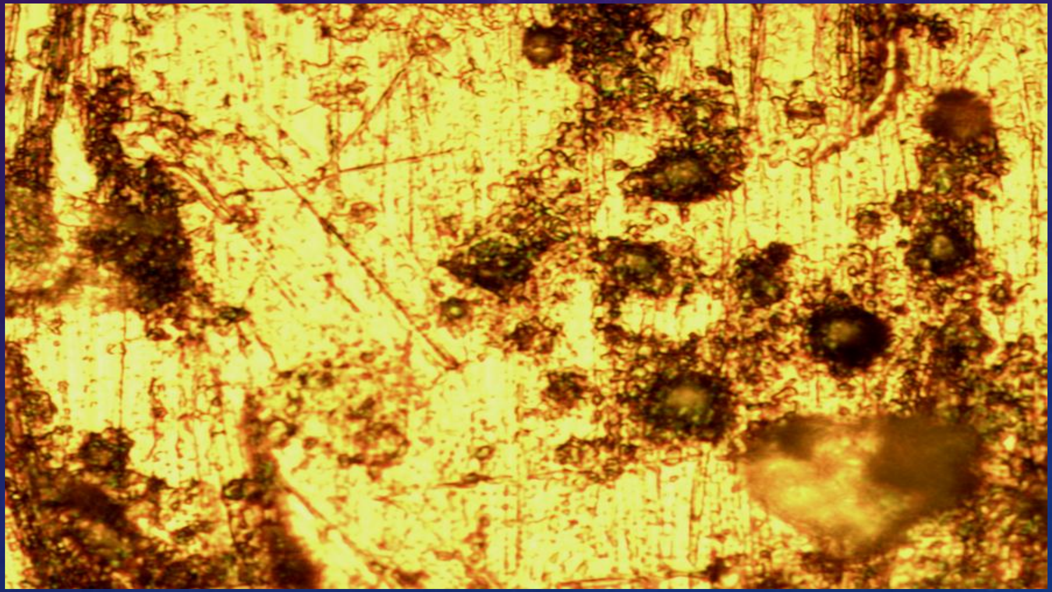

x 400

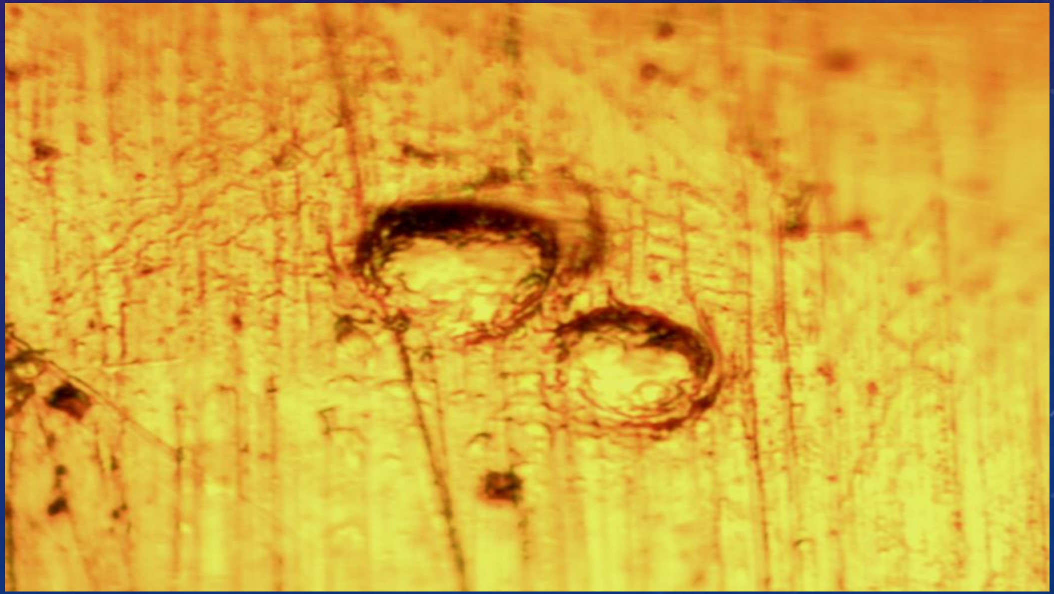

Blisters appearance is related with MeV electrons irradiation damaging

Cathode radiation damages

E-H – sample, Dose = 0.35×10^{-3} Gy/cm2

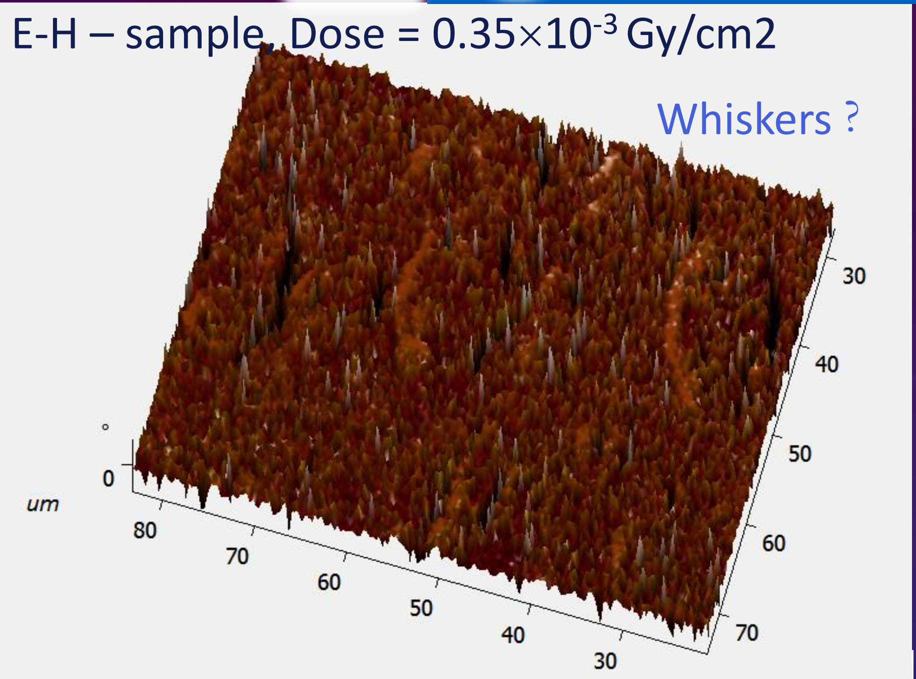

C– sample, Dose = 0.5×10^{-4} Gy/cm^2

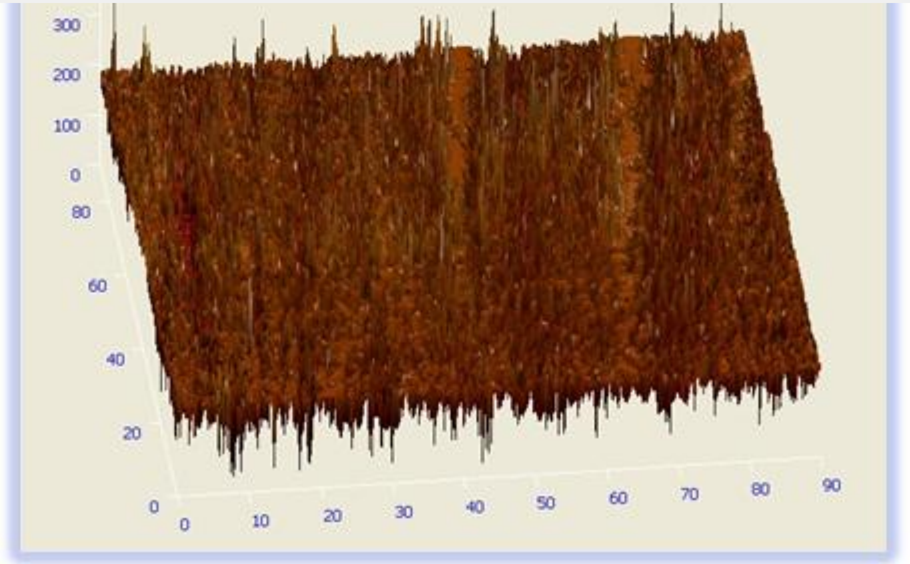

Blisters

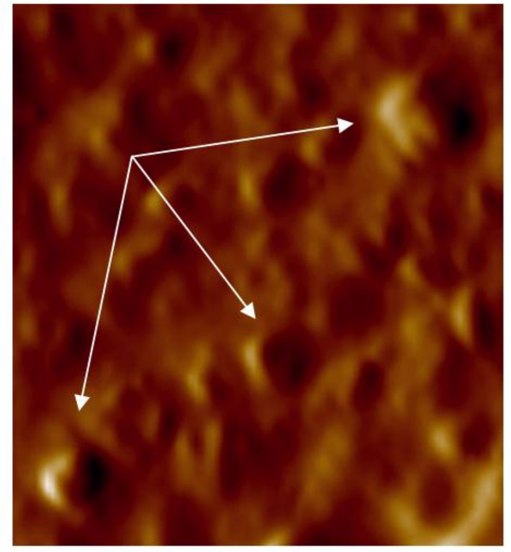

Craters

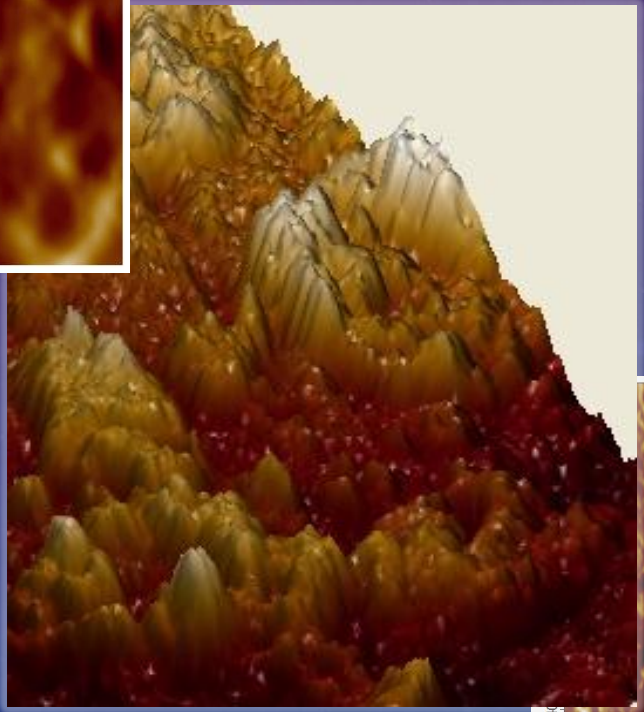

Flaking

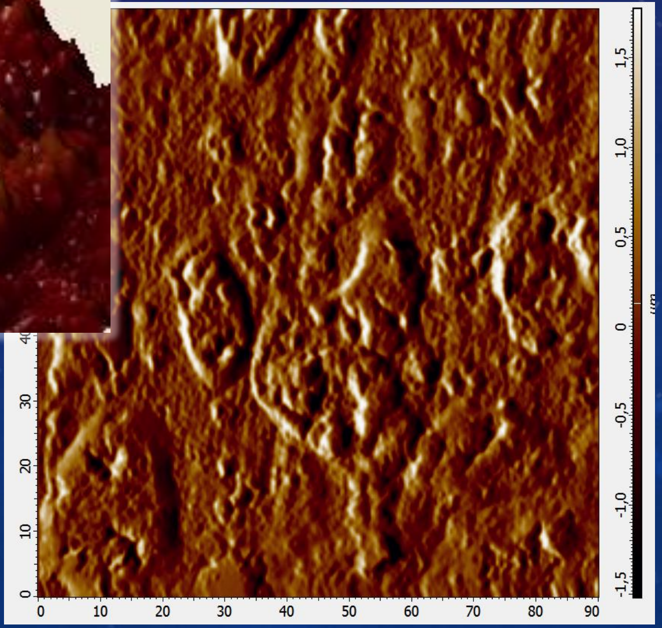

Whiskers on the AFM phases scan
have a different colour.
Perhaps, this means oxidation at E-H sample

Whiskers at room temperature and in space

The Art of Metal Whisker Appreciation: A Practical Guide for Electronics Professionals

Lyudmyla Panashchenko
NASA Goddard Space Flight Center
lyudmyla.p@nasa.gov

Human Hair vs. Metal Whisker

Metal Whiskers are commonly
1/10 to <1/100 the thickness of a human hair

Optical comparison of Human Hair vs. Tin Whisker

SEM comparison of Human Hair vs. Metal Whisker

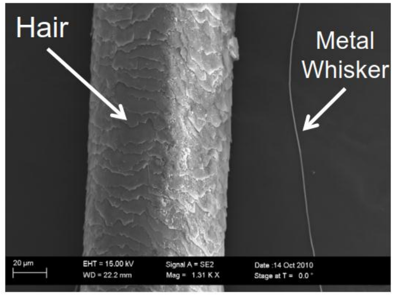

Electrical Behavior of Whiskers

- Variations expected in whisker resistance
  - $R = \rho \frac{L}{A} = \rho \frac{L}{\pi (d/2)^2}$
  - ρ is metal resistivity, L is whisker length, d is whisker thickness
  - Since both length and thickness vary, so does resistance
- Whiskers are coated with insulative oxide layers
  - Mechanical contact with a whisker does not mean electrical contact
  - Dielectric breakdown of insulative layers required for conduction to occur
- Whiskers will melt with enough current through them!
  - How to protect circuits under failure analysis from burning out a whisker?

Tin, Zinc, Cadmium – Whisker Family Album

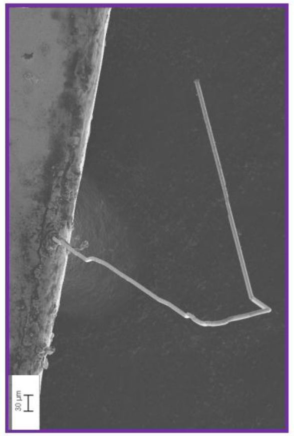
Sn whisker

Cd whisker

Zn whisker

The Miracle of Whisker Initiation

All of these theories were proposed back in 1950s and 1960s.
No clear proof yet exists for any of them.

Stress?

Dislocations?

Entropy?

Recrystallization?

Impurities?

Inclusions?

Whiskers are making a mockery of 60 years of research.

Tin Whisker Resistance at Room Temperature for Different Lengths and Thicknesses

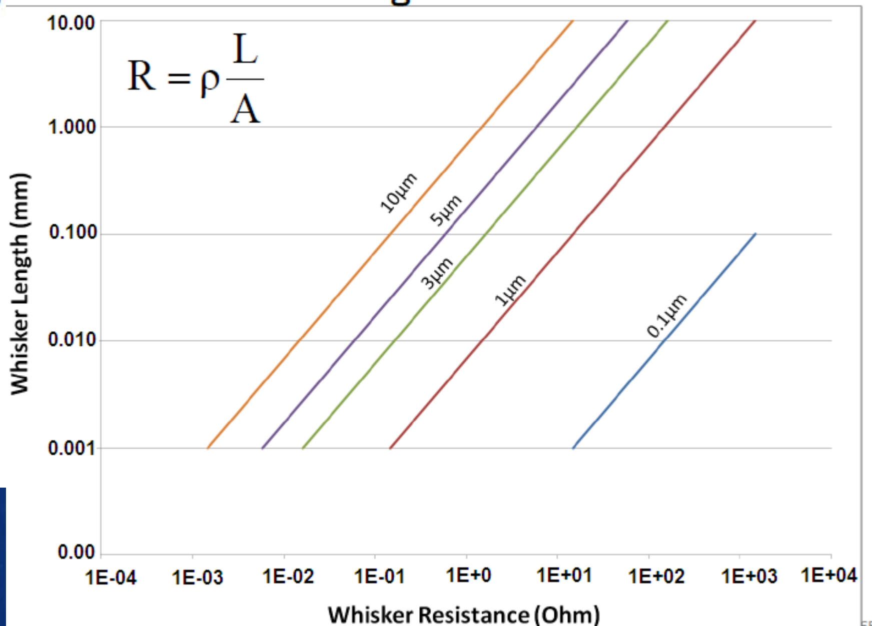

Metal Whiskers on Components

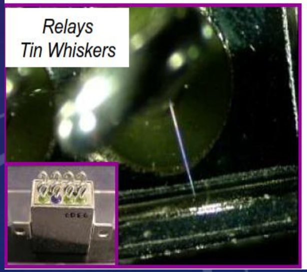

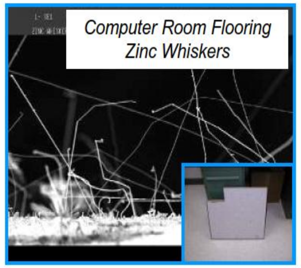

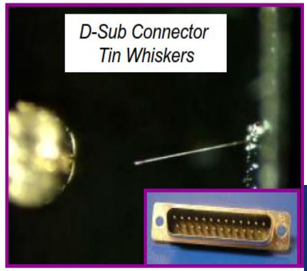

УДК 537.52

А. А. Петров[1,2], *Р. Х. Амиров*[3], *Е. В. Коростылев*[2], *И. С. Самойлов*[3]

[1]Физический институт им. П. Н. Лебедева РАН
[2]Московский физико-технический институт (государственный университет)
[3]Объединенный институт высоких температур РАН

Исследование эрозии катода в отрицательном коронном разряде

Materials Physics and Mechanics 19(2014) 88-95
“Cooper oxide nanowhiskers: Method of production, structure specific, and mechanical properties.”
A.N. Abramov et al.

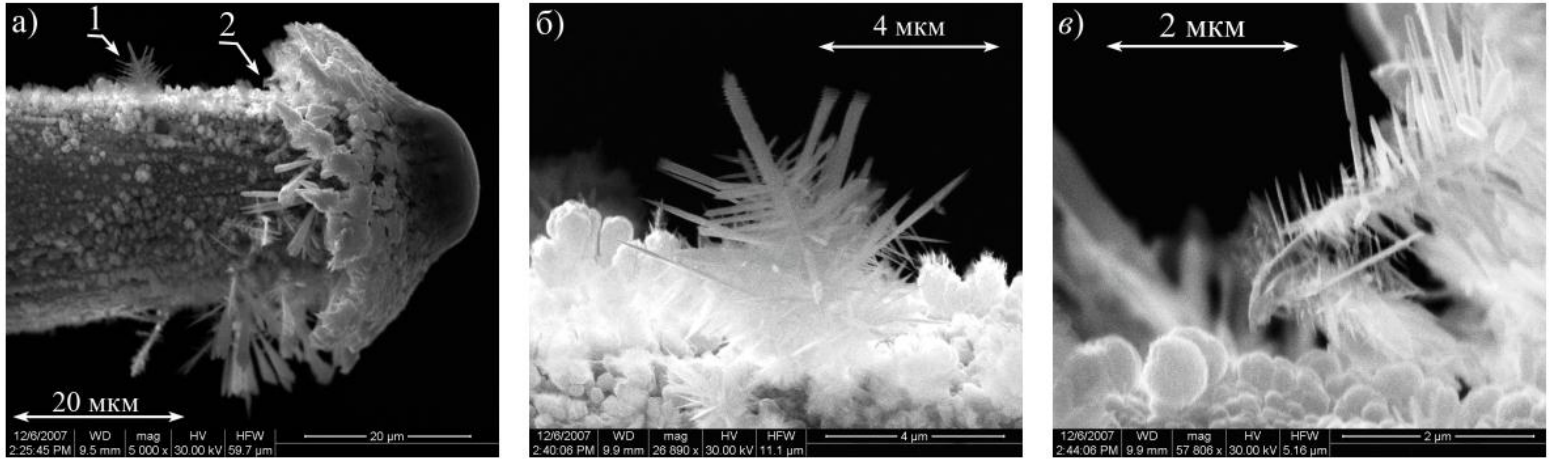

Cooper cathode after Trichel discharges (<100 uA)
a) General view of the cathode (1,2 – nanocrystals, formed on the Cu-cathode as a result of recycling products corrosion)
b) a crystal formed 30 um apart from the cathode end cup
c) crystals formed as a result of recycling on the collar of the peak.

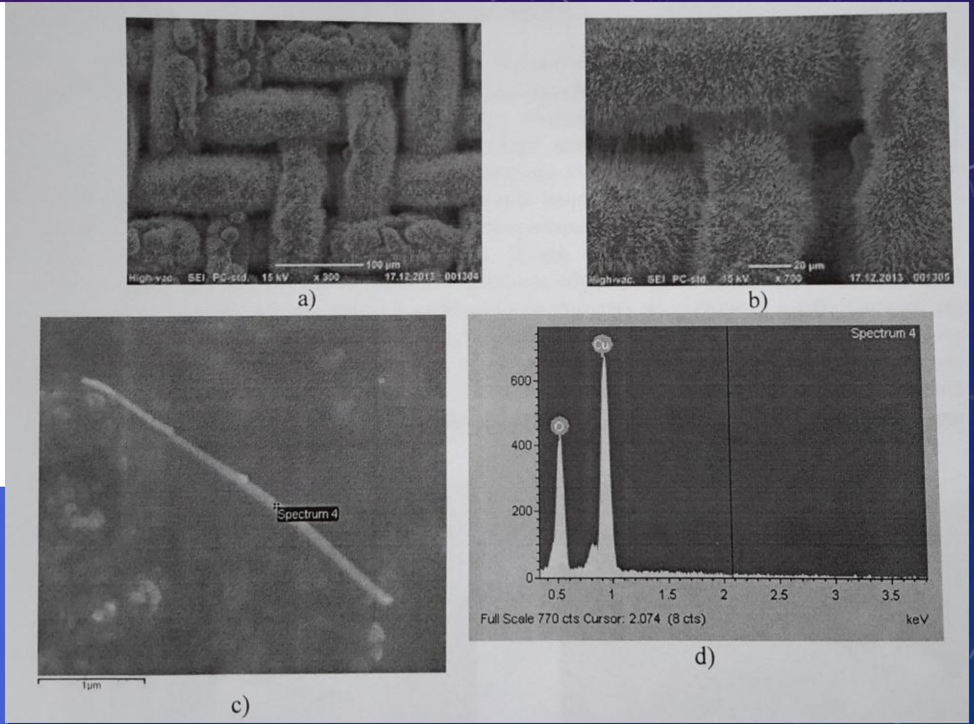

Growth of CuO whiskers is related with annealing at 400-700° C at presence of oxygen

3-D image of the cooper foil in the irradiation zone. Craters and locally melted zones are seen.

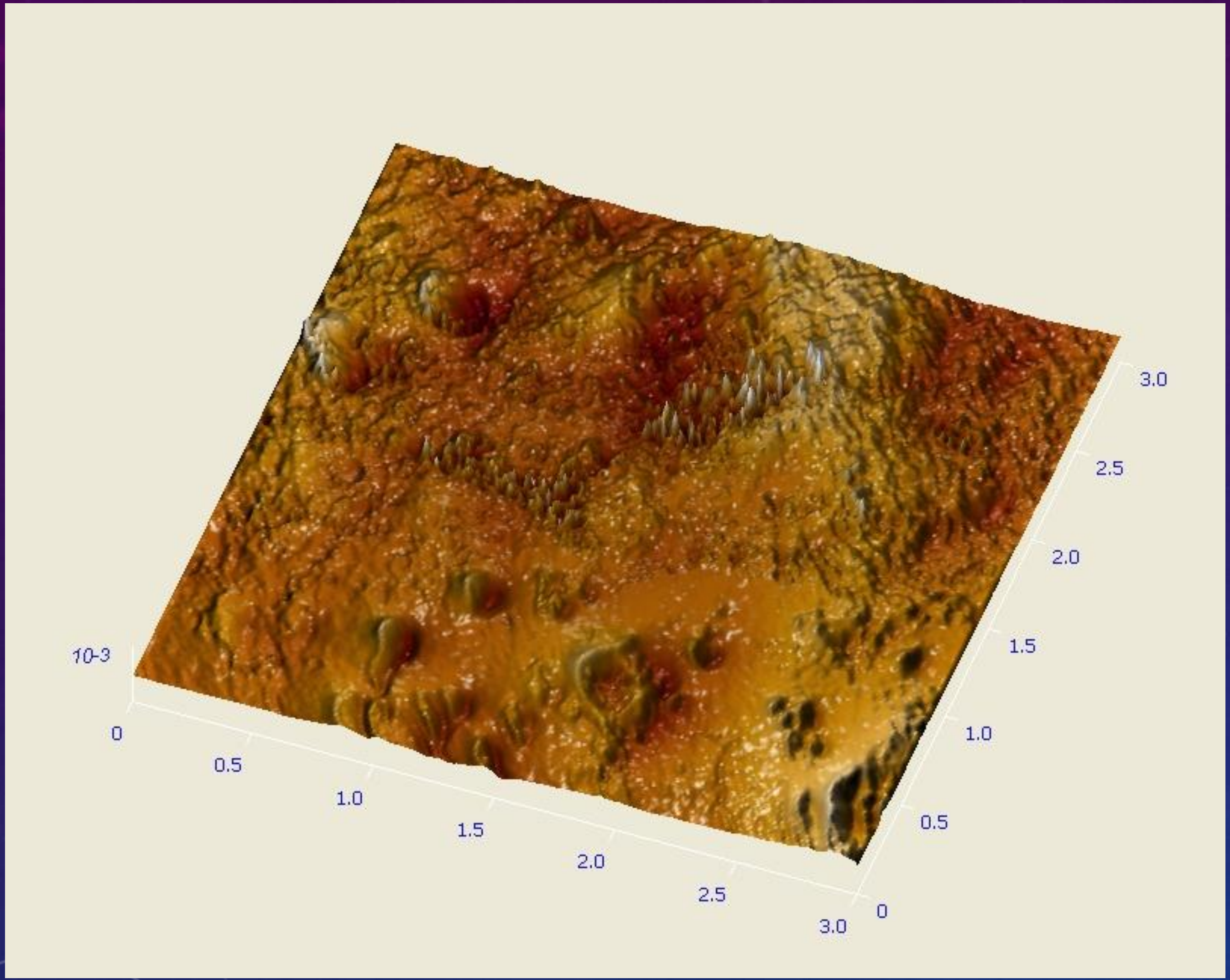

Phase image of the sample. Dark colour area means an appearance of new material: Cu oxides?

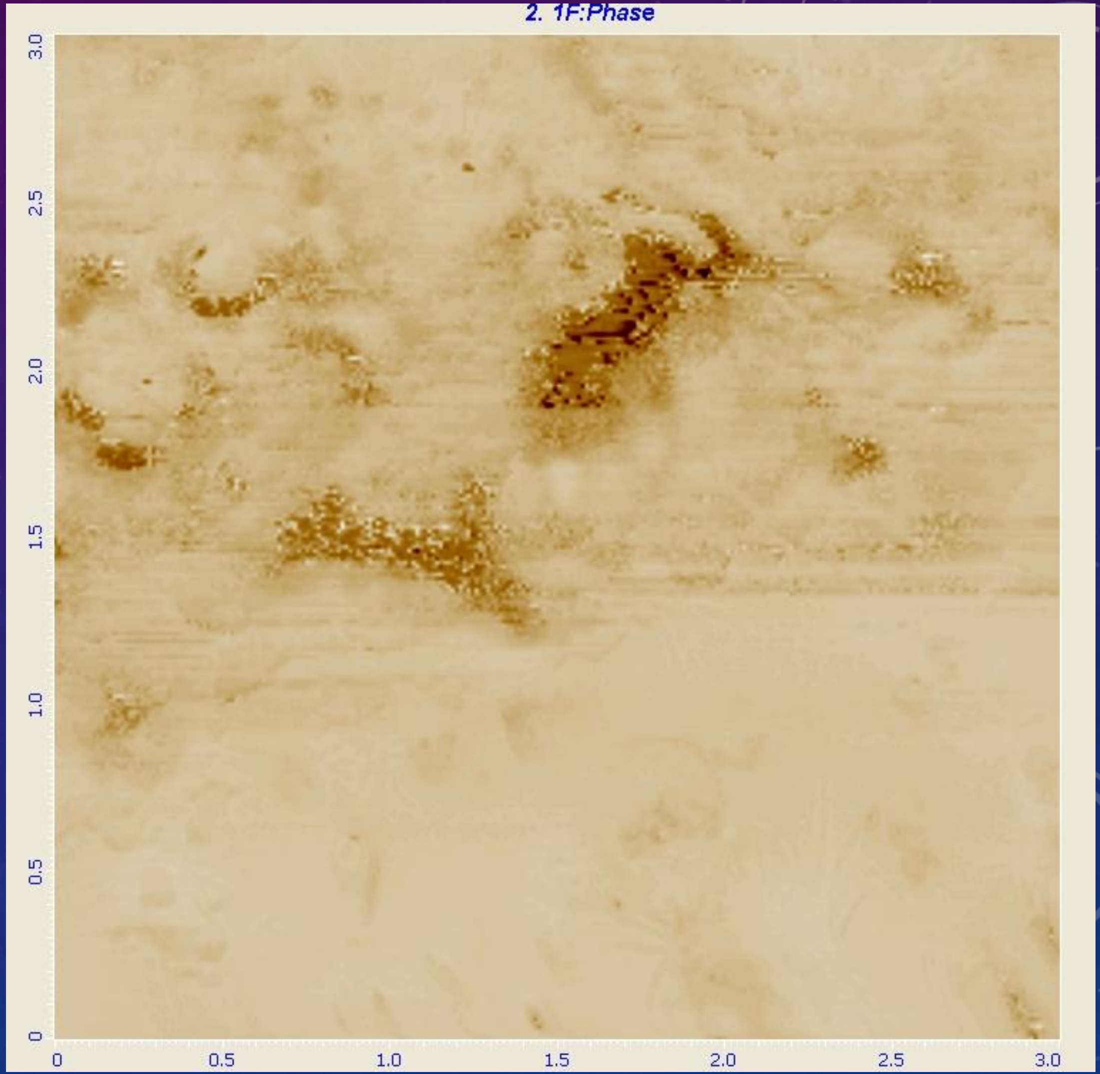

D-E point

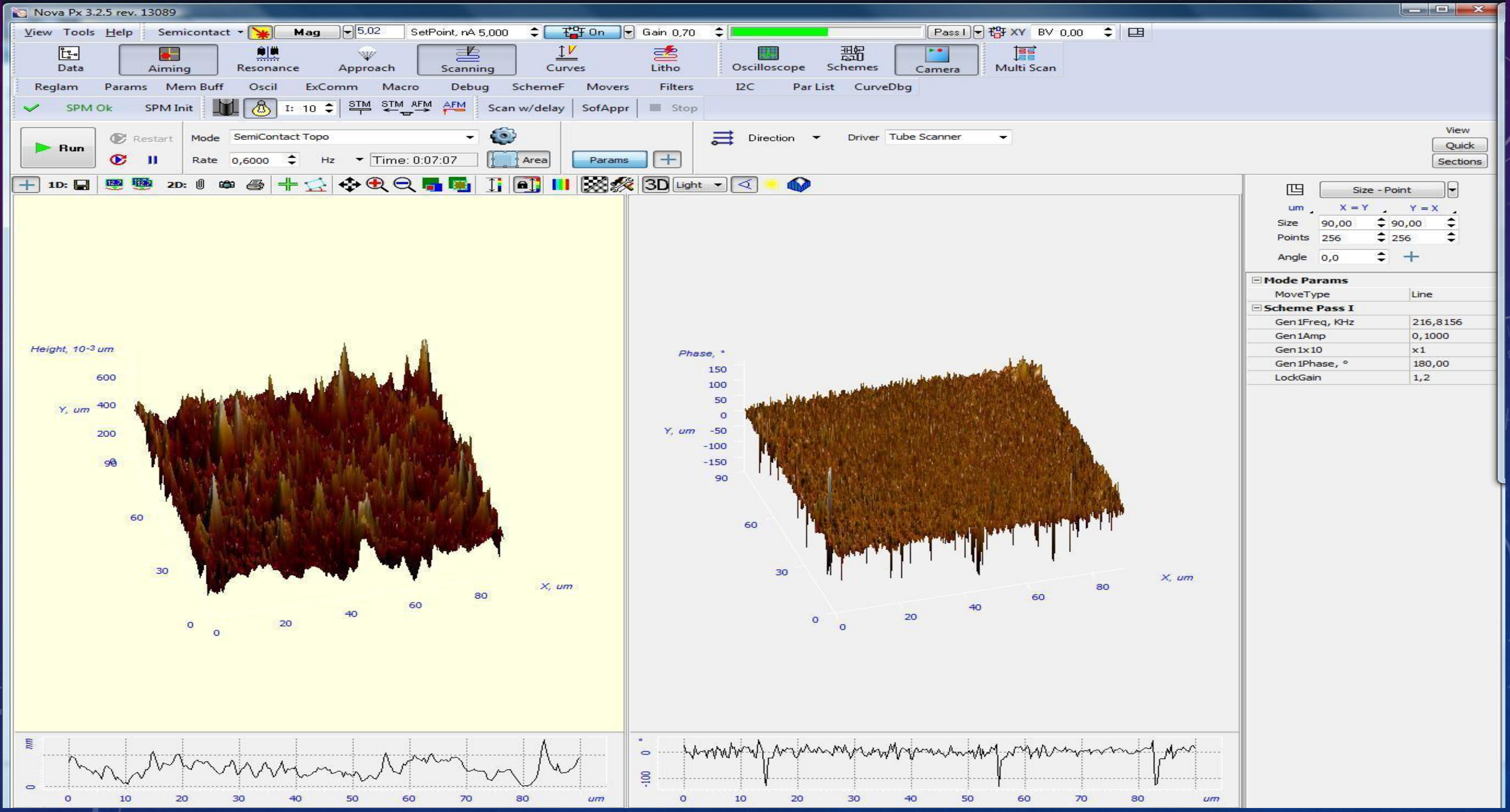

Nova Px 3.2.5 rev. 13089
View Tools Help
Semicontact
Mag
5,02
SetPoint, nA 5,000
On
Gain 0,70
Pass I
XY
BV 0,00
Data
Aiming
Resonance
Approach
Scanning
Curves
Litho
Oscilloscope
Schemes
Camera
Multi Scan
Reglam
Params
Mem Buff
Oscil
ExComm
Macro
Debug
SchemeF
Movers
Filters
I2C
Par List
CurveDbg
SPM Ok
SPM Init
I: 10
STM
AFM
Scan w/delay
SofAppr
Stop
Run
Restart
Mode
SemiContact Topo
Rate
0,6000
Hz
Time: 0:07:07
Area
Params
Direction
Driver
Tube Scanner
View
Quick
Sections
1D:
2D:
3D
Light
Size - Point
um
X = Y
Y = X
Size
90,00
90,00
Points
256
256
Angle
0,0
Mode Params
MoveType
Line
Scheme Pass I
Gen 1Freq, KHz
216,8156
Gen 1Amp
0, 1000
Gen 1x10
x1
Gen 1Phase, °
180,00
LockGain
1,2
Height, 10-3 um
600
400
200
Y, um
X, um
Phase, °
150
100
50
0
-50
-100
-150
um

E - H point

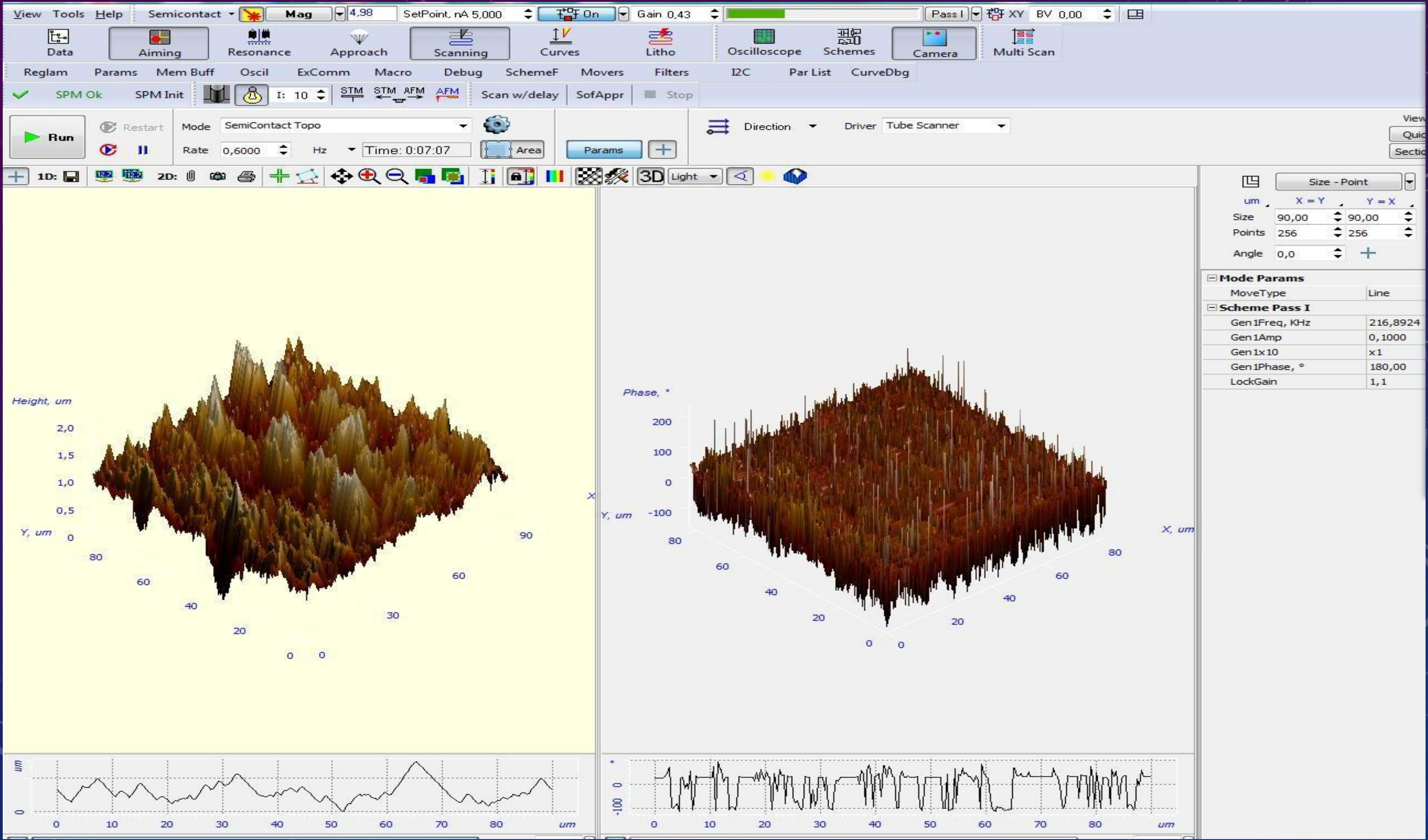
View Tools Help Semicontact Mag 4,98 SetPoint, nA 5,000 On Gain 0,43 Pass I XY BV 0,00
Data Aiming Resonance Approach Scanning Curves Litho Oscilloscope Schemes Camera Multi Scan
Reglam Params Mem Buff Oscil ExComm Macro Debug SchemeF Movers Filters I2C Par List CurveDbg
SPM Ok SPM Init I: 10 STM STM AFM AFM Scan w/delay SofAppr Stop
Run Restart Mode SemiContact Topo Rate 0,6000 Hz Time: 0:07:07 Area Params
Direction Driver Tube Scanner
Size - Point
um X = Y Y = X
Size 90,00 90,00
Points 256 256
Angle 0,0
Mode Params
MoveType Line
Scheme Pass I
Gen1Freq, KHz 216,8924
Gen1Amp 0,1000
Gen1x10 x1
Gen1Phase, ° 180,00
LockGain 1,1
Height, um
Phase, °
Y, um
X, um

AFM MICROSCOPY STUDIE

Scanning spreading resistance microscopy

Scanning spreading resistance microscopy and spectroscopy for routine and quantitative two-dimensional carrier profiling

P. Eyben, M. Xu, N. Duhayon, T. Clarysse, S. Callewaert, and W. Vandervorst

1.US Pat. 4992728.
2.J. Vac. Sci. Techn. B, 20 (1), 471 (2002).

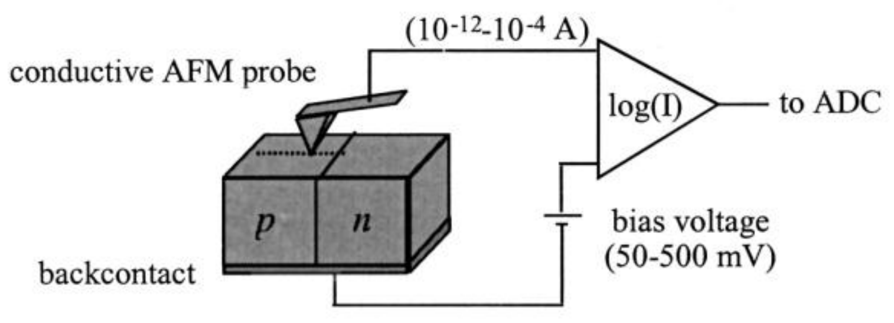

FIG. 1. Basic scheme of SSRM.

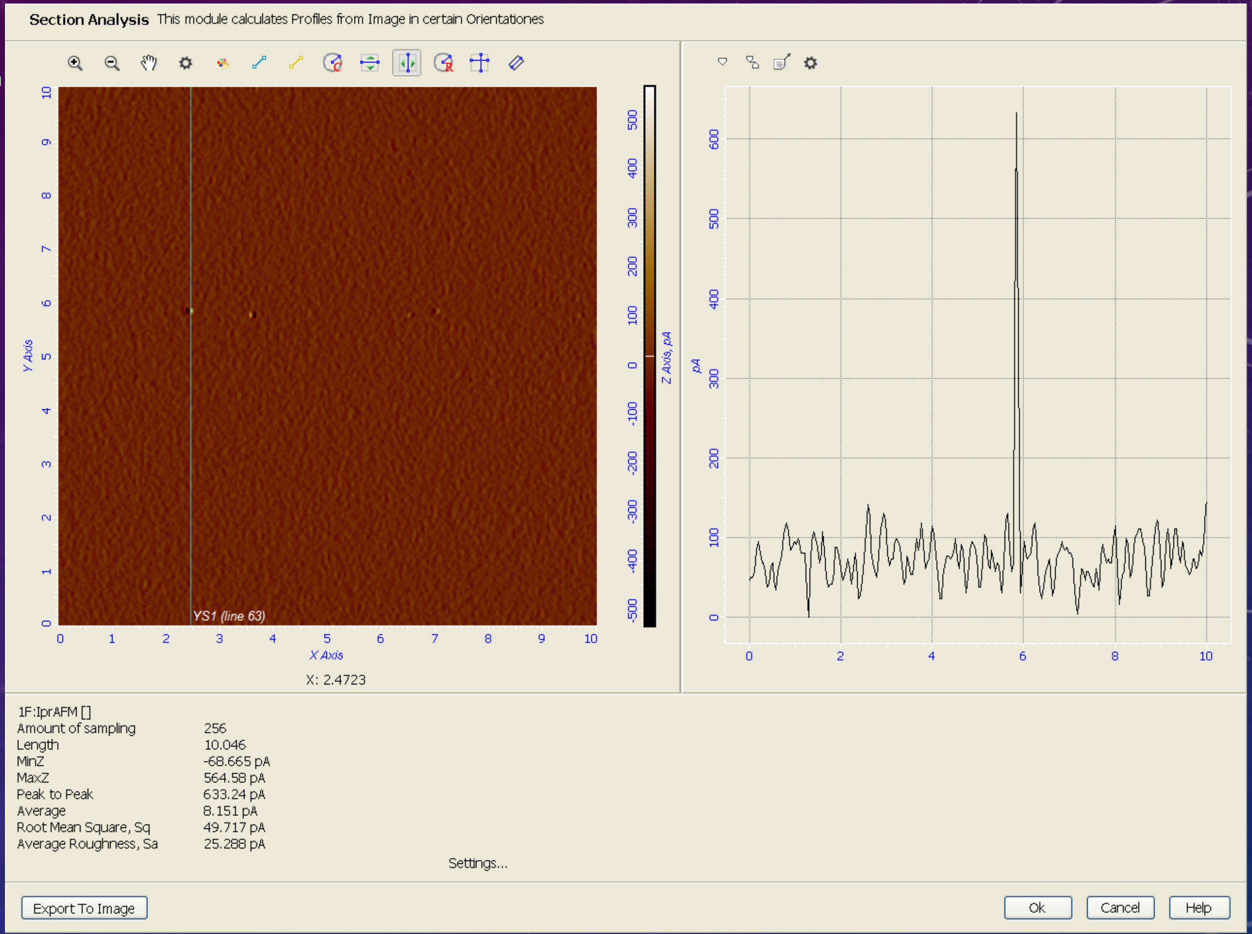

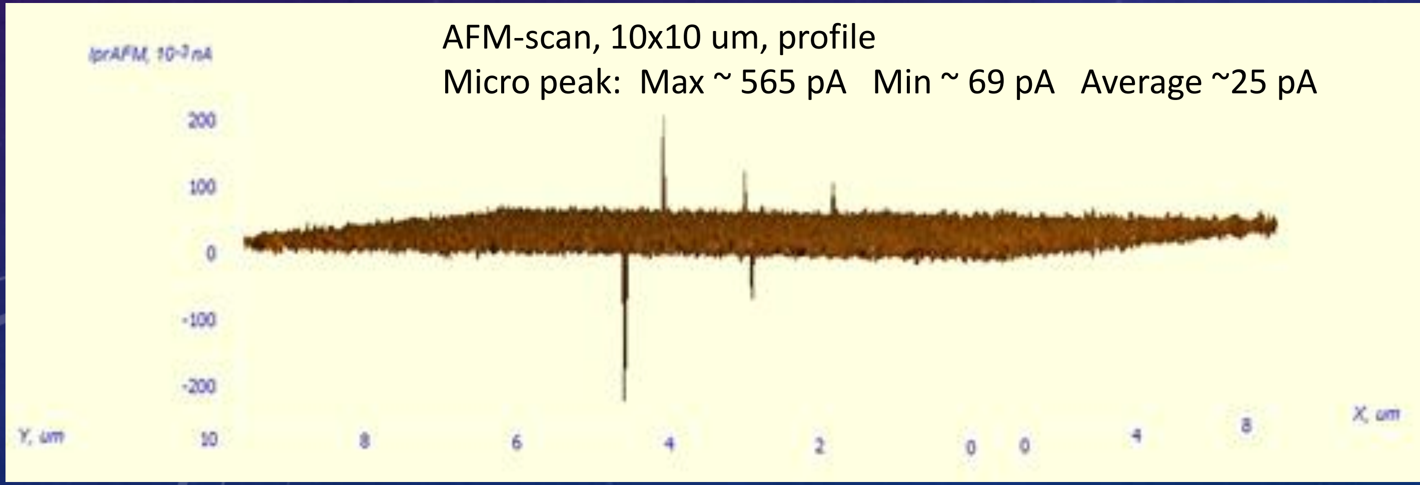

AFM-scan, 10x10 um, profile
Micro peak: Max ~ 565 pA Min ~ 69 pA Average ~25 pA

In SSRM, a very small conductive tip is used to measure the local spreading resistance, which is linked directly proportional to the local resistivity, provided the tip pressure is high enough to locally induce a b-tin phase transformation under the tip.

The basic principle is to apply a bias voltage between a back contact and the tip and to measure the current flowing through the sample using a logarithmic amplifier ~Fig. 1!.

A spatial resolution set by the tip radius typically 10–15 nm!

SUMMARY

- Cathode surface definitely suffers from oxidation by the gas radicals, ions, and radiation damages. Besides of Cu a presence of Si, O, F, C is observed, too. That might be: SiO_2, Cu_2O, and Si. All of them are high resistive materials.
- At the edges of the strips in the centre and apart of the irradiated zone the signs of the FR4 chemical components are observed, that is: Br, Ca, Si (crystals).
- Three sources of self-sustained current emission are available:

- autoemission from the whiskers;

- gas ionization initialised by photons from Cu_2O grains;

- Malter effect from dielectric deposits.

BACKUPS

AFM image of the copper foil surface of FR4 after irradiation

SAMPLE E^F

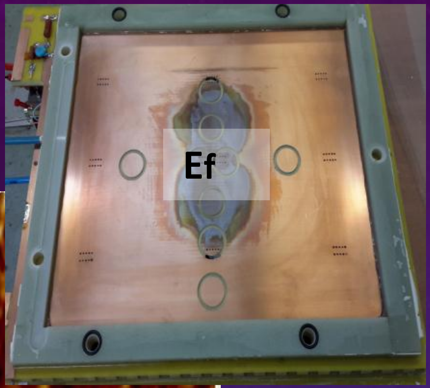

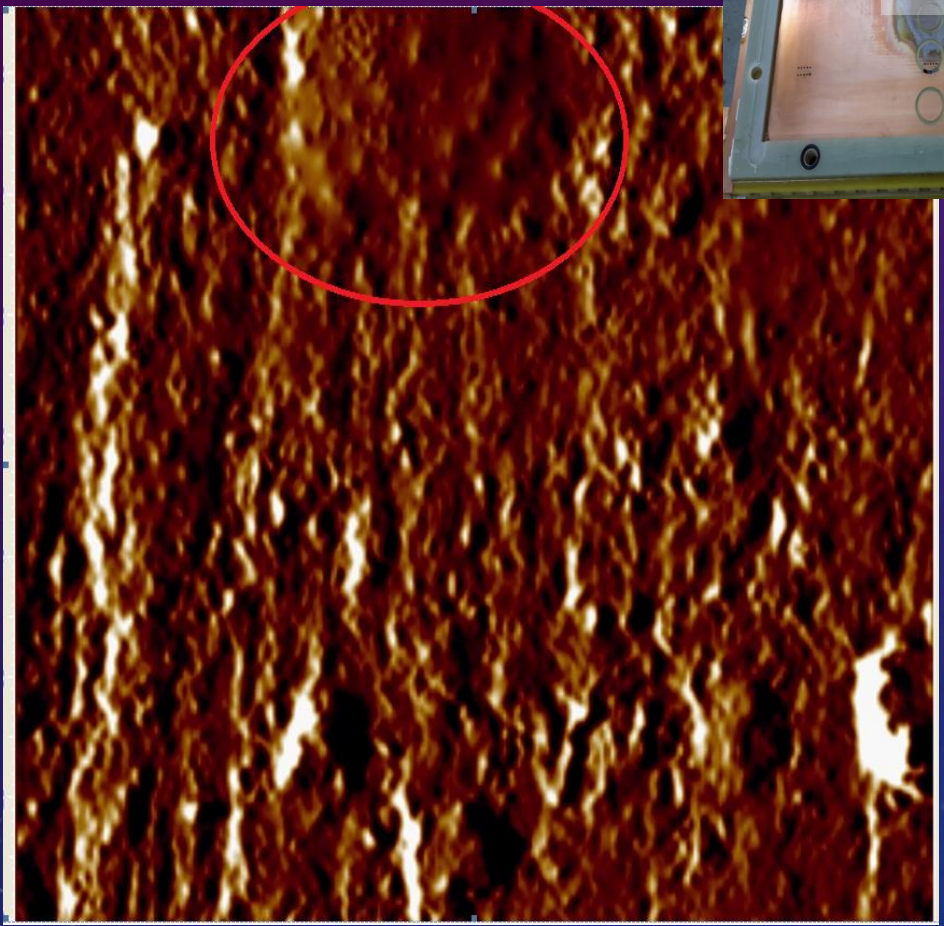

Sample H

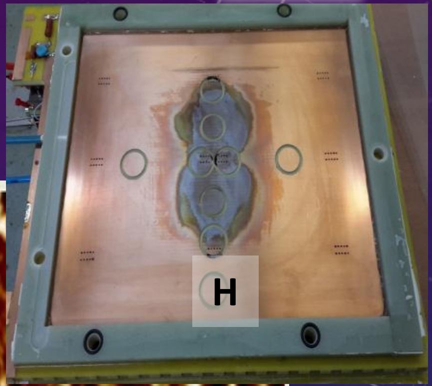

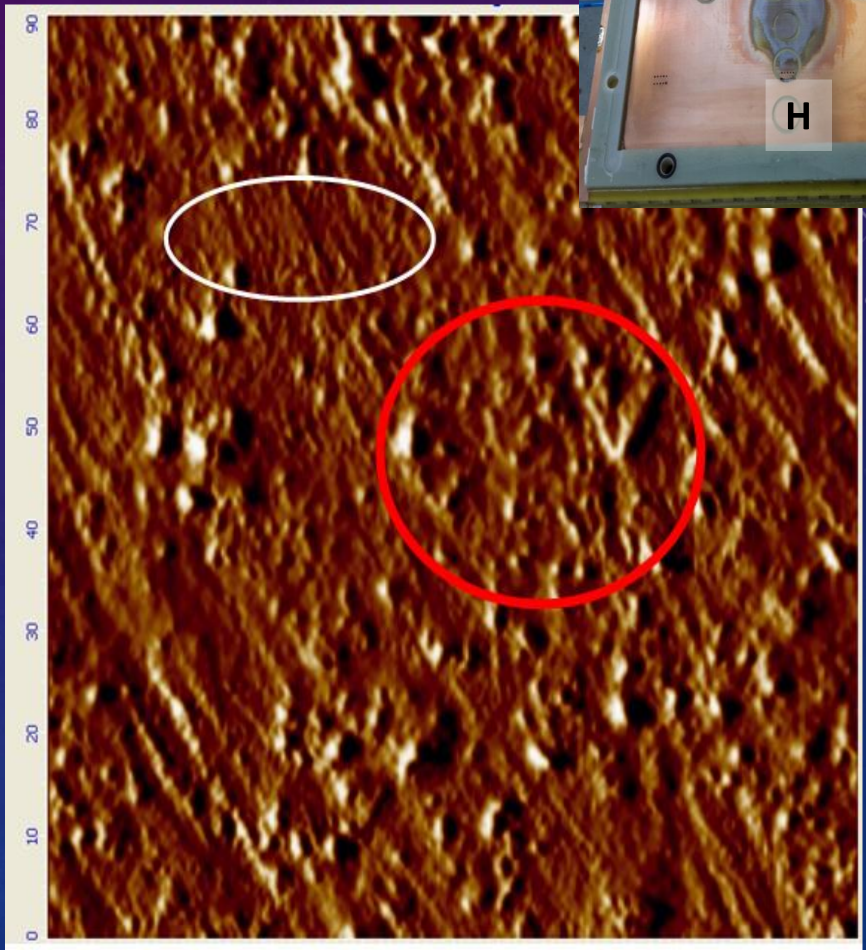

Presence of clear damages on the cooper foil surface indicates that besides of the intensive oxidation processes cathode suffer as well from radiation damage.

THE BEHAVIOUR OF COPPER IN VIEW OF RADIATION DAMAGE IN THE LHC LUMINOSITY UPGRADE

R. Flukiger, T. Spina, CERN, Geneva, Switzerland

Table 1: Radiation sources and track length fraction in LHC upgrade and approximate energies at the maximum of distribution

Radiation source	Track length fraction (%)	Energy at distribution maximum (MeV)
Photons	88	~ 0.5
Electrons/positrons	7	~1 – 10
Neutrons	4	1
Pions	0.45	100 - 200
Protons	0.15	100 - 200

Table 2: Mean energy, flux and dpa, averaged over four hot spots (data from Mokhov [10])

Particle j	<E> (GeV)	RMS (GeV)	Flux ($cm^{-2}s^{-1}$)	DPA/yr	DPA (%)
p	2.93	10.7	1.3e8	1.75e-5	5
n	0.22	3.7	2.3e9	8.24e-5	26
π, K	13.8	41.6	5.4e8	4.78e-5	15
μ	11.3	19.7	6.3e5	1.70e-9	-
γ	0.018	0.35	8.6e10	~2.e-5	6
e	0.077	0.5	9.8e9	2.47e-5	8
Sub-thresh.					40

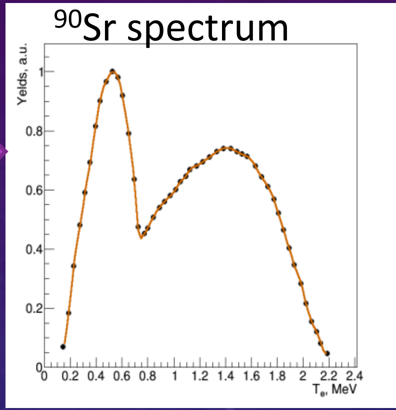

Образец облученной медной фольги на катоде прототипа

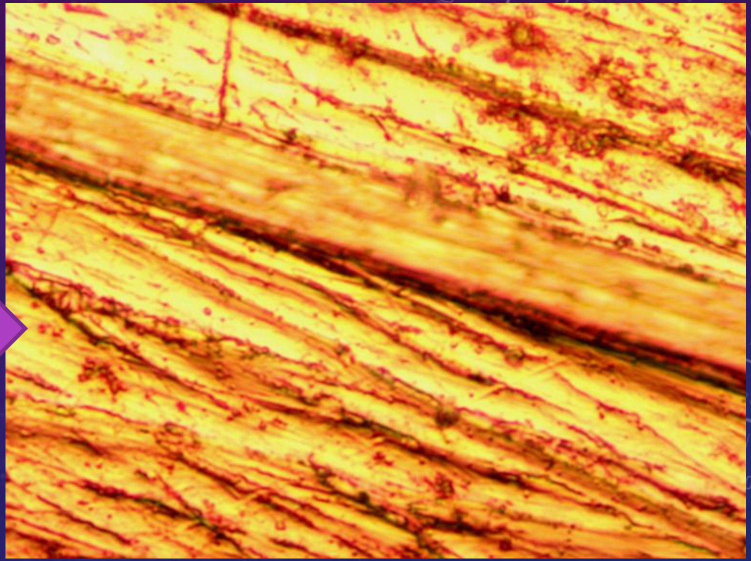

X 400

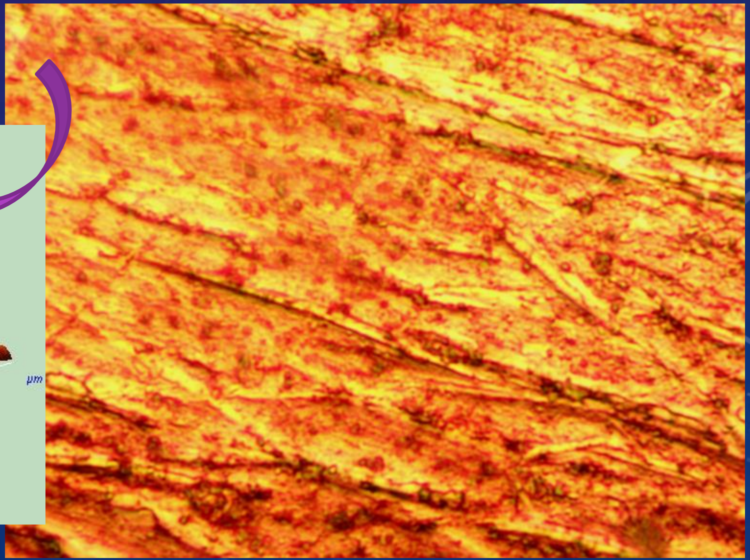

X 200

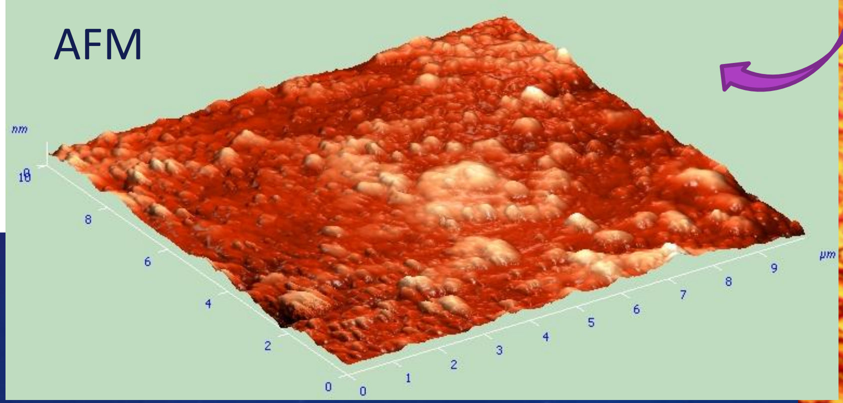

Table 2.4. Values of threshold and average displacement energies

Element	Crystal structure	Threshold E_d (eV)	Average E_d (eV)
Al	FCC	16 [Jung, 1981]	27 [Lucasson, 1975] 25 [ASTME521]
Cu	FCC	19 <110> [Vajda, 1977] 19 <100> [Vajda, 1977] 45 <111> [Vajda, 1977] 19 [Jung, 1981]	29 [Lucasson, 1975] 30 [ASTME521]
Ni	FCC	22 <110> [Vajda, 1977] 35 <100> [Vajda, 1977] 60 <111> [Vajda, 1977] 23 [Jung, 1981]	33 [Lucasson, 1975] 40 [ASTME521]
Ag	FCC	23 <110> [Vajda, 1977] 24 [Jung, 1981]	39 [Lucasson, 1975]
Au	FCC	36 <110> [Vajda, 1977] 36 <100> [Vajda, 1977] 36 <111> [Vajda, 1977] 34 [Jung, 1981]	43 [Lucasson, 1975] 40 [Vajda, 1977]
Pb	FCC	12.5-15 [Jung, 1991]	19 [Lucasson, 1975] 25 [ASTME521]
Co	FCC	23 <110> [Vajda, 1977] 30 <100> [Vajda, 1977]	
Pt	FCC	39 <110> [Vajda, 1977] 37 <100> [Vajda, 1977] 34 [Jung, 1981]	44 [Lucasson, 1975]
Pd	FCC	34 [Jung, 1981]	41 [Lucasson, 1975]
Th	FCC	35 [Jung, 1991]	44 [Lucasson, 1975]
Ge	Diamond cubic	14 [Corbett, 1966]	18 [Loferski, 1958] 20 [Poulin, 1980] 30 [Vitovskii, 1977]
Si	Diamond cubic	13 [Corbett, 1966] 13 <111> [Loferski, 1958]	
C (diamond)	Diamond cubic	32 <110> [Steeds, 2011] 27 <100> [Steeds, 2011] 34 <111> [Steeds, 2011]	40 [Zinkle, 1997]
C (graphite)	HCP	25 [Corbett, 1966]	30 [Zinkle, 1997]
V	BCC	39 <110> [Vaj, 77] 30 <100> [Vaj, 77] 35 <111> [Vaj, 77] 25 [Jung, 1981]	40 [ASTME521]

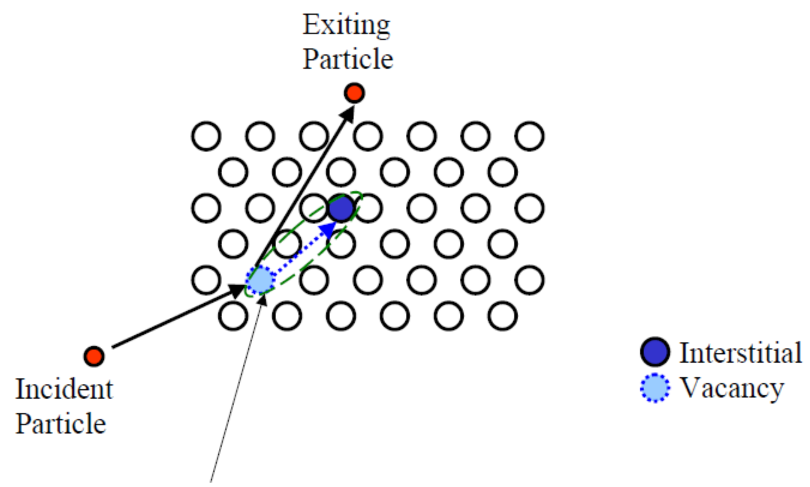

A Frenkel pair consists of a vacancy and an interstitial atom.

Atomic displacement damage occurs ballistically through kinetic energy transfer. Displacement damage is due cumulative long-term non-ionizing damage from ionizing radiation. The particles producing displacement damage include protons of all energies, electrons with energies above 150 keV, and neutrons.

$$N_d(T_d) = \begin{bmatrix} 0 & ; & T_d < E_d \\ 1 & ; & E_d < T_d < 2E_d/0.8 \\ \dfrac{0.8T_d}{2E_d} & ; & 2E_d/0.8 < T_d < \infty \end{bmatrix}$$

$$T_d = \frac{2(E+2mc^2)E}{Mc^2}$$

T_d – energy available for damage;
E_d – threshold displacement energy;
N_d – number of dislocations.

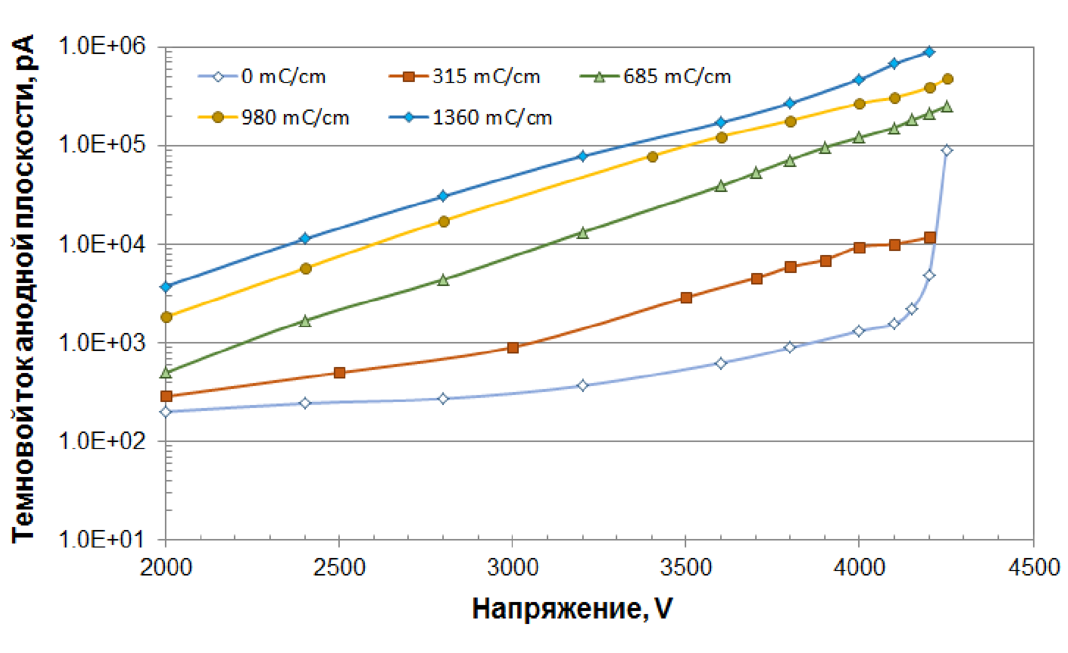
Темновой ток анодной плоскости, pA
1.0E+06
1.0E+05
1.0E+04
1.0E+03
1.0E+02
1.0E+01
2000
2500
3000
3500
4000
4500
Напряжение, V
0 mC/cm
315 mC/cm
685 mC/cm
980 mC/cm
1360 mC/cm

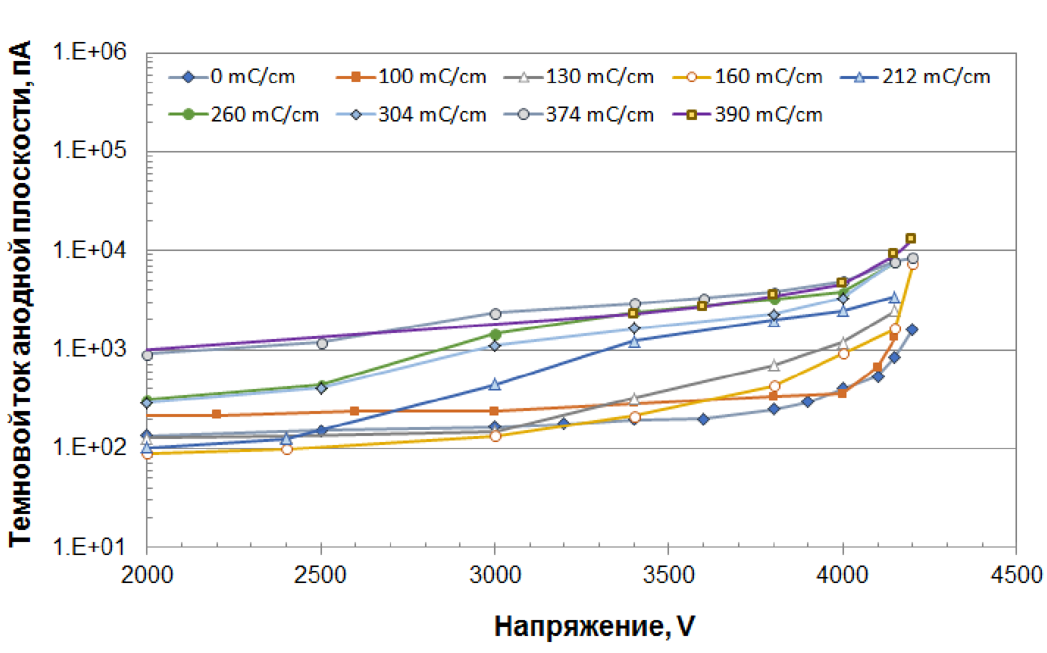
Темновой ток анодной плоскости, пА
1.E+06
1.E+05
1.E+04
1.E+03
1.E+02
1.E+01
2000
2500
3000
3500
4000
4500
Напряжение, V
0 mC/cm
100 mC/cm
130 mC/cm
160 mC/cm
212 mC/cm
260 mC/cm
304 mC/cm
374 mC/cm
390 mC/cm

Flora M. Li et al., Low temperature (<100 °C) deposited P-type cuprous oxide thin films: Importance of controlled oxygen and deposition energy, Thin Solid Films 520 (2011) 1278–1284

Copper forms two types of oxides: cuprous oxide (Cu_2O) and cupric oxide (CuO), each with unique material properties as highlighted in Table 1. Cu_2O is a highly transparent, yellow, p-type semiconductor, while CuO is typically an opaque, more conductive material. Although Cu_2O is the native oxide of copper, it is often difficult to form pure Cu_2O films and requires precise control of the stoichiometry. Even moderate excess of oxygen and/or reaction energy tends to favour the formation of CuO instead of Cu_2O. Fig. 1 provides a simplified illustration of the oxidation pathway to form Cu_2O and CuO from copper.

Increasing Oxygen (O_2)

$$2Cu \longrightarrow 2Cu + O^- \longrightarrow Cu_2O \longrightarrow Cu_2O + O^- \longrightarrow CuO$$

Fig. 1. Simplified illustration of the oxidation reaction of copper for the formation of Cu_2O and CuO.

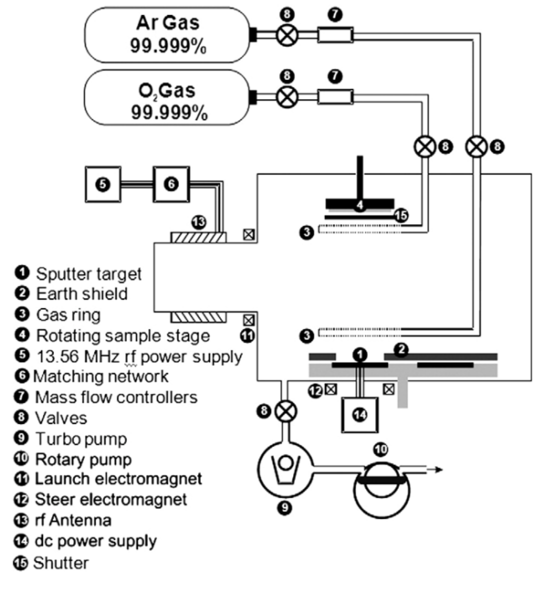

Fig. 2. Schematic illustration of a HiTUS sputtering system, with a remote plasma chamber where the substrate/sample is removed from the sputtering plasma. Illustration adapted from Ref. [13].

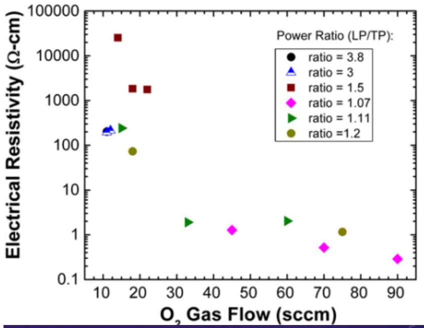

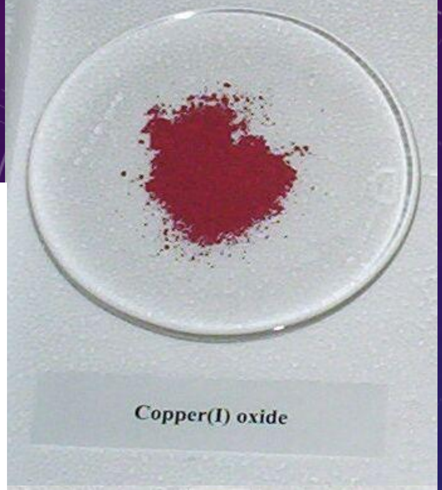

Table 1
Comparison of the different oxides of copper [3,6].

Name	Molecular formula	IUPAC name	E_g (eV)	Resistivity (Ω-cm)	Type	Crystal structure	Appearance
Cuprous oxide	Cu_2O	Copper (I) oxide	2.0–2.6	10^3–10^8	P	Cubic	Yellow/Red, semi-transparent
Cupric oxide	CuO	Copper (II) oxide	1.2–1.6	0.01–1	N/P	Monoclinic	Darker colour

CSC CMS PROTOTYPE LONGEVITY TEST

Photos of the disassembled detector after accumulation of Q=1.36 C/cm

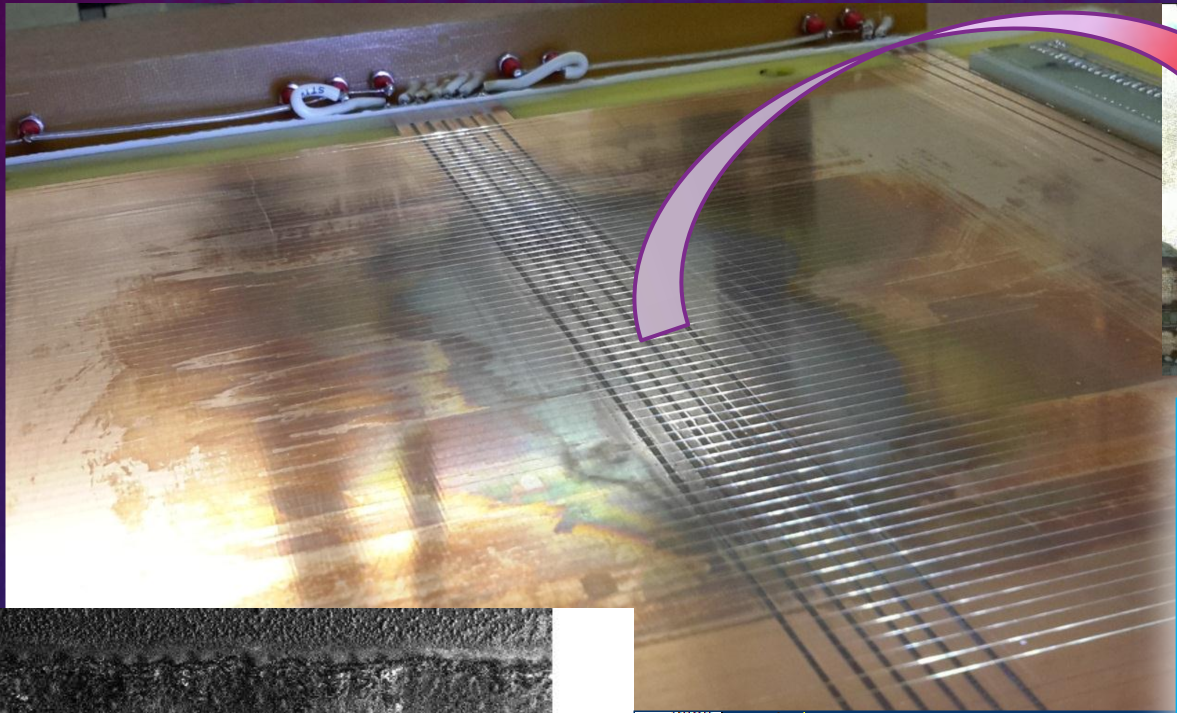

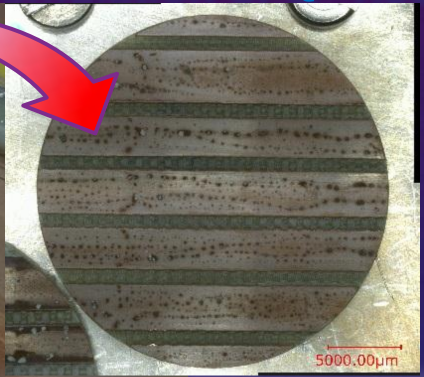

Centre of the irradiated zone

Traces of liquid
(plasticizers from FR4 ?)

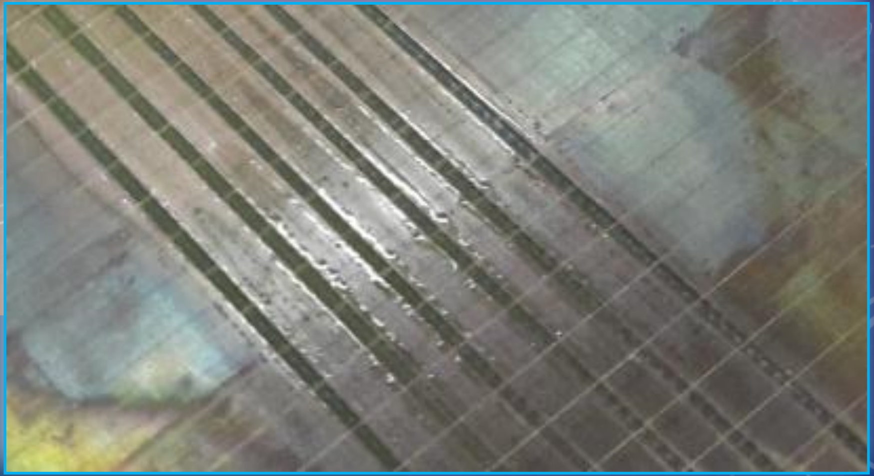

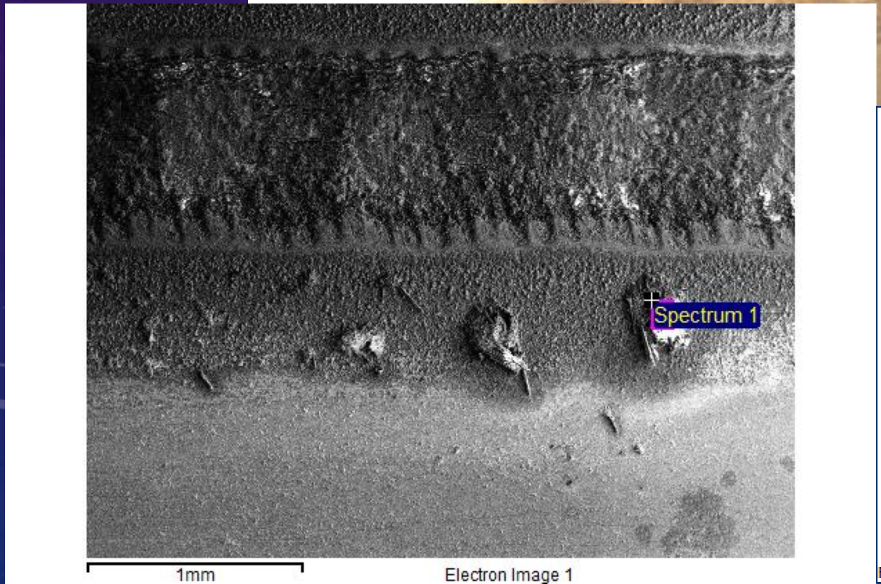

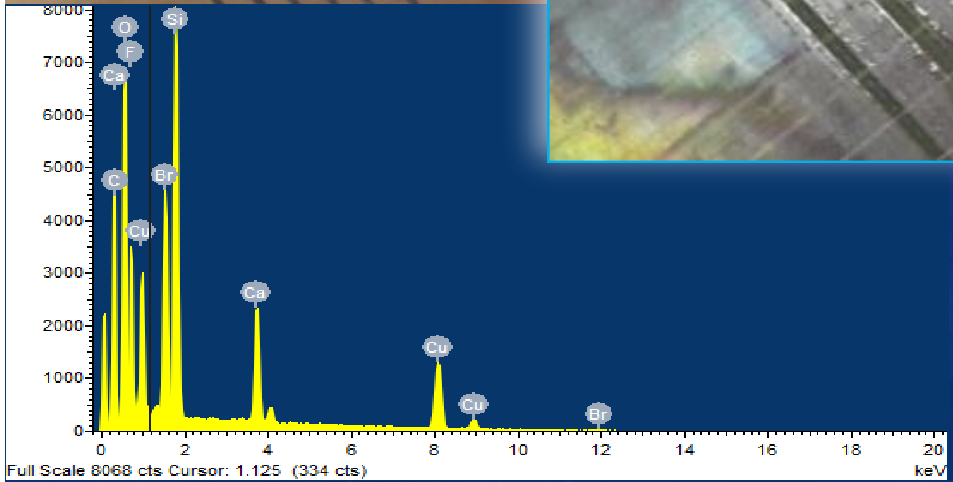

J. Phys. D: Appl. Phys., Vol. 10, 1977. Printed in Great Britain. © 1977

LETTER TO THE EDITOR

Electroluminescence produced by high electric fields at the surface of copper cathodes

R E Hurley and P J Dooley
General Electric Company Limited, Hirst Research Centre, Wembley, Middx HA9 7PP

Received 20 June 1977, in final form 15 August 1977

Abstract. Spots of light have been observed on the surface of OFHC copper cathodes following the application of high electric fields. The spectrum of the radiation shows a sharp peak at about 640 nm and its intensity obeys the Alfrey–Taylor relationship for electroluminescence. Within the light-emitting regions, discharges have been seen which it is believed are caused by the breakdown of dielectric inclusions trapped at defects in the crystal structure. Observations are consistent with the inclusions having semiconducting properties and emitting light by recombination of conduction electrons with holes produced by impact ionization within their crystal lattice structure.

In the range of E = 50-100 kV/cm light emission from the spots have been observed with wave length 660 nm.
Most probable source Cu_2O crystals or other semiconducting impurities on the cooper surface.

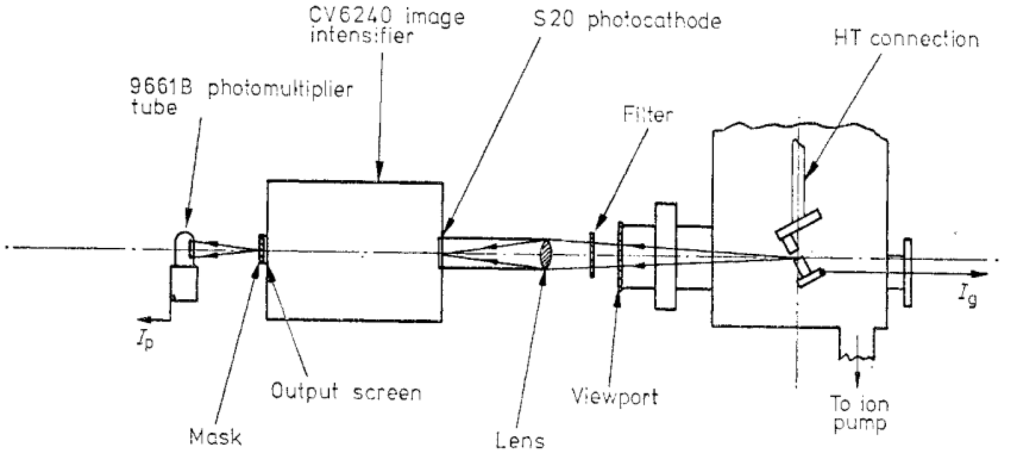

Figure 1. Experimental arrangements.

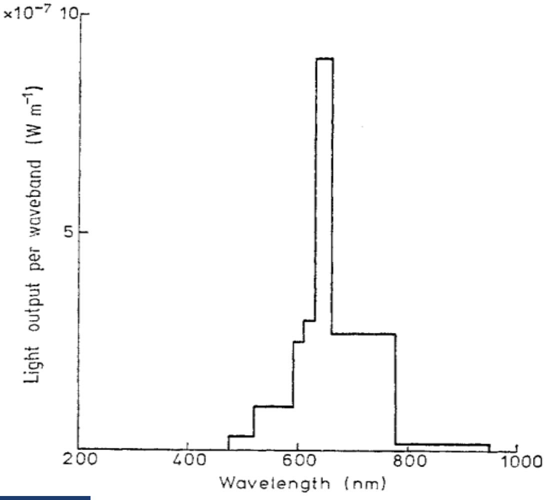

Spectrum of light emitted from a single cathode spot: 4·8 mm gap, 61 kV DC.

The emitted light intensity obeys the Alfrey–Taylor relationship which represents strong evidence that lattice atoms or emission centres are ionized by the acceleration of conduction electrons. The source of these electrons may be Cu which will form junctions with Cu_2O or other semiconducting impurities, or alternatively it may be donor levels existing near the conduction band. Assimos and Trivich (1974) have shown that surface donor levels can exist in single crystal Cu_2O and in addition there is the possibility that the substitution of n-type impurities can occur at Cu atom sites—for example, Fe which has more valence electrons than Cu and is a known impurity in OFHC Cu (see table 1).